FINAL REPORT

DEPARTMENT OF SUPPLIES AND SERVICES CANADA

CONTRACT # : OSUS1-00117

FILE # : 23SU-3600-1-0155

PROJECT TITLE : Magnetically Stabilized Plasma Torch For Chemical Vapour Deposition

PROPOSED STARTING DATE : Nov. 1/83

PROPOSED COMPLETION DATE : April 1/84

PROJECT DIRECTOR : Dr. H. J.J. Seguin
Department of Electrical Eng.
University of Alberta
Edmonton, T6G2G7
ph. (403) 432-3335

SCIENTIFIC AUTHORITY : Dr. Derwin C. Johnson
Communications Research Center (C.R.C.)
P.O. Box, 11490, Station H , Shirley Bay
Ottawa, Ontario
ph. (613) 596-9230

TECHNICAL STAFF : Dr. A.K. Nath
Dr. D.M. Antoniuk
Mr. H. Resheff
Ms. D. O'Shea

PERSONNEL SPECIFICS :

Dr. Nath is a research engineering from the Atomic Energy Research Institute in India. He has been working with our group for about a year , as a research associate in the area of high powered lasers and plasma physics. He has been able to lend considerable and valuable experience to the project.

Dr. Antoniuk is a recent Ph.D graduate from the laser group, at the University of Alberta. He has worked on the Magnetic Discharge Stabilization process almost exclusively , and consequently has been able to render much assistance to the undertaking in question.

Mr. Reshef is highly experienced electro-mechanical technician possessing numerous well developed skills in the electronics and fabrication fields. His services have been indispensable to the contract work outlined herein.

Ms. O'Shea is a specially trained materials technologist having extensive expertise in the preparation and evaluation of material samples produced by a variety of methods. Ms. O'Shea has become an invaluable member of the research team, particularly in the researching and documentation of "Prior Art"in this area. A report on Plasma Assisted Chemical Vapour Deposition of Vitrious Silicon Dioxide prepared by Ms. O'Shea is included in appendix A of this document.

Our machine shop is staffed by a group of 6 highly qualified specialists machinists , who have been working within the general area of laser -plasma research for many years. As a consequence they have acquired considerable knowhow in this area of activity and have been able to assist us , not only in the fabrication of special apparatus and equipment, but additionally in the design of the devices themselves.

INTRODUCTION :

With the ever increasing demand and usage of optical fibers for communication and the transmission of information new and improved technologies for the manufacture of the optical fibre itself are becoming of even greater scientific and economic interest.

The speedy, high quality and low cost production of very large preforms, from which these minute optical fibers are drawn in a continuous and unbroken thread, is thus of major importance at this point in time.

At the present state-of-the-art two different preform manufacturing processes have gained prominence. These are:

1. The standard C.V.D. multilayer internal soot depostion method, utilizing an external gas or hydrogen powered torch as reaction heat source and subsequent vitrifaction.

2. The axial M.C.V.D. continuous growth, bulk depostion method, employing a combined internal oxi-hydrogen torch to simultaneously drive both the decomposition and deposition reaction , as well as the vitrifaction process.

Both of the above production techniques have been demonstrated to provide good quality preforms at an acceptable cost. However the standard C.V.D. process is relatively slow and not conducive to very large preform fabrication. The M.C.V.D method on the other hand can be easily adapted to produce very large preforms relatively quickly, but high quality ,low optical absorption and index control are much more difficult to achieve on a consistent basis.

The research project which forms the framework of this DSS contract is thus directed at the development of an alternative method for optical fibre preform manufacture. One which hopefully will incorporate the best features of the previously developed processes into a single cost-effective method, amenable to operation in a continuous production manner.

PROJECT DESCRIPTION :

The nature of the research work considered here involves the utilization and adaptation of a " Magnetic Discharge Stabilization " Technique ,developed recently in our laboratory for laser applications, to the field of chemical vapour deposition . In particular we wish to study the feasibility of using specially profiled magnetic fields, interacting with a low voltage, high current electrical discharge, to produce an intense , hot plasma possessing a high velocity azimuthal motion. Such a "MAGNETICALLY STABILIZED PLASMA TORCH " is anticipated to exhibit good high temperature spacial uniformity and reliability , particularly with electro-negative host gases or vapours. In this manner it is envisaged that an efficient and clean , electrically powered heat source for chemical vapour deposition applications will be realized.

Brief Description of Method:

Extensive research work, both theoretical and experimental , in our laboratories over the past several years has documented that the " LORENTZ " JxB forces produced on charged particles in properly designed crossed electric and magnetic fields can be utilized to effectively suppress electrothermal plasma instabilities , thereby producing exceptionally stable discharges in a variety of gases. Further investigation has revealed that these relatively weak gasdynamic forces can be used to impart a significant and highly sheared motion to the plasma in question.

In a co-axial type geometry this magnetically induced plasma motion produces a strong outward directed radial flow of all gas species contained within the discharge volume ; due to heavy ion-neutral coupling. As a consequence it should be possible to use this " magnetic discharge stabilization and centrifugal gas pumping action" to generate a very high temperature, fast moving ionized gas stream ; which could conceivably be useful for initiating and sustaining desired eletro-chemical re ctions. Because of the relatively wide insensitivity of these interacting processes to pressure and ionized species, a wide variety of gases and mixtures , including electronegative materials , appear to be amenable to chemical vapour deposition reactions. If in fact such a "magnetically stabilized plasma C.V.D. torch " becomes technically viable , it should provide a welcome alternative to the classical oxy-hydrogen heat source presently widely utilized in the industry.

Project Major Tasks:

The original project proposal, dated Oct. 24/83, identified several tasks that were to be accomplished during the development of this contract. Thus in order to facilitate the discussion of our achievements in this undertaking these tasks are again reproduced below.

(1). Design a small scale , high pressure, plasma torch with a magnetic stabilization feature.

(2) Fabricate the above device in our machine shop.

(3) Test and debug the plasma torch under high pressure conditions, and with a number of inert and electronegative gases.

(4) Perform a parametric study on the operational characteristics of the torch in question. The study will include data on temperature profiles, gas velocity distribution,heating efficiency and uniformity, under a wide variety of input electrical drive conditions, and with a number of host gases, both inert and electronegative.

(5) If the above tasks # 1 through # 4 are successful we will proceed to investigate the potential of this high pressure magnetic stabilized plasma torch to perform steady state chemical vapour deposition of materials of interest to the electronics and optical communications industries. Here special emphasis will be given to the continuous growth of high quality silica preforms for use in optical fiber manufacture.

(6) Under take an indepth study of the physical properties of the various materials deposited and ascertain their usefulness in the electronics industry.

PROJECT ACCOMPLISHMENTS :

TASK # 1 through # 4 have thus far been accomplished.

TASK # 5 is presently underway and will be continued over the next several months; possibly over the summer period, by a third year engineering summer student.

TASK # 6 has not been initiated due to lack of time and the relative shortness of this present contract.

PROJECT DETAILS :

Magnetically stabilized plasma glow torch design :

As indicated previously our intention was to adapt our previous experience in magnetically stabilized gas discharges to attempt to develop a Plasma Glow Torch suitable for initiating and sustaining chemical reaction of interest for vapour deposition applications.

The particular geometrical features utilized in the first plasma torch constructed for this preliminary investigation are shown in the schematic sectional diagram of Fig. 1. The photographs of figures 2 and 3 reveal actual fabrication parameters. As can be seen the device is exceedingly simple, consisting essentially of a water-cooled anode and cathode electrode structure mounted in a close proximity co-axial configuration.

Provision has been made in the design to introduce the reactants co-axially through a chemically resistant small bore ceramic tube, built directly into the center of the water-cooled cathode electrode. A shielding flow of inert Argon gas is passed co-axially up this cathode structure, between the copper electrode inner wall and the ceramic reactant tube, so as to protect the cathode electrode face from chemical attack by the reactants. An Argon purge is also used in the main plasma chamber to provide similar protection for the water-cooled anode electrode annulus.

In operation a high current (typically 150 amps) distributed glow discharge is initiated and maintained between the extremities of the anode and cathode annulus. The interaction of this D.C. current with a superimposed magnetic field , produced by a surrounding solenoid, generates an electromagnetic force that results in a high velocity rotation being impressed upon the discharge region.

Theory of operation :

Figure 4 depicts the magnetic field profile generated by the particular electromagnet solenoid developed for this experiment. This data was obtained from a special " Potent " computer code perfected in our laboratory . The axial magnetic field component Bz produced by this magnet, when crossed with the radial component of the discharge current Jr , gives rise to a LORENTZ force Jr x Bz . This azimuthally directed force in turn produces a circular and sheared driving action on the plasma bulk, which spins up the discharge volume to a relatively high rotational velocity .

The particular MagnetoGasDynamic interactions involved in this process were extensively analyzed for a somewhat similar co-axial discharge geometry, used in a laser pumping system. Details of this computer modelling are enclosed in appendix B . Although the results obtained in this previous laser-plasma case are not directly applicable for the range of parameters considered here, the analysis does never-the-less clearly illustrate the manner and profiles in which these crossed electric and magnetic fields can produce large sheared mixing flows and gas transport in a co-axial discharge volume.

In order to gain a more detailed insight into the parameters of significance for the plasma torch case considered here a new graduate student was recruited and is presently engaged in adapting this previous computer modelling to accommodate the specific geometrical and operational parameters of this new plasma torch. Some of these specific features are illustrated in the model of figure 6 ; which was developed to simulate the actual physical construction displayed in figure 1. In this computer modelling we hope to obtained relevant expectation operational features and values ; and additionally gain some much needed information into the salient features associated with an optimum design of such a magnetically stabilized plasma glow torch.

This phase of the project has progressed well and preliminary results are presented in figures 7 through 11. It is expected that this computer simulation will be further pursued and hopefully completed over the coming summer months.

Figure 7 illustrates the current density, as a function of radial and axial position, with reference to the model used in figure 6. No azimuthal dependence in J was assumed in this analysis. The expected velocity profiles , developed within the rotating plasma disc in the torch, under transient and steady state conditions, are depicted in figures 8 and 9. Figure 8 shows the "short-time" velocity distribution unfolding within the interelectrode volume, after a run period of about 100 microseconds. The fully developed steady state velocity characteristics are given in figure 9. Examination of the above two figures reveals that although initially the plasma begins to spin relatively uniformly , to soon begins to assume a highly sheared nonuniform distribution ; with the highest velocities of almost 200 meters per second developing near the anode electrode. This highly sheared , high velocity plasma rotational feature produced with the torch interaction volume is particularly useful in that it promotes a high degree of mixing of the plasma constituent gases and vapours. This aspect is more fully illustrated in figures 10 and 11. Figure 10 depicts the transient evolution of this secondary gas mixing process after a period of

about 100 microseconds. The fully developed steady state gas mixing feature is shown in figure 11.

All of the computer simulation results shown in figures 7 through 11 were obtained for a typical operational condition of 100 amps total discharge current , 100 Torr total gas pressure and 1000 gauss magnetic field.

Another new third year summer student has been hired on to perform an ongoing series of tests upon the full spectrum of actual physical and electrical parameters associated with the operation of this torch. These test are expected to provide design data for a modified and hopefully improved version of the torch ; which will be much smaller physically and incorporate compact permanent magnets, instead of the bulkier electromagnets used in the work thus far. We anticipate that much of this development will be done over the summer months.

EXPERIMENTAL RESULTS :

Plasma rotational velocity :

Although, as indicated previously a detailed parametric study of the operational characteristics of the torch is still to be performed, some preliminary experimental data has never-the-less been collected. This data is outlined in the following section.

The photographs of Fig. 12 show this first torch design under actual operating conditions. As can be seen the device produces considerable visible side-light.

It is well known that the reactant utilization efficiency of any CVD torch is a very important parameter in the overall cost-effectiveness of the process. Previous work has shown that his utilization efficiency is a direct function of the quality and uniformity of mixing and heating of the reactant feedstocks achieved within the torch's fireball. Consequently the magnitude and profile of the rotational velocity achieved with this first magnetically stabilized torch design are of paramount importance. This being the case an attempt was made to utilize this side-light emission to measure the spacial and rotational velocity of the plasma, using both photographic and electrical techniques.

Firstly, high speed photographs (1/1000 of a sec.) were taken of the plasma fireball , using a variety of special optical filters, so as to provide some information on plasma uniformity and special profile. Typical photos thus obtained are shown in figure 13. However , as can be seen from these high speed photographs there is some structure in the rotating plasma disc, the rotational velocity is much too high to be resolved by the 1/1000 of a second speed of the camera used.

For the physical velocity measurements a special double photodiode pickup , developed earlier for laser plasma studies, was used. However the results obtained were inconclusive , ostensibly because there was insufficient plasma structure to provide a clean output electrical from the timing photodiode system.

We hope in the future to successfully repeat the experiments described above by using a high speed storage video camera system, which is due to be acquired by other plasma researchers within our department.

Temperature profile :

The temperature profile generated by the torch , as a function of input current , is shown in figures 14 through 16, for several pressures and gas mixtures. The initial thermocouple available to us did not permit measurements beyond about 1200 degrees C. (ie. the thermocouple itself melted when brought within about 1 cm. of the cathode electrode). Despite this however the data obtained did clearly indicated that the torch can indeed easily generate a sufficiently high temperature to sustain the desired $SiCl4 + O2 = SiO2 = Cl2$ reaction, at approximately 1200 to 1400 degrees C. The temperature profile also drops off sufficiently rapid in the axial direction to allow boule condensation . A more extensive and higher temperature profile investigation will be undertaken when our higher temperature (Rhodium) thermocouple is delivered.

Electronegative gases :

The experimental data presented previously in this report was taken for the test condition that only the inert gas Argon was flowed through the plasma torch. However, since in most chemical vapour depostion situations the majority of the reactant gas species of interest are particularly electronegative , it was necessary to investigate the discharge stability of the torch under this type of gas feed. This task was first attempted using

oxygen and then later the relatively nontoxic , Carbon tetracholride vapour as feedstock. The results, typical examples of which are shown in figures 17 through 19, documented that this magnetically stabilized torch concept does indeed provide stable plasma operation under relatively high concentrations of an electronegative species.

Deposition studies :

In order to evaluate the potential of this magnetically stabilized torch for silica preform manufacture, a series of actual SiO_2 deposition experiments are scheduled. However due to a shortage of time these have not yet been undertaken .

The experimental arrangement to be used is similar to that shown in Fig.7 of the literature survey contained in appendix A. Oxygen gas will be bubbled through a $SiCl_4$ bath and subsequently feed up the central region of the hollow cathode electrode . Argon buffer gas will again be flushed through both the cathode annulus and the main plasma chamber, so as to assist in plasma stability and electrode surface passivation and protection. A seed quartz rod will be positioned just above the plasma fireball to provide a site for SiO_2 condensation.

Reaction rates :

As indicated previously there has been insufficient operational time to permit the determination of reaction rates and deposition efficiencies. However, we hope to be in a position over the summer months to investigate these parameters in some depth.

Electrode contamination :

During operation of the torch , both with and without reactive feedstocks, it was observed that a dark deposit gradually accumulated on the upper anode electrode and the transparent quartz sidewall torch enclosure. It is believed that this deposit was due to " sputtering " of the cathode electrode , due to the heavy positive ion impact present at these elevated discharge currents. Up to the present time we have investigated only 3 different materials for fabrication of the cathode electrode surface; heavy metal , copper and stainless steel. We intend shortly to begin additional experiments using tungsten as the cathode surface. Hopefully a combination less prone to this

sputtering mechanism will be achieved.

We are also investigating the use of the " hollow cathode " concept in the construction of the cathode electrode. The photos of figure 21 show some of these hollow cathode geometries thus far investigated. The particular current confining operational feature characteristic of a hollow cathode electrode could conceivably be utilized to eliminate much of the sputtering action of the cathode electrode ; since the only high current density active area of the electrode would be that encompassed within the hollow ring annulus. Figure 21 is a drawing of a new hollow cathode design which we intend to investigate in the near future.

It is not clear at this stage of the investigation exactly what effect this electrode sputtering effect will have upon the quality of the chemical vapours deposited. In the worst case it is conceivable that such an " electrode contamination " could render the deposited material completely unsuitable for preform applications. Clearly much more work needs to be done in this area before any definitive statements can be made, either pro or con.

DISCUSSION AND CONCLUSION :

We believe, from the work that has thus far been accomplished, that an effective magnetically stabilized plasma glow torch can indeed be developed which provides sufficient temperature and stability to be of use for chemical vapour deposition. Considerable further work will however be necessary to determine if the electrode sputtering phenomenon and possible concomittent contamination observed can be suitably accommodated ; or if the contamination so produced is too detrimental for the production of high quality silica preforms.

FIGURES :

1. Schematic cross-sectional diagram of first Magnetically Stabilized Plasma Torch design.

2. Photos of plasma torch component anode and electrode parts dissassembled.

3. Photos of plasma torch with component parts assembled.

4. Computer generated magnetic equipotentials for solenoid used.

5. Magnetic field profile obtained from "Potent" Code.

6. Geometrical model used for computer simulation studies.

7. Current density profile used in simulation studies

8. Computer simulation of transient plasma rotational velocity distribution , after a running time of 100 microseconds.

9. Computer simulation of steady state plasma rotational velocity distribution.

10. Transient secondary gas flow in plasma torch.

11. Steady state scondary gas flow developed in plasma torch, showing mixing effect.

12. Photo of operating plasma torch.

13. Photos of rotating plasma taken at 1/1000 of a second and with variable density bandpass optical filter.

14. Temperature profile of plasma torch as a function of plasma current for 50 Torr Argon gas.

15. Same as above, but for 100 Torr Argon.

16. Same as 14, but for 150 Torr Argon.

17. Temperature profile of plasma torch as a function of plasma current for 50 Torr Argon and Oxygen gas.

18. Same as 17, but for 100 Torr Argon and Oxygen.

19. Same as 17, but for 150 Torr.

20. Photos of hollow cathodes tested.

21. Drawing of proposed hollow cathode design to reduce sputtering effect.

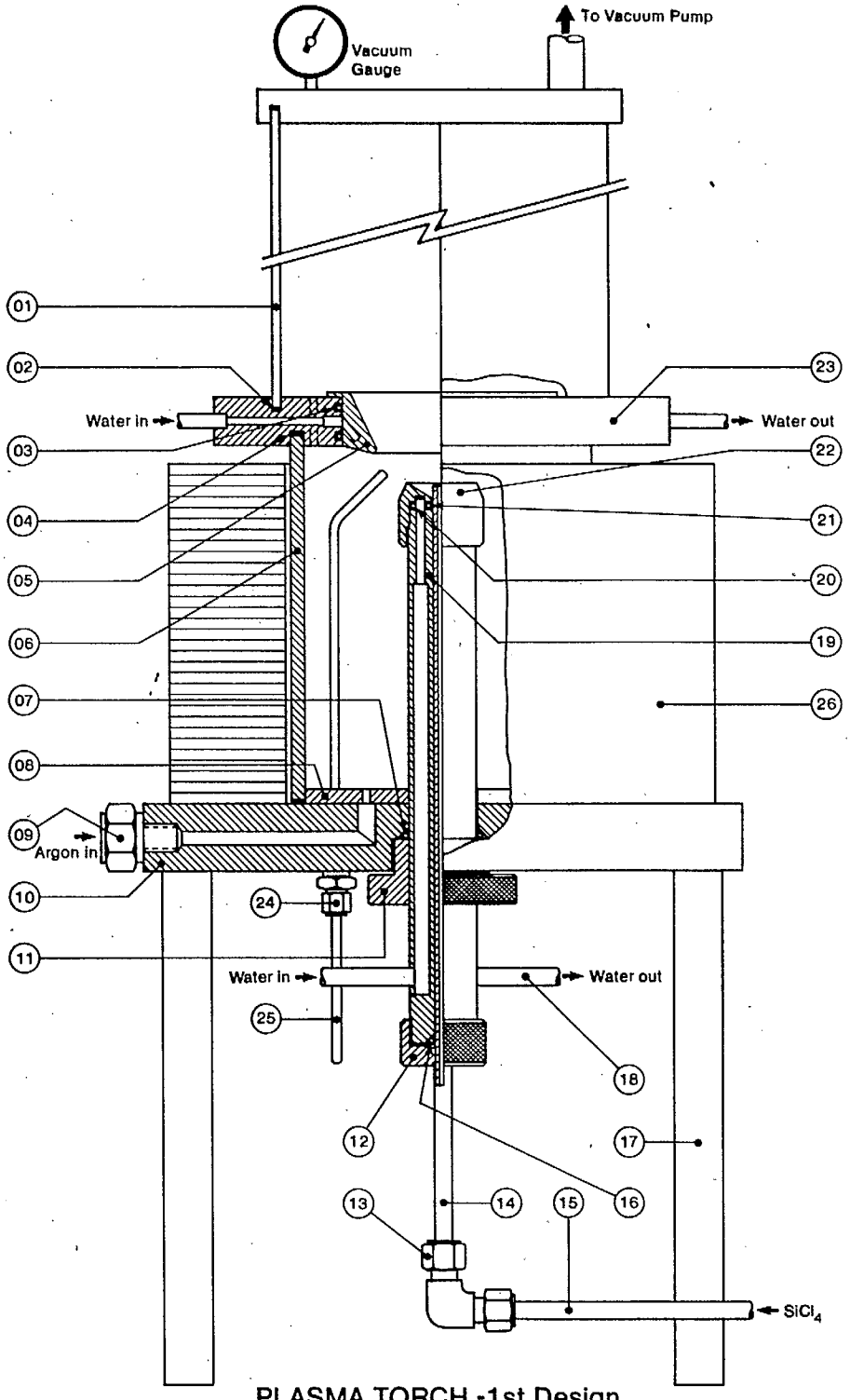

PLASMA TORCH -1st Design

Parts List

No.	Name	Description	Qu./ Unit		No.	Name	Description	Qu./ Unit	
01	Shield	Quartz(128"OD•123"ID•12"L)	1		14	Ceramic Tube	Mullite MXRS-0142 12"L	1	Std.
02	Gasket	Rubber	2		15	Teflon Tube	9038-008-004 Johnston	1	Std.
03	O-Ring	# 041	2	Std.	16	O-Ring	# 10	1	Std.
04	Gasket	Rubber	2		17	Support	Aluminum	4	
05	Anode	Copper	1		18	Copper Tube	¼" OD	4	Std.
06	Shield	Mullite 4½" OD•4⅛" ID	1	Std.	19	Cathode Cooler	Brass	1	
07	O-Ring	# 120	1	Std.	20	O-Ring	# 19	1	Std.
08	Gas Spread	Perspex	1		21	O-Ring	# 11	1	Std.
09	O-Seal Connector	B-400-1-OR Swagelok	1	Std.	22	Cathode	Tungsten	1	
10	Base	Perspex	1		23	Anode Cooler	Brass	1	
11	Sealing Nut	Aluminum	1		24	O-Seal Connector	B-200-1-OR Swagelok	1	Std.
12	Sealing Nut	Aluminum	1	Std.	25	Spark Electrode	Tungsten Rod ⅛" dia.	1	
13	Union Elbow	T-400-9 Swagelok	1	Std.	26	Electro-Magnet		1	

FIG. 1. Schematic cross-sectional diagram of first Magnetically Stabilized Plasma Torch design.

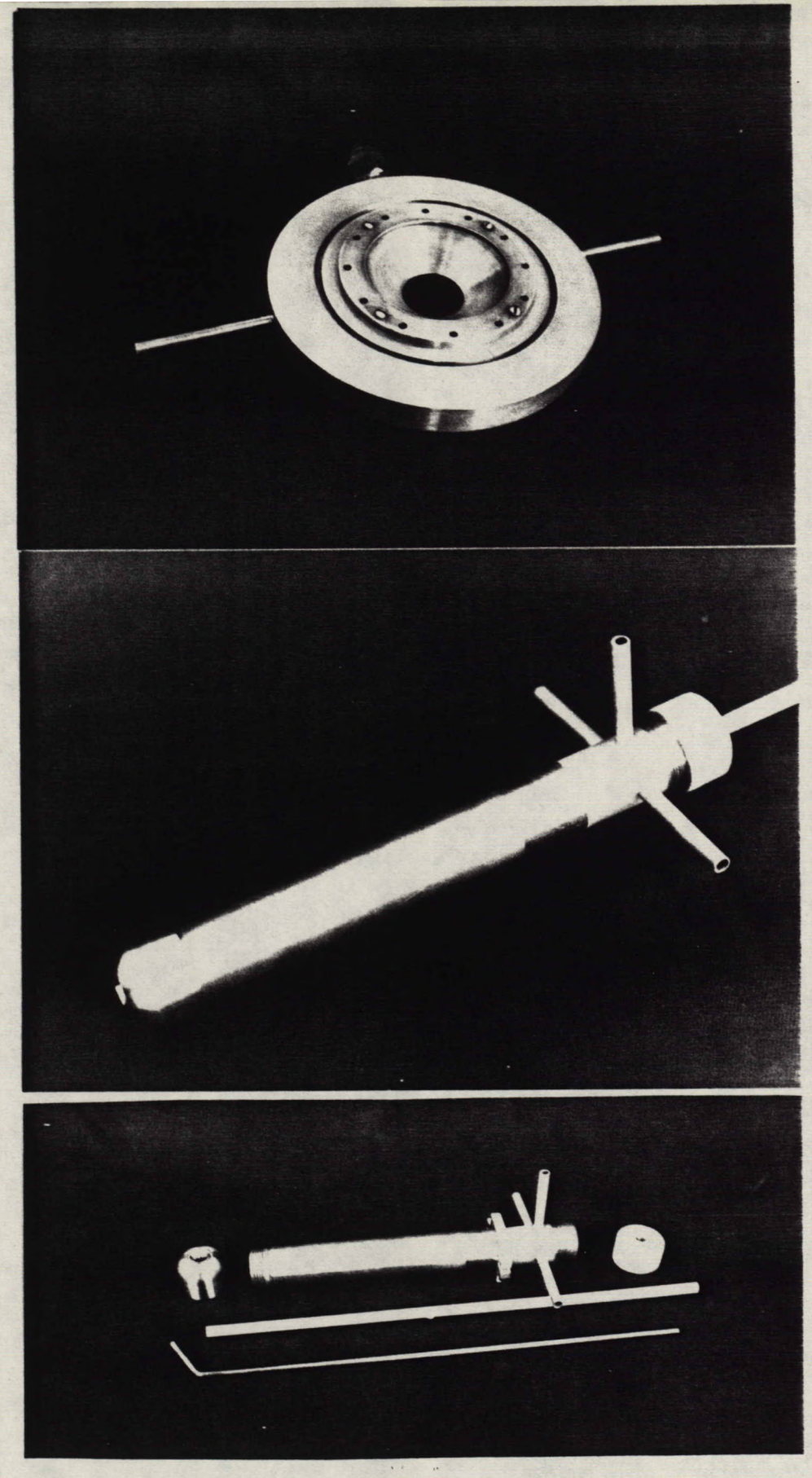

FIG. 2. Photos of plasma torch component anode and electrode parts dissassembled.

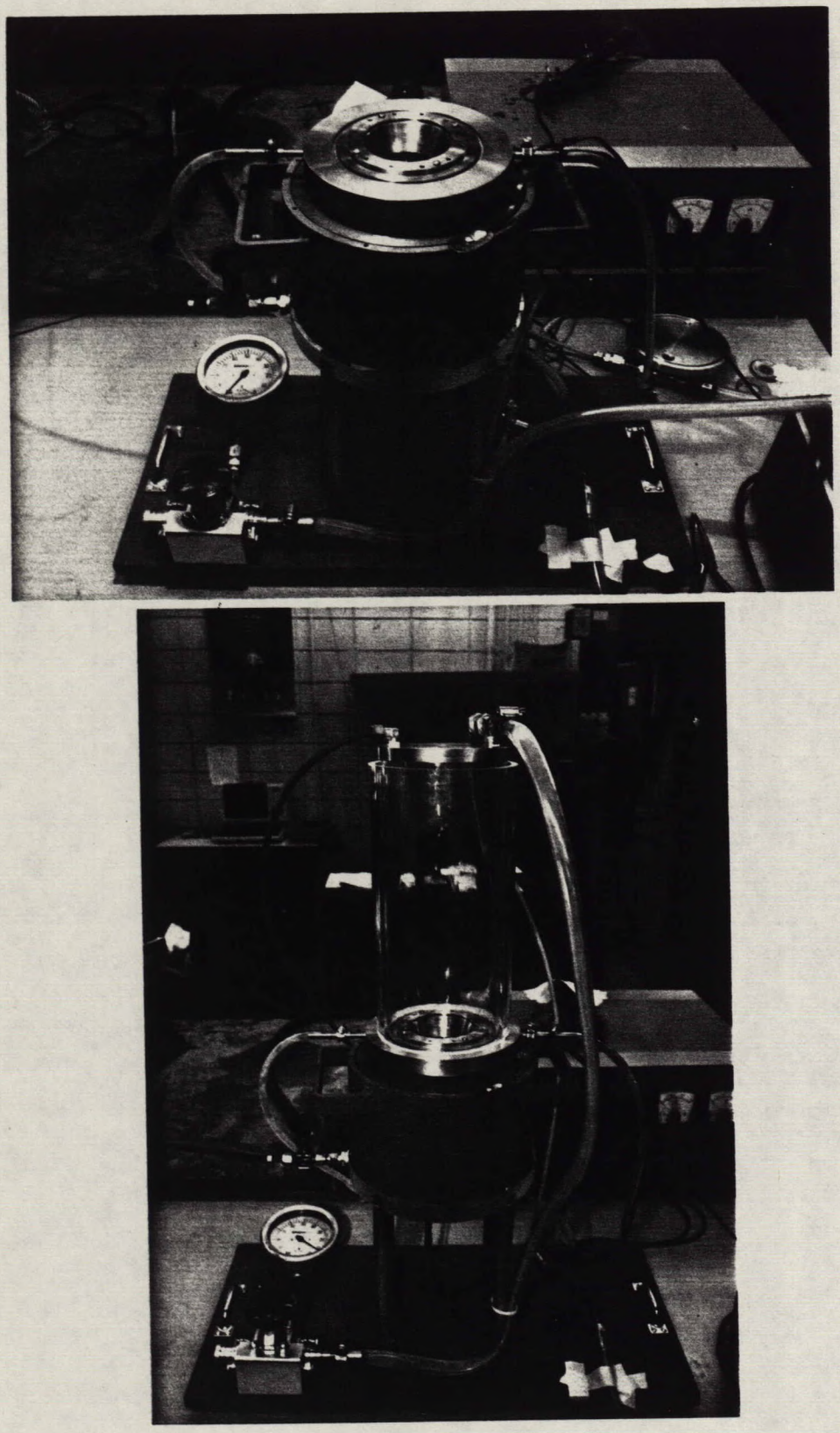

FIG. 3. Photos of plasma torch with component parts assembled.

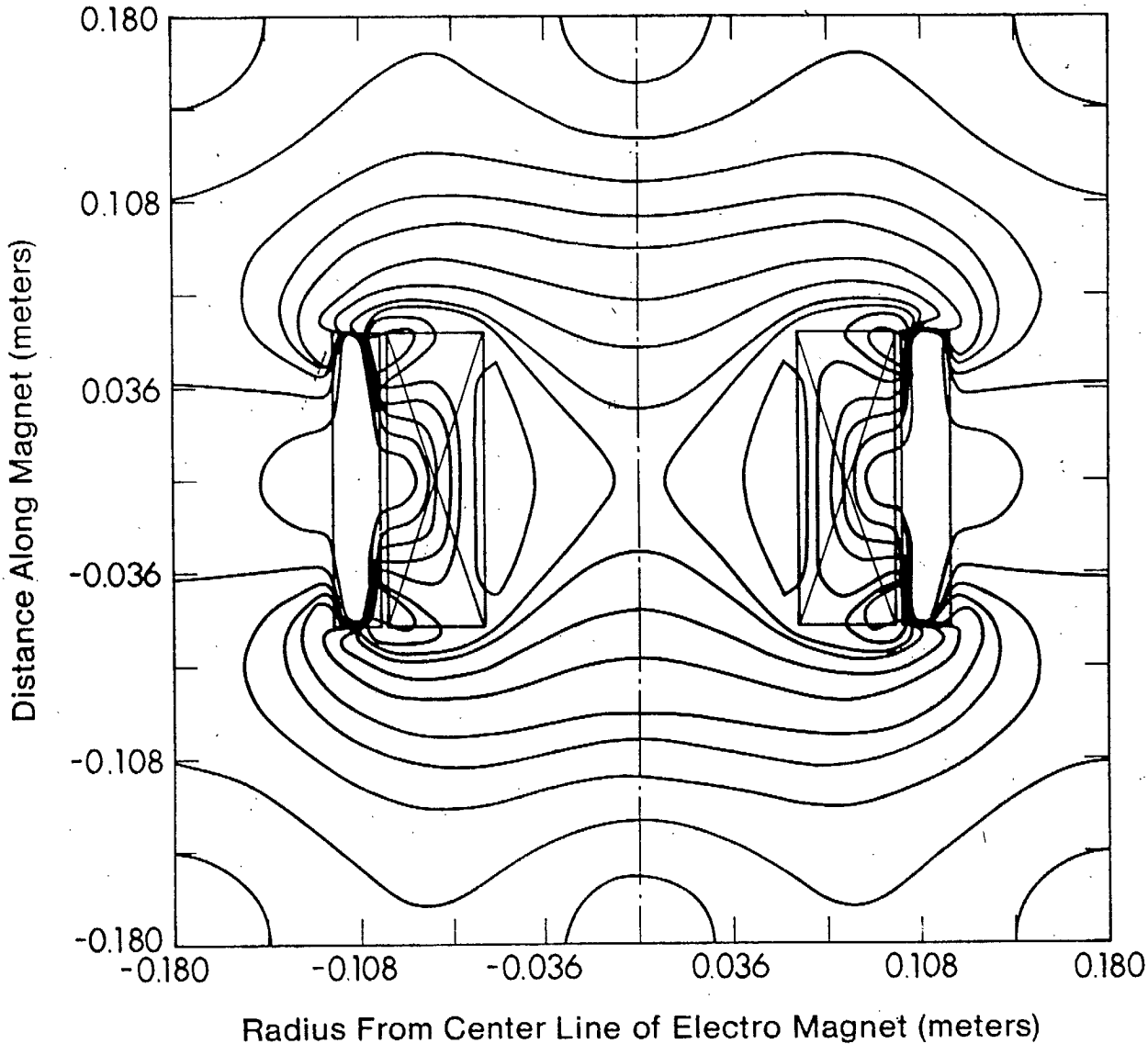

FIG. 4. Computer generated magnetic equipotentials for solenoid used.

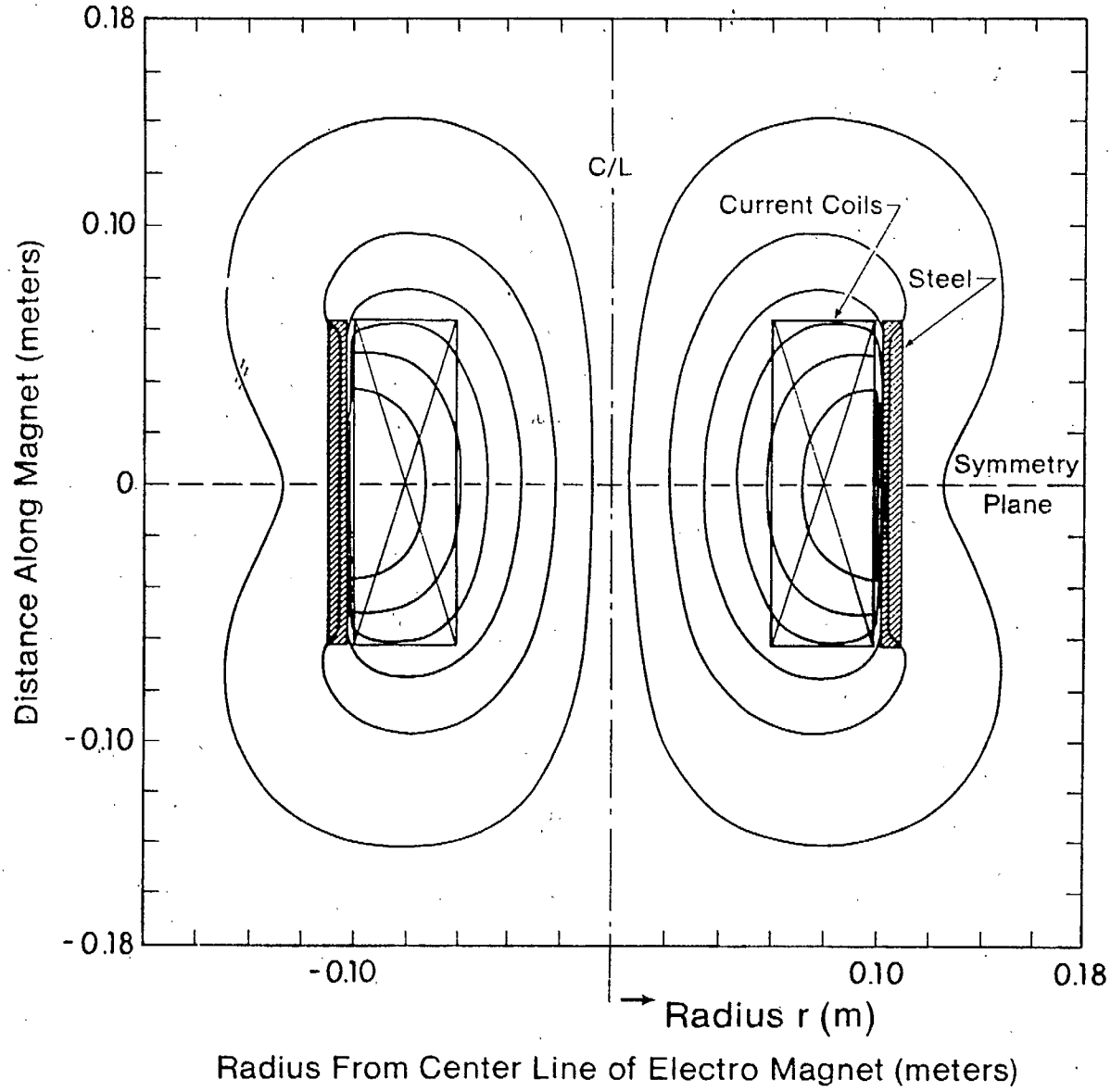

FIG. 5. Magnetic field profile obtained from "Potent" Code.

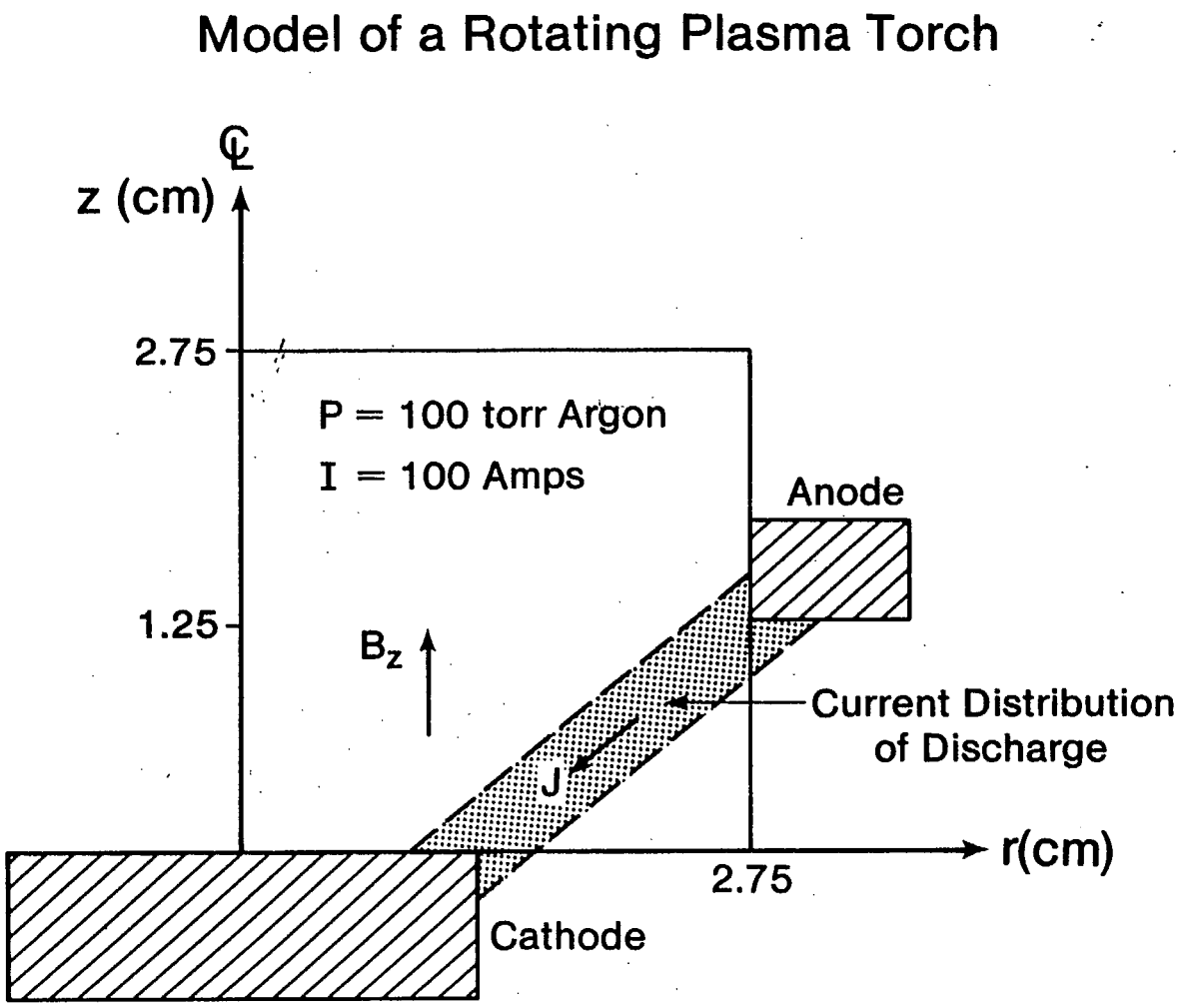

FIG. 6. Geometrical model used for computer simulation studies.

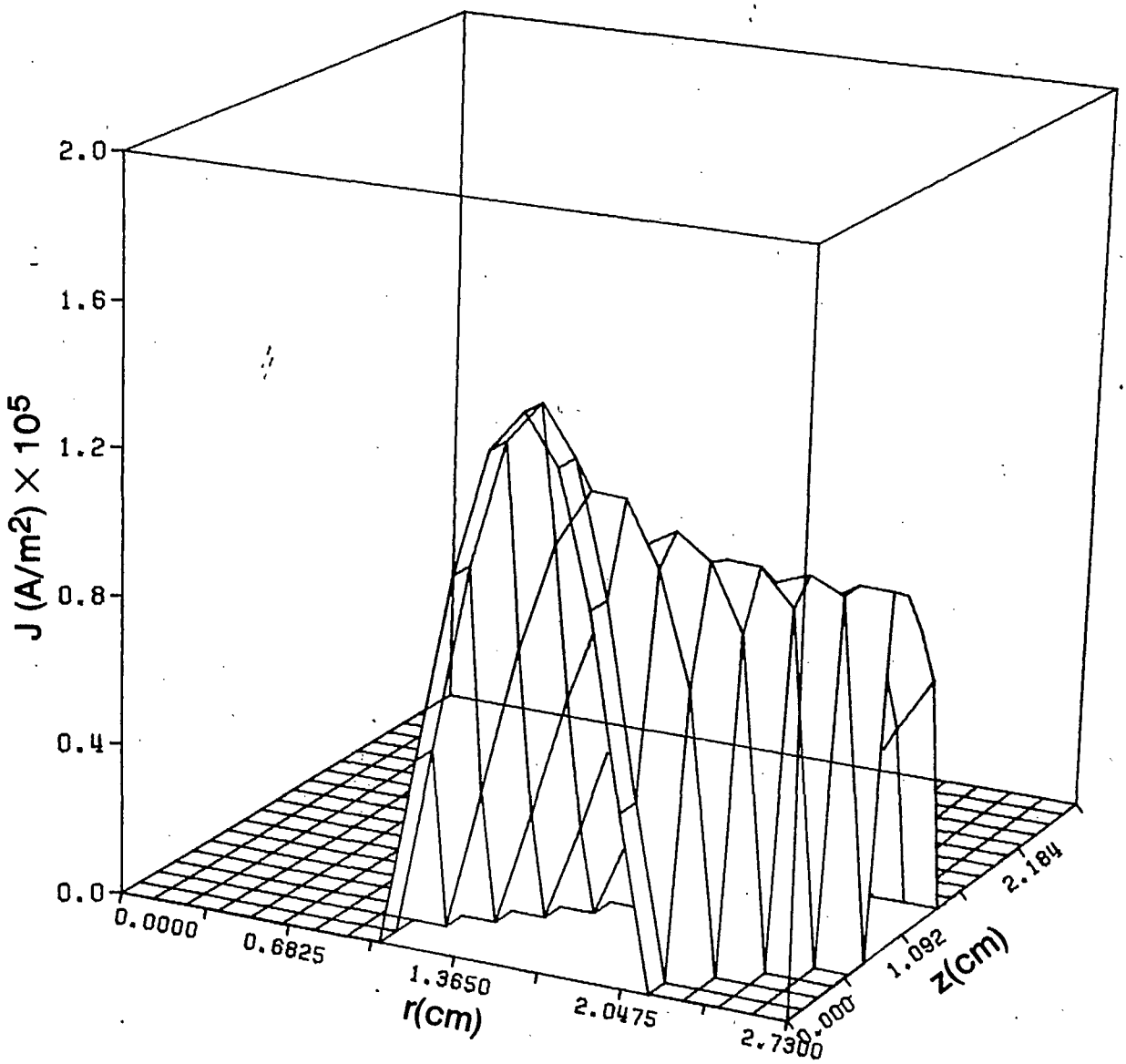

FIG. 7. Current density profile used in simulation studies

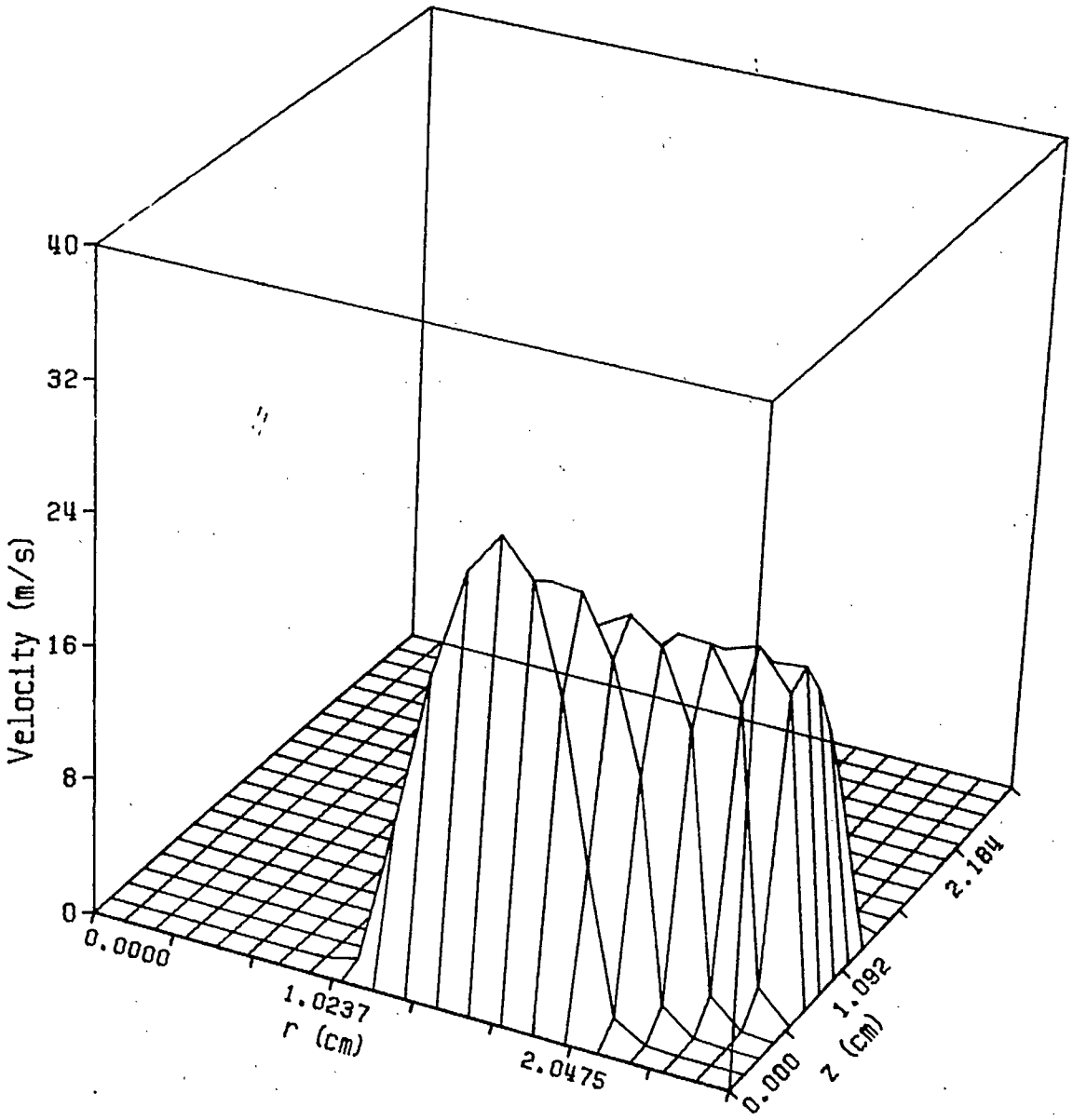

FIG. 8. Computer simulation of transient plasma rotational velocity distribution, after a running time of 100 microseconds.

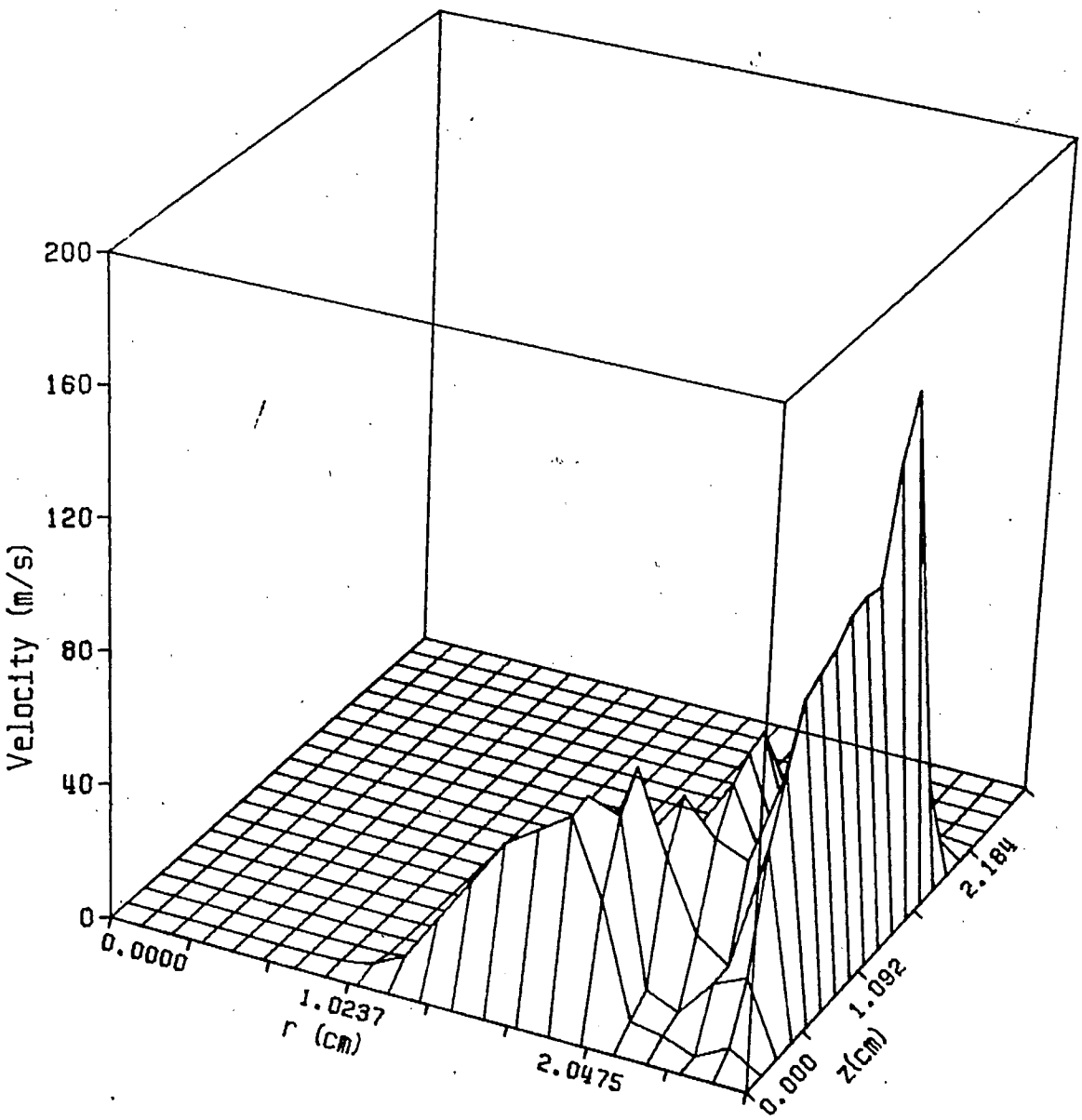

FIG. 9. Computer simulation of steady state plasma rotational velocity distribution.

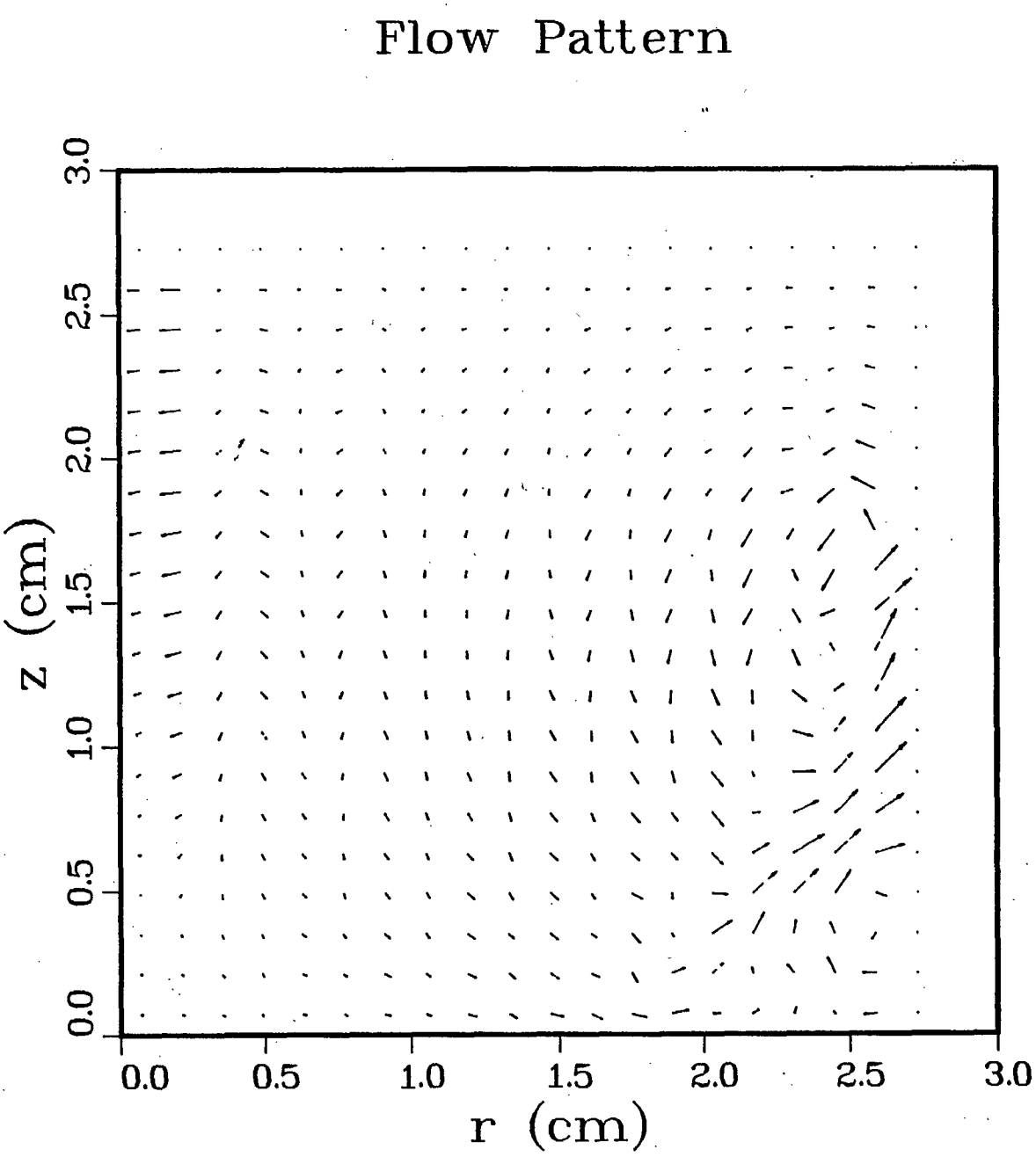

FIG. 10. Transient secondary gas flow in plasma torch.

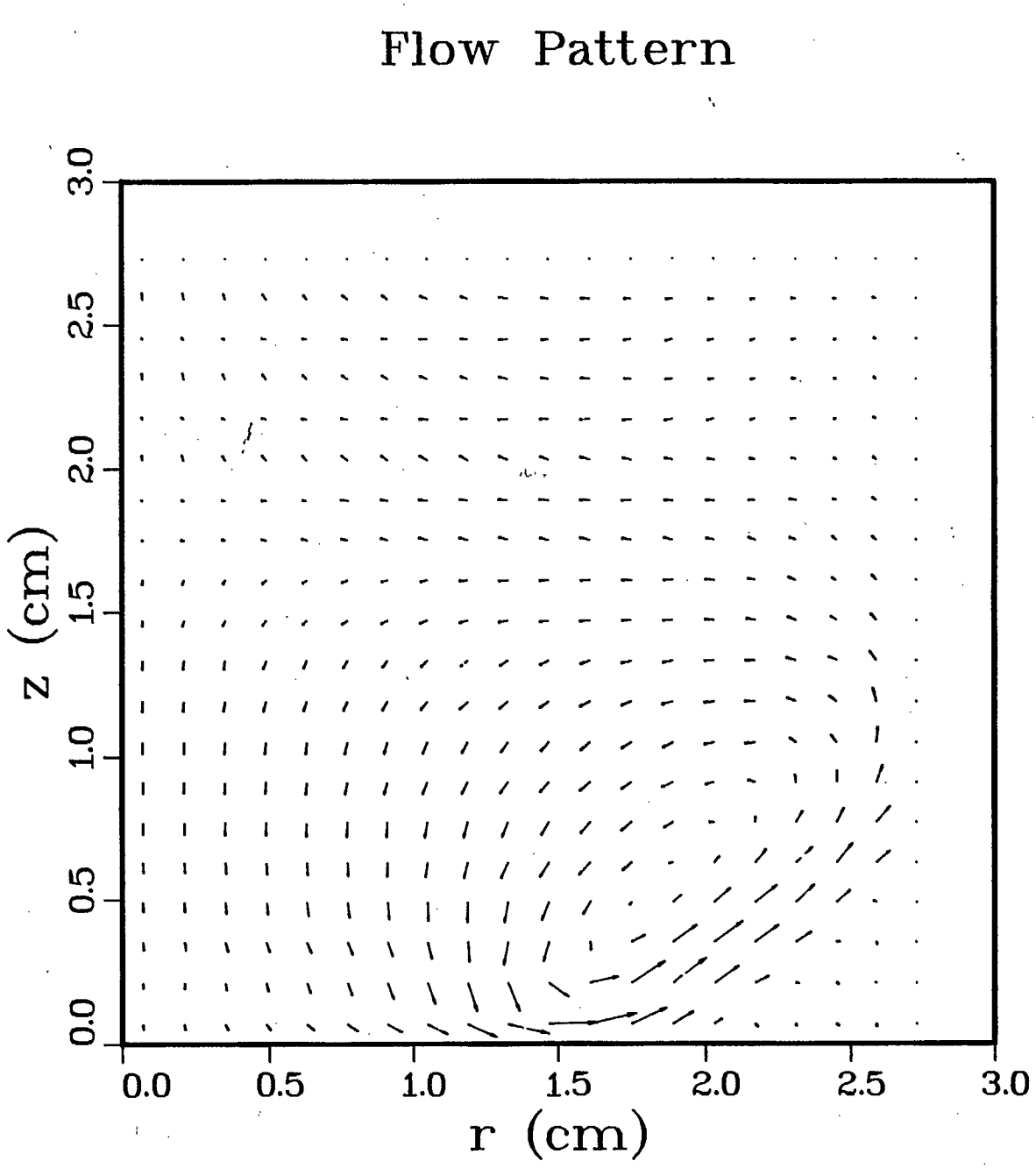

FIG. 11. Steady state scondary gas flow developed in plasma torch, showing mixing effect.

FIG. 12. Photo of operating plasma torch.

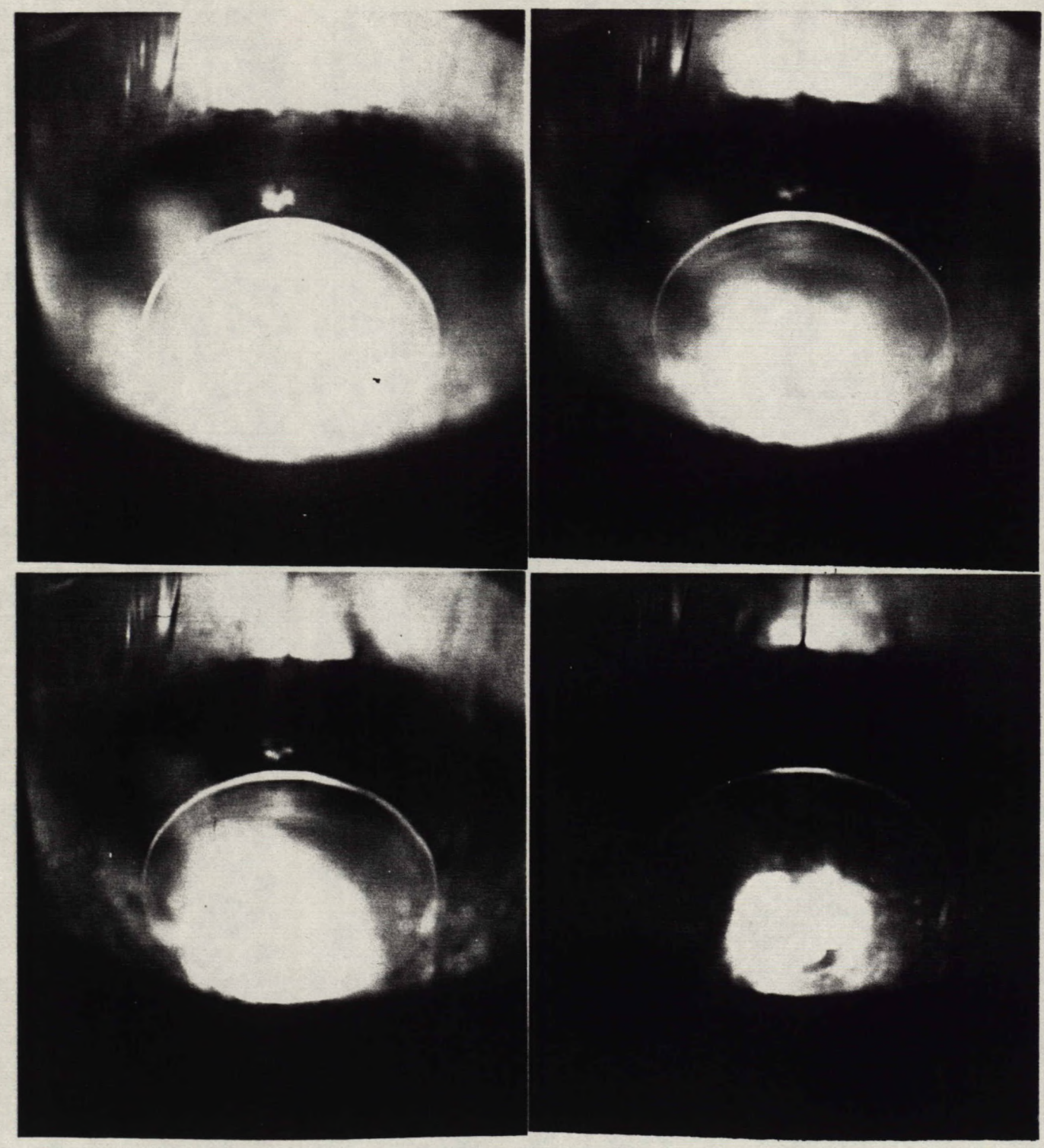

FIG. 13. Photos of rotating plasma taken at 1/1000 of a second and with variable density bandpass optical filter.

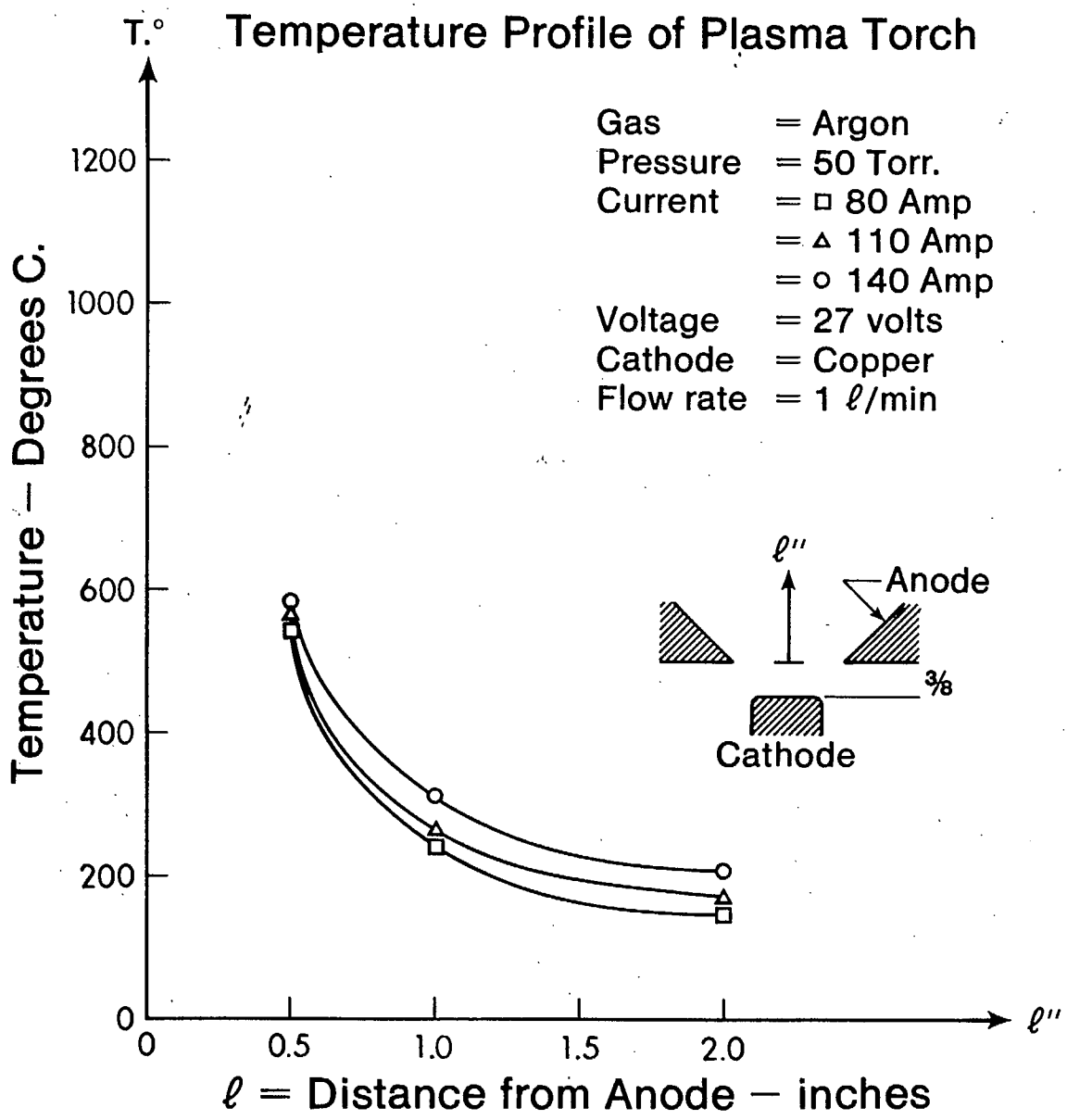

FIG. 14. Temperature profile of plasma torch as a function of plasma current for 50 Torr Argon gas.

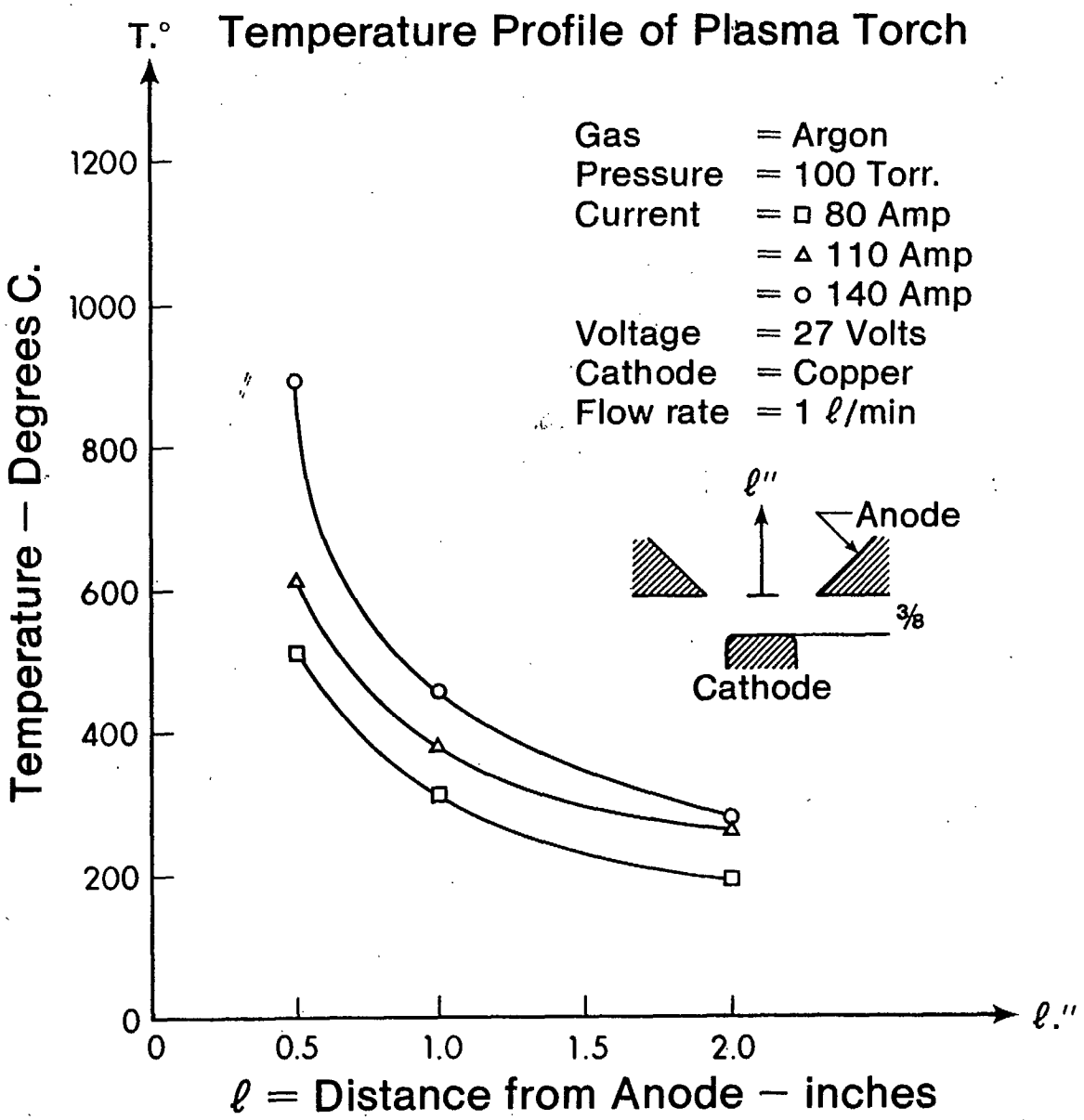

FIG. 15. Temperature profile of plasma torch as a function of plasma current for 100 Torr Argon gas.

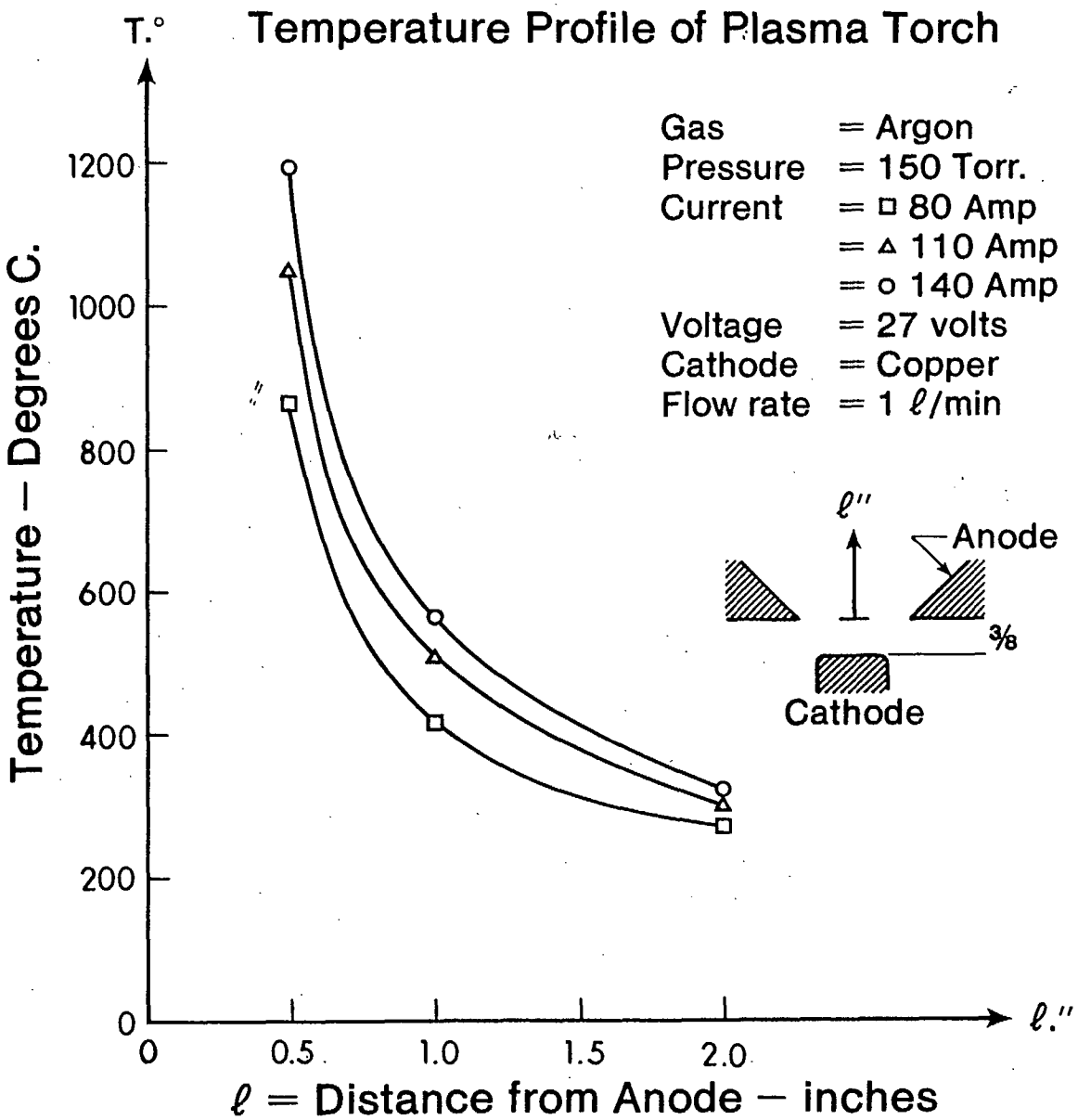

FIG. 16. Temperature profile of plasma torch as a function of plasma current for 150 Torr Argon gas.

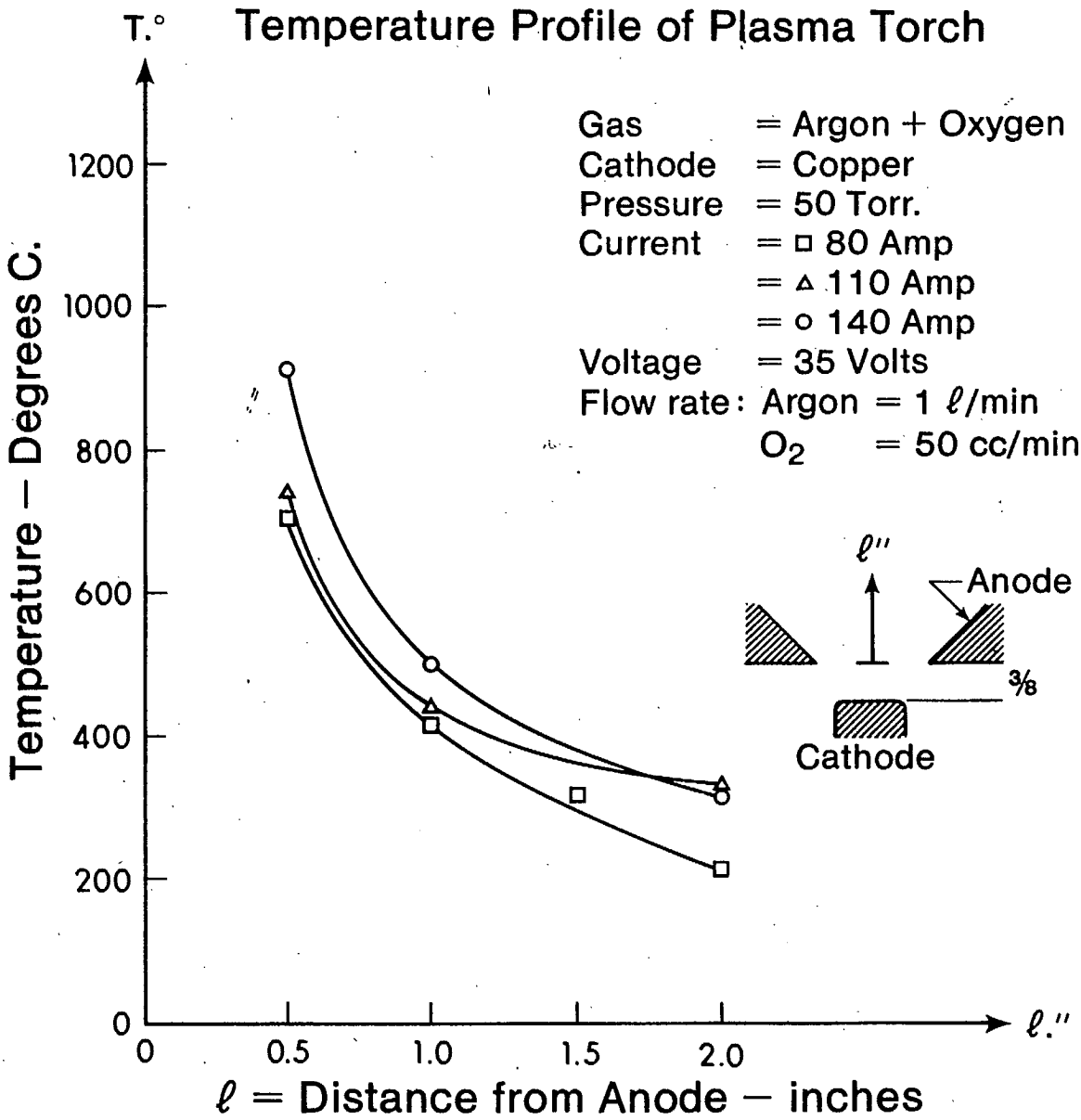

FIG. 17. Temperature profile of plasma torch as a function of plasma current for 50 Torr Argon and Oxygen gas.

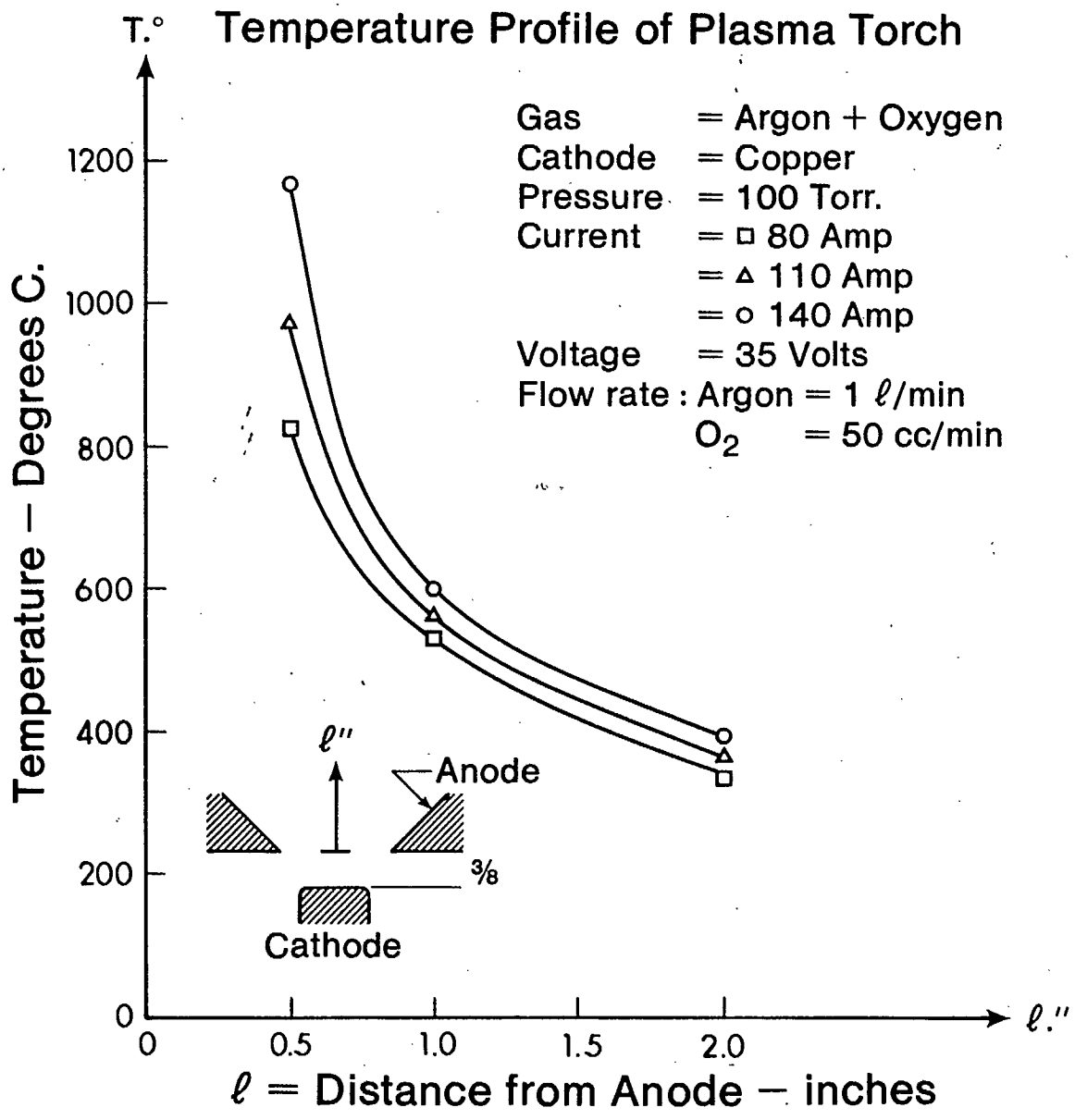

FIG. 18. Temperature profile of plasma torch as a function of plasma current for 100 Torr Argon and Oxygen gas.

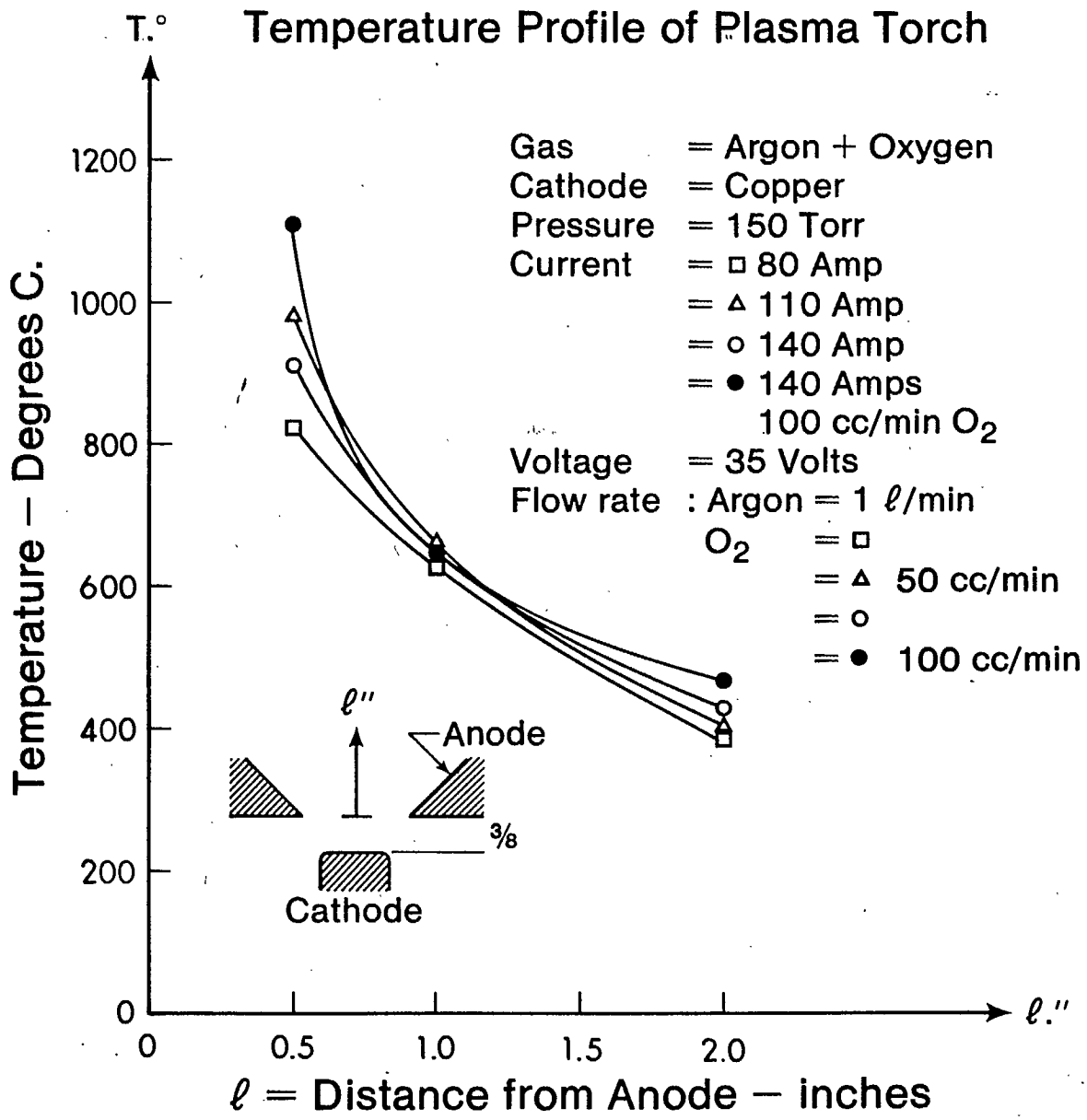

FIG. 19. Temperature profile of plasma torch as a function of plasma current for 150 Torr Argon and Oxygen gas.

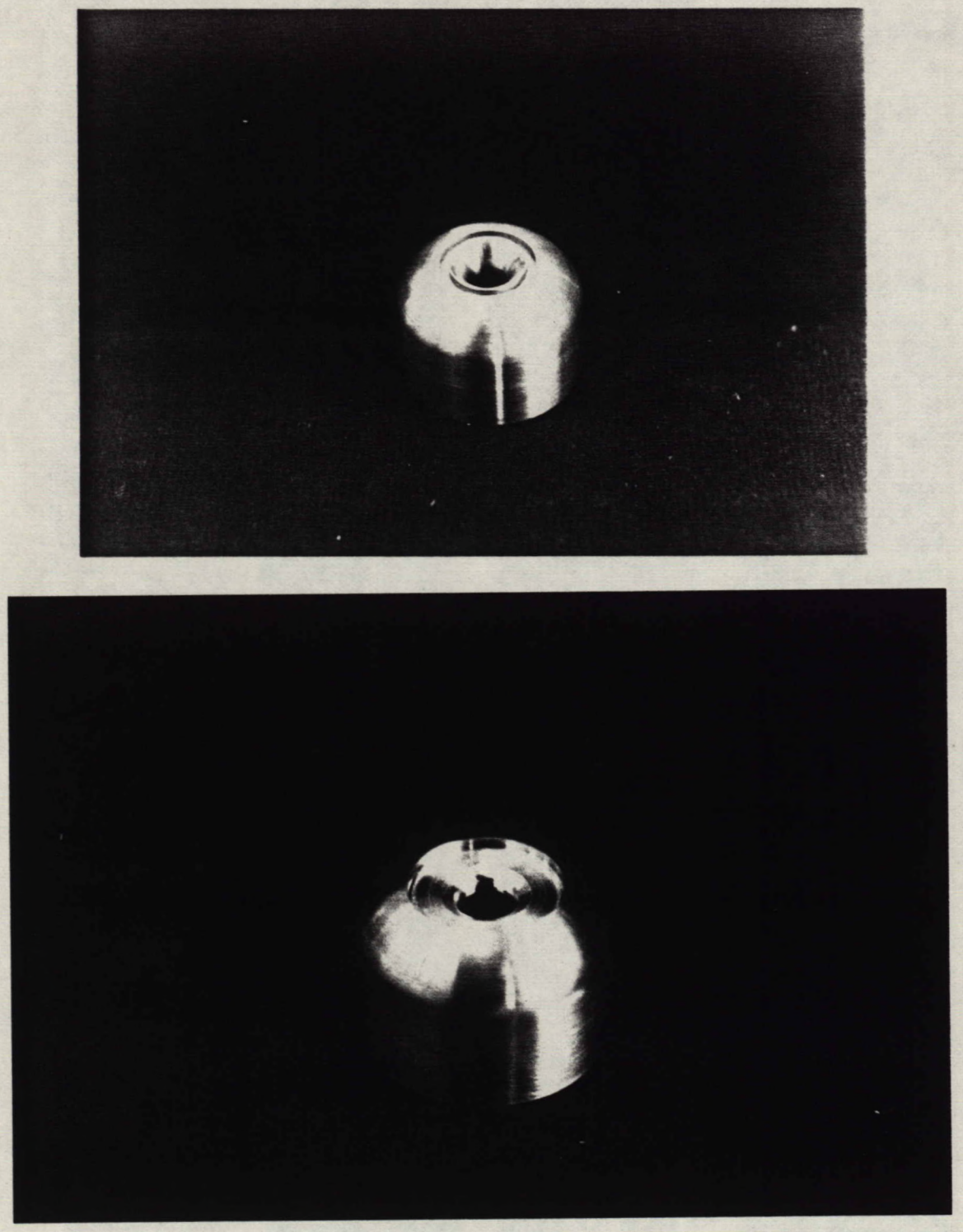

FIG. 20. Photos of hollow cathodes tested.

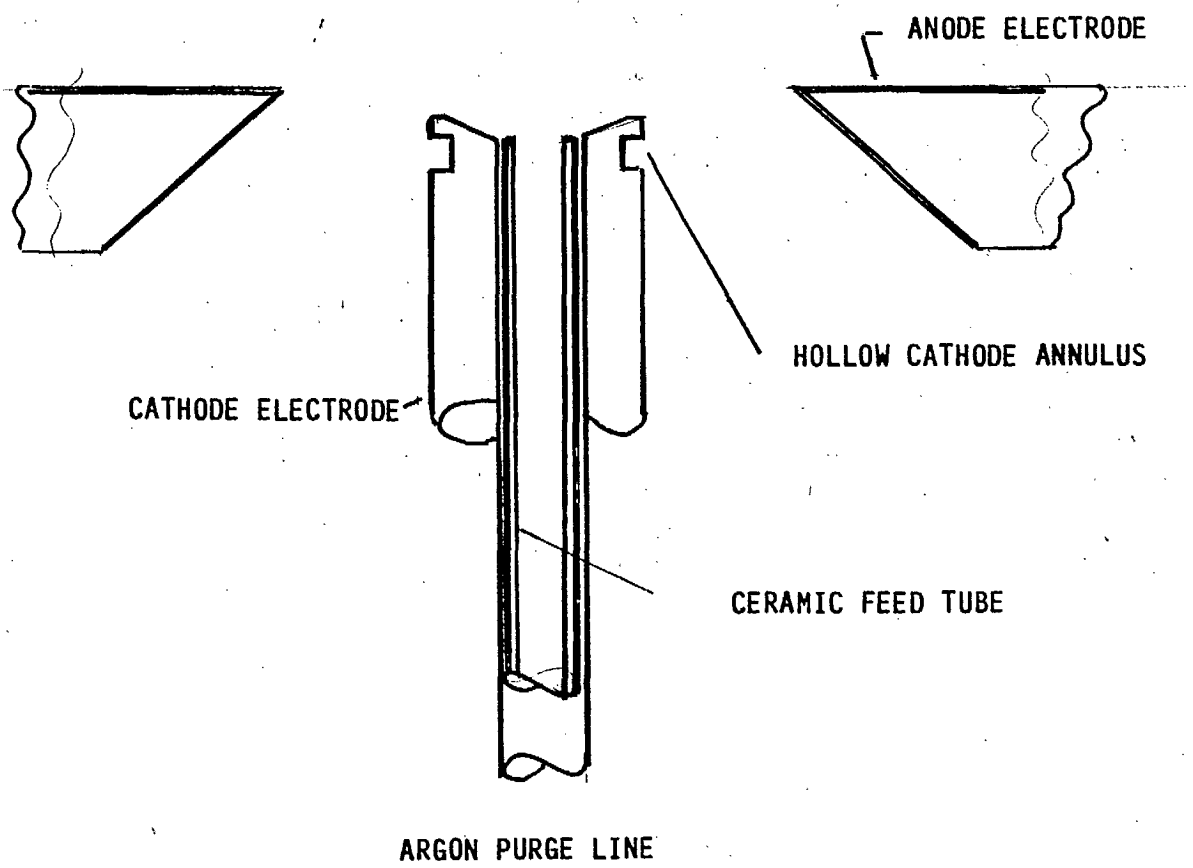

FIG. 21. Drawing of proposed hollow cathode design to reduce sputtering effect.

APPENDIX A

Investigative Report on:

PLASMA ASSISTED CHEMICAL VAPOR DEPOSITION OF VITREOUS SILICON DIOXIDE

For:

Dr. H. H. Seguin

Department of Electrical Engineering

University of Alberta

By:

Darleen O'Shea

Research Associate

Date:

January, 1984

INTRODUCTION

The object of this study is to develop a plasma torch system to transform liquid silicon tetrachloride into vitreous silicon dioxide. The silicon dioxide will then be drawn into a fibre to be used in fibre optics. The reaction to produce silicon dioxide from silicon tetrachloride requires high temperatures in the area of 1200° - 1500°C. A plasma torch provides quick thermal reactions for materials with high melting temperatures.

The first stage of this study involves the design, construction and operation of a plasma torch. A plasma torch is a device designed to heat gases to very high temperatures by using the high conductivity of a ionized gas. Conventional plasma torches require electrodes to supply energy to the gas. They operate on direct current (dc) carried by thermionic or high-field cathodes and water cooled anodes (1). Because of the high conductivity of partially ionized gas (e.g. conductivity of argon at 15,000°K is about $120(\text{ohm-cm})^{-1}$), these torches are characterized by a high current (100-1000 amps) and a low voltage (10-100V). An axial magnetic field may be added to rapidly rotate the plasma, thereby increasing heat output and stabilizing the plasma. Electrode-coupled dc plasma torches are limited in their operation because the electrodes are subject to attack by such gases as oxygen and nitrogen.

An induction-coupled plasma torch heats gases to 10,000°-20,000°K using a standard radio-frequency (rf) power supply (1). Plasma is initiated within the rf field (usually a coil) by a heated carbon rod, tungsten wire or a tesla coil. The heating of plasma gases in the vicinity of the hot rod lowers the breakdown potential of the gases sufficiently for the plasma to be established in the presence of the high rf field. An rf induction plasma torch is typically operated at a maximum power output of 10 kW and a frequency of 4 Mc. Since there are no electrodes, this torch can be operated in inert, oxidizing or

reducing gases, i.e. Ar, He, N_2, O_2 and H_2. Argon is most commonly used as a starting plasma gas as it has low heat capacity and ionization potential. The introduction of gases or powders is simpler because the electrode is absent. It should be noted that the induction-coupled (rf) plasma torch will not be used in this project; other than for comparative purposes.

The second stage of this study deals with the chemical vapor deposition (CVD) of vitreous silicon dioxide from liquid silicon tetrachloride. Simply put, CVD is the condensation of elements or compounds from the vapor state to form solid deposits. These deposits are formed by chemical reactions which take place on, at, or near the deposition surface. There are a number of reactions that describe the transformation of silicon tetrachloride into silicon dioxide. These are discussed in the section on CVD.

Following the dicussion on CVD is a description of the silicon dioxide growth process. The silicon dioxide is to be deposited and grown as a glass preform or "boule". The growing boule is pulled away from the plasma flame at the same rate as it is growing towards the flame. Consequently, the growth front is always at the same location within the plasma flame.

Since the silicon dioxide boule is to be used for fibre optics, it must be free of undesired contaminants. Sources of contaminants include: the reactants, electrodes, gases, and apparatus materials. Therefore, all gases and reactants must be purified and apparatus materials must be inert at high temperatures. Impurities within a silicon dioxide fibre affect certain glass properties, e.g. refractive index, electrical conductivity, and viscosity.

PLASMA TORCH DESIGN (2,3)

A basic plasma torch consists of three concentric quartz tubes with three independent gas flows (see figures 1(3) and 2(2)). A large diameter outer tube

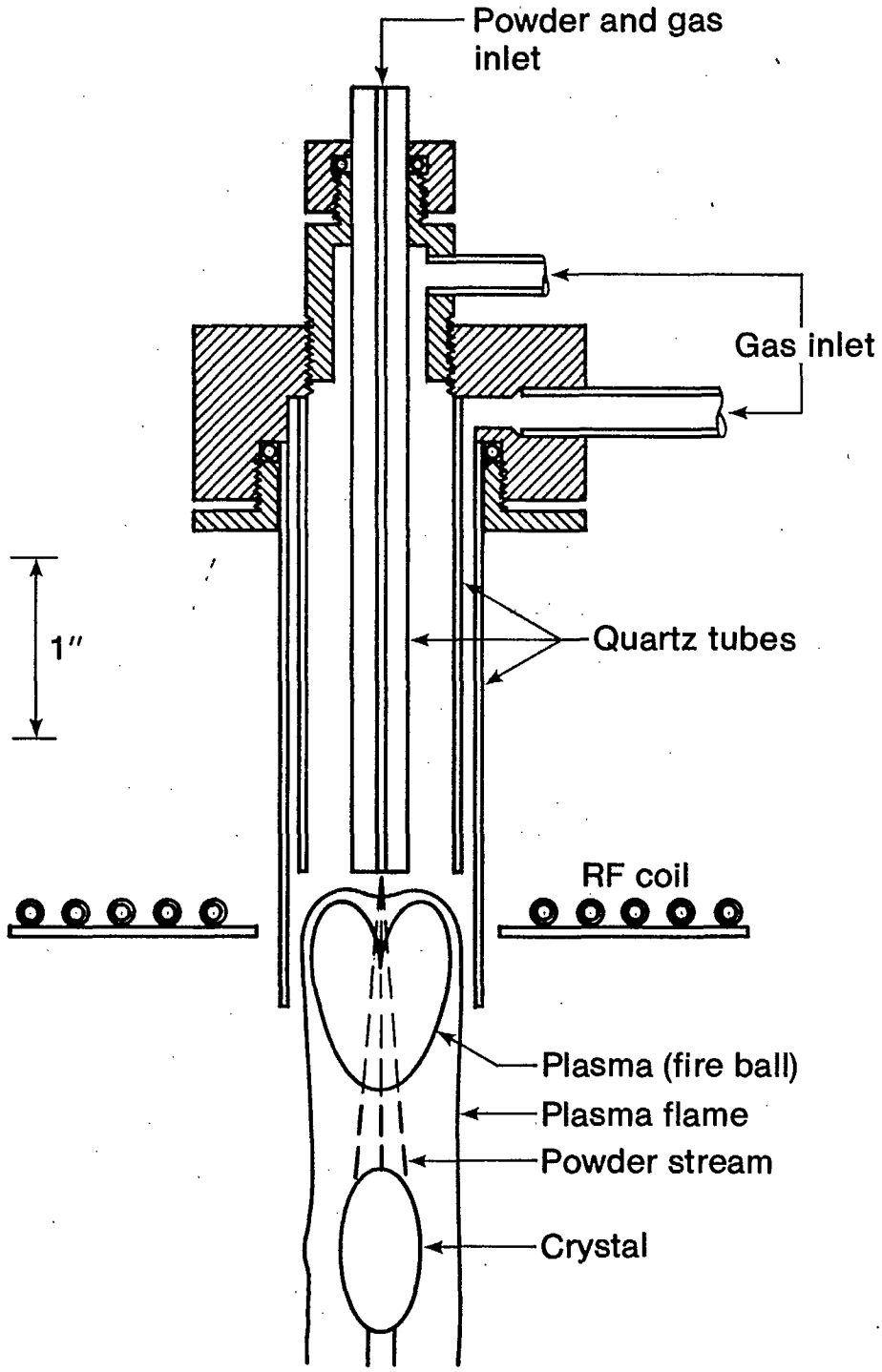

Fig. 1. Modification of induction-coupled plasma torch for crystal growth.

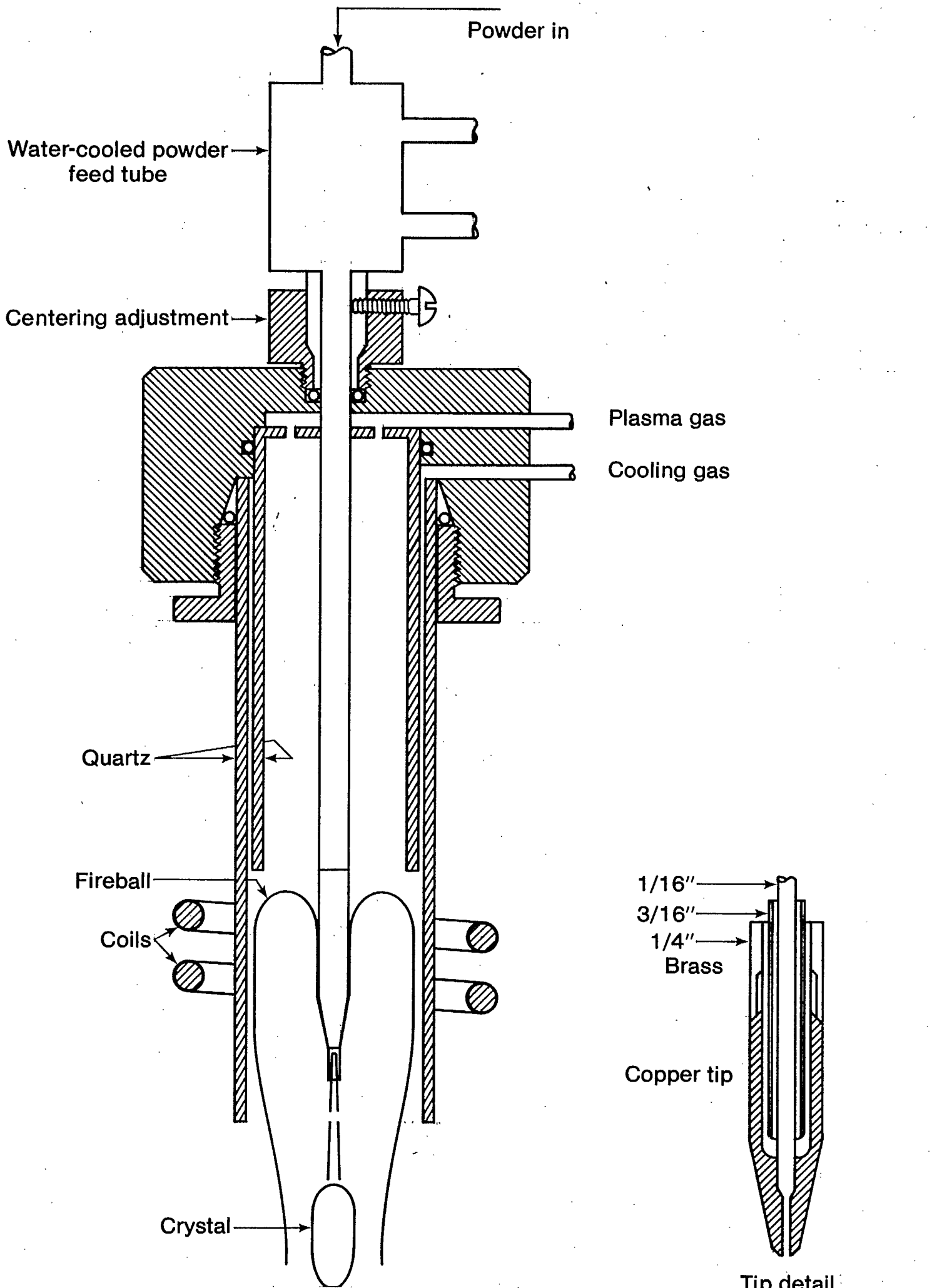
Powder in
Water-cooled powder feed tube
Centering adjustment
Plasma gas
Cooling gas
Quartz
Fireball
Coils
Crystal
1/16″
3/16″
1/4″
Brass
Copper tip
Tip detail

forms a nozzle to shape the plasma into a long laminar flame. Gas flow at high velocity between this tube and the intermediate tube keeps the outer tube from melting and to create recirculation in the plasma region. Gas which flows at low velocity through the intermediate tube forms the main body of the plasma. Finally, gas flowing at high velocity through the center tube carries the powder or gaseous material through the plasma to the molten cap of the growing boule.

Gases or powders introduced into the center of the plasma should not be done tangentially as it creates an upstream flow. The probe introducing the gases or powders is typically one-quarter (1/4) inch outside diameter and water cooled. The probe can terminate in the fireball or pass right through the plasma and inject the reactant into the tailflame. Figure 2 shows in detail, the probe and tip in the plasma. This is an advantage for solids which may evaporate at the highest temperature, or where it is desired to maintain a composition beyond the plasma which would generate too much heat if introduced into the fireball. The cooling gas is introduced along the edge of the intermediate tube which stops short of the plasma. This tube must be accurately centered because it determines the symmetry of the plasma and keeps the plasma from touching the walls. Although the torch system as shown in figures 1 and 2 is for rf induction coupled plasma, it can be modified for dc electrode plasma.

There are two main methods for plasma generation. One method is direct current (dc) electrode-coupled heating which uses a gas sheath or magnetic field for plasma stabilization. The second method is radio-frequency (rf) induction heating which uses vortex stabilization for the plasma.

D. C. PLASMA TORCH (4)

A dc plasma torch operates under the condition where a dc arc is formed between electrodes. Rapid gas flow through the arc directs the plasma ahead of the electrodes. It is common for dc plasma torches to run at tens or hundreds

of volts and currents of several hundred to several thousand amperes. Plasma stabilization is extremely difficult. At worst, the plasma blows from between the electrodes and is extinguished. At best, the plasma tends to fluctuate in intensity and wander in position. Plasma stabilization can be obtained by using gas sheaths or magnetic fields.

Controlling the velocity and direction of gases passing between the electrodes helps to stabilize the plasma. In the dc plasma torch in figure 3, the arc goes from a tungsten cathode to a hollow water cooled anode. The arc remains within the chamber and is prevented from striking the wall by a sheath of gas that is considerably larger than the wall thickness. D.C. plasma torches can be operated in inert, reducing and oxidizing atmospheres. However, oxidizing atmospheres create difficulties in maintaining an arc for any length of time. The electrodes are subject to oxide attack. Furthermore, the self-induced magnetic field exerts a force on the conducting gas between the electrodes.

Magnetic Stabilization (2)

Location and motion of the arc discharge can be controlled by a self-induced or externally applied magnetic field. For the induced-field configuration the arc discharge is caused to rotate by interaction with an axial-magnetic field produced by an external solenoid. Figure 4 shows magnetic stabilization by induced and applied magnetic fields. In this case the low enthalpy (3500 BTU/lb) capability is associated with poor coupling between the discharge and the gas flow. High currents of 10,000-20,000 amperes and 1000 volts in the induced magnetic field arc required to rotate the discharge.

A rotating arc plasma jet has been developed by Mahawili and Weinberg (5) which uses a magnetic field coil (see figure 5). A dc arc is struck between a central tungsten cathode and a circumferential copper anode. Reactants are passed through this arc to form the plasma. An axial magnetic field rotates the

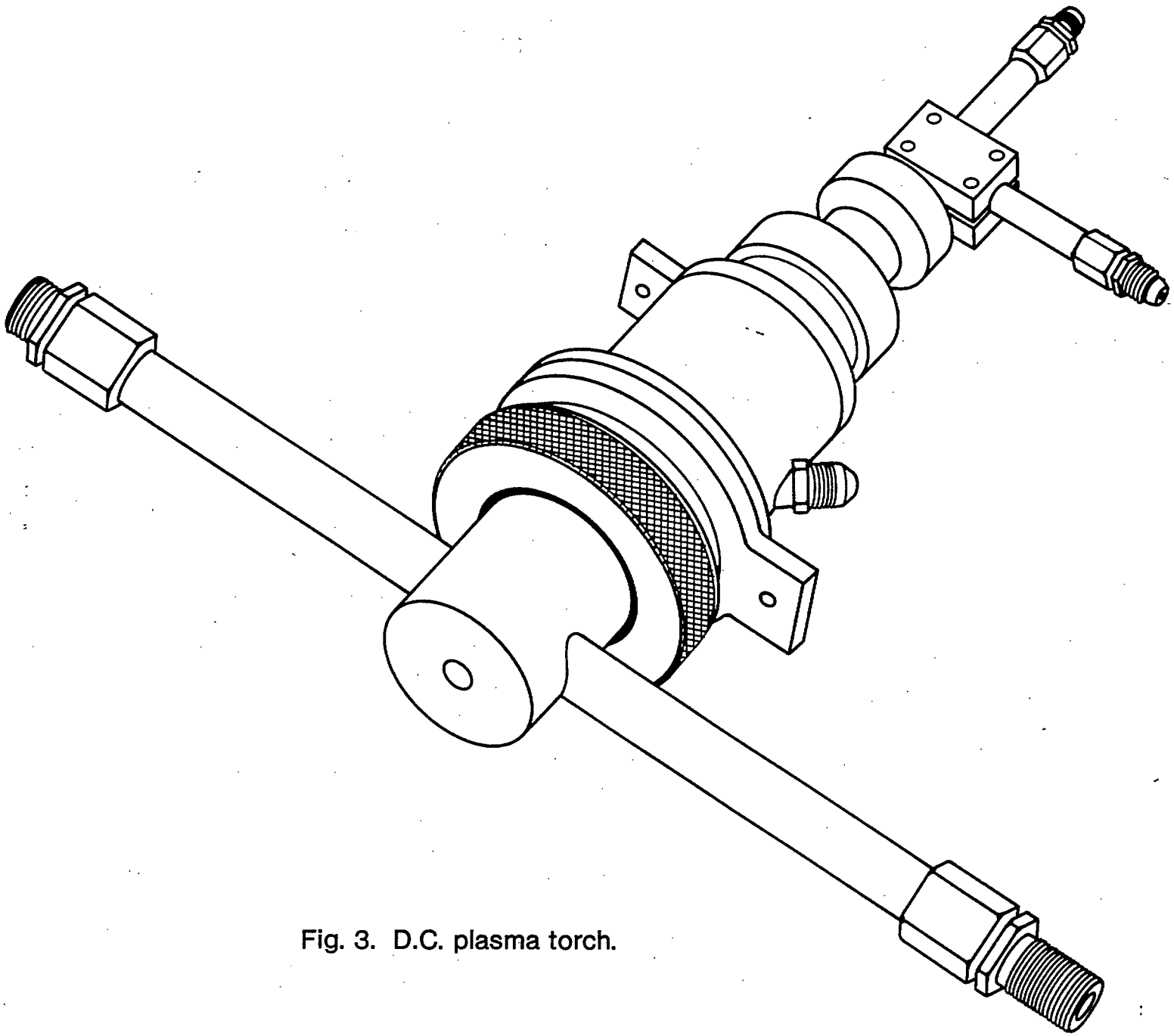

Fig. 3. D.C. plasma torch.

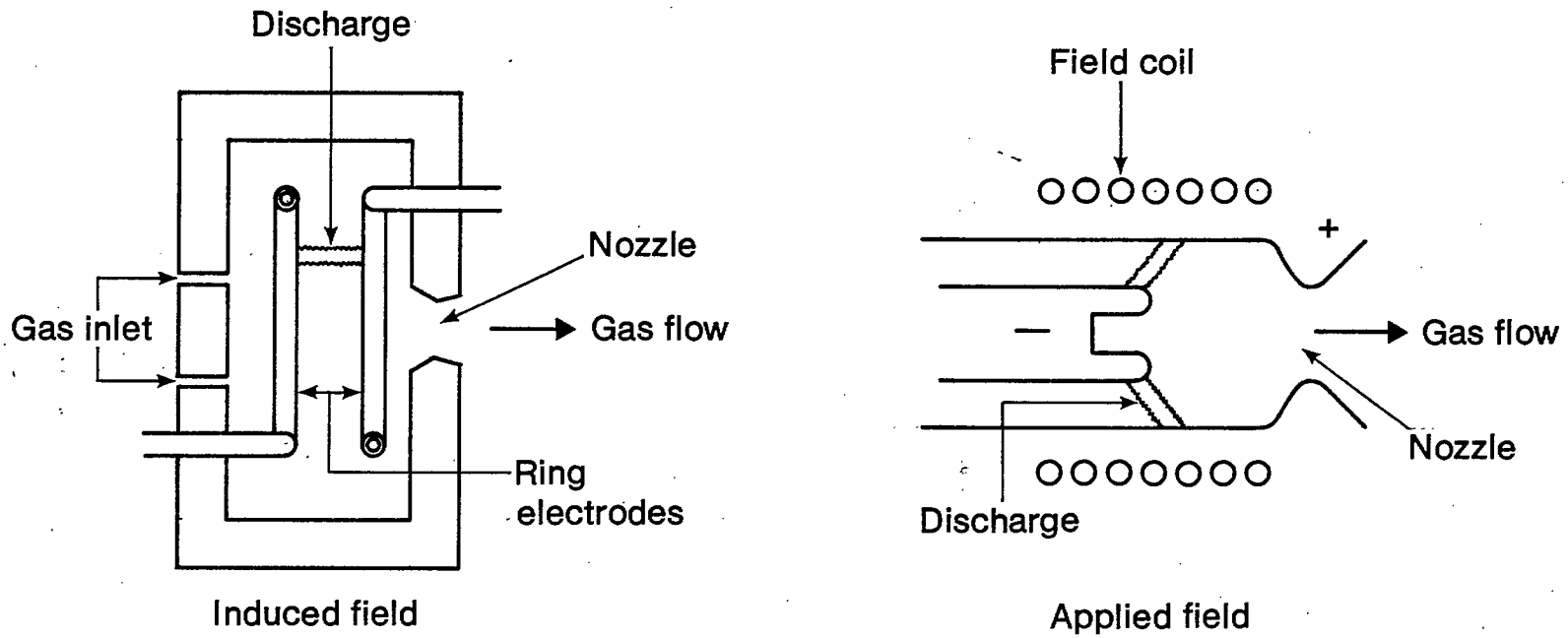

Fig. 4. Magnetic stabilization.

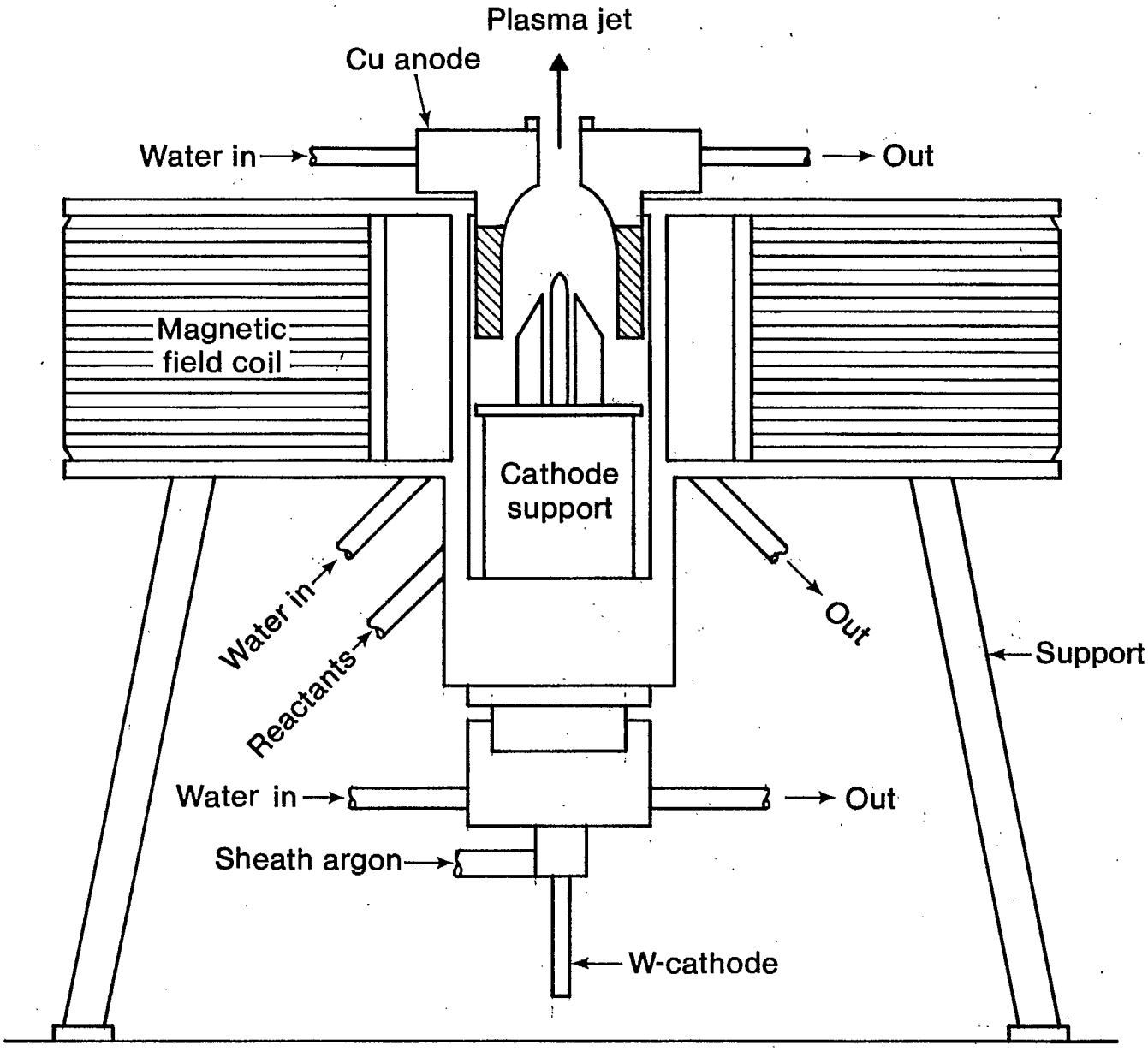

Fig. 5. Schematic of the rotating arc plasma jet.

plasma at high speeds, which is a rapid and efficient way of supplying a great deal of heat in a short distance. The axial magnetic field is produced by passing a direct current through a water cooled coil. In this case, the coil is made up of 4,200 turns of 22-awg copper wire covered with a high-temperature-resistant enamel. A small annulus surrounding the cathode allows a sheath of argon to pass over, thereby cooling the cathode and protecting it from direct chemical attack by the reactants.

RF PLASMA TORCH (2)

A second method for generating plasma is by using rf induction heating. Resistivity of a well ionized gas is about 10^{-2} ohm-cm, only a little higher than that of graphite. Therefore, the gas can be heated and maintained by currents of tens or hundreds of amperes. A simple form of an induction coupled plasma torch is viewed in figure 2 (2). An rf coil surrounds a quartz tube, 1-1½ inches diameter. Gas is introduced into the tube tangentially to provide axial stabilization. The coil, near the end of the tube, is energized by a generator with a capacity of a few kW or more, and a frequency of 4 MHz or more. Larger torch diameters with higher powers permit the use of lower frequencies, i.e. about 50 kHz. The torch is usually started in argon, the simplest gas to ionize, by inserting a metallic (i.e. tungsten) or carbon rod or using a tesla coil. Once started, it can be operated in argon or any other gas if sufficient power and cooling are available. Argon plasmas can be maintained with 2 kW, pure oxygen requires 10 kW, while hydrogen, nitrogen, and helium require as much as 20 kW power. When changing gases it may become necessary to vary the impedance matching. Also, argon and some mixtures can be operated without cooling the quartz tube, but pure diatomic gases (i.e. H_2, N_2, O_2) and helium require water cooling.

Discharge Initiation (2)

A carbon rod or tungsten wire is often used for plasma initiation. The heated tip lowers the breakdown potential and allows formation of a thermal plasma which is maintained by the rf energy. Once plasma has been initiated, the carbon rod or tungsten wire is removed. Tungsten wire has the advantage that it eliminates sparking between the metallic head and the discharge region, eliminates carbon contamination, and can be completely gas tight.

Plasmas of diatomic gases need more power than argon plasmas. Therefore, when one of these gases is added to the argon, the power must be increased. For a given composition and flow rate, the diameter of the plasma increases with the power. However, due to their thermal conductivity, diatomic plasmas tend to be more contracted than argon plasmas. Thus, the discharge can always be kept at a reasonable distance from the tube if the addition of power and the increase in flow rate of diatomic gas are synchronized. Too fast an increase of diatomic gas concentration leads to extinction of the discharge, while too fast an increase in power can cause destruction of the tube. Typical gas flow for plasma is 10-20ℓ NTP/min with a power input of 1-10kW.

Plasma Stabilization (3,4)

Plasma in rf torches is controlled by vortex stabilization. Gas flow is introduced tangentially to the circumference of the tube. The gas flows spirally down the walls and creates a low pressure area in the center, i.e. forms vortex. Some of the plasma extends farther upstream as gas flow increases. Gas flow along the walls tends to keep the plasma centered and away from the walls. At the same time, the tube walls are cooled, making it possible to operate at higher power levels.

PLASMA (2)

The plasma flame generally shows two clearly distinguished regions. In the

region of the coil there is the fireball with temperatures ranging from 10,000°-20,000° K and anywhere from a few percent to full ionization. Below this is the plasma-flame region, generally much less luminous in the permanent gases but becoming quite luminous when various materials with lower ionization potentials are injected into the plasma. Plasma is generally very quiet, except for any audio frequency variations in the power supply being broadcast by it. A well-filtered power supply will be almost inaudible, but a thyratron power control will roar.

COMPARISON OF ELECTRODE AND INDUCTION PLASMA GENERATION (2)

When comparing electrode generated plasma with induction coupled plasma, many interesting characteristics can be found. One of the main problems with electrode generated plasma is the chemical compatibility and cooling of the plasma by the electrodes. The electrodes are often situated where it would be convenient to inject material into the plasma. Injection through the electrode will interfere somewhat with its operation. Electrodes cause a magneto-hydrodynamic compression to be applied to the plasma leading to plasma streaming. Depending on the situation, this can be beneficial or deleterious. Electrode plasma torches tend to be high in velocity and low in cross-section compared to induction plasmas at the same power level. Power generation by electrodes has the advantage of using low cost dc power.

Induction plasma has low velocity and a wide cross-section so that it can completely envelope the growing boule and has no tendency to blow the molten cap away. High velocity plasma can be obtained if a constricting nozzle is used. For some applications increased dwell time in the induction plasma may be an advantage; for others it may be a disadvantage. Induction plasma has the advantages that any gas can be used, various materials are easily injected, and has excellent visibility. Power utilization efficiences are comparable for electrode and induction plasma generation.

CHEMICAL VAPOR DEPOSITION (7)

Chemical vapor deposition (CVD) is a method of producing a layer of deposits by heterogeneous gas-solid or gas liquid chemical reactions at the surface of a substrate. A volatile compound of the substance or element to be deposited is first vaporized. The vapor is then thermally decomposed, or reacted with other gases or vapors, at, near, or on the substrate to yield non-volatile reaction products. These reaction products are deposited on the substrate as a coating or layer. Due to the large number of available chemical reactions, CVD is regarded as a process of potentially great complexity, versatility and flexibility. CVD is basically an atomistic process (i.e. layers are built up atom by atom). It is capable of producing deposits of maximum density and of closely reproducing fine detail in the substrate surface. CVD does not require the use of ionizing compounds nor a degree of electrical conductivity in both the substrate and the deposit for successful application. Compounds which are too unstable to be deposited without marked change in composition can be successfully deposited by CVD. Finally, CVD can be carried out over a pressure range from superatmospheric down to subatmospheric.

In the following sections the most important fabrication methods that employ vapor phase reactions will be briefly discussed.

Inside Vapor Phase Oxidation (IVPO) (8)

The inside vapor oxidation (IVPO) process involves vapor deposition of glassy layers on the inside wall of a glass (vitreous silica) tube. Soot may be formed which deposits on the tube wall, and is subsequently sintered (usually by a moving external flame). Direct deposition of a sintered glass may occur by heterogeneous reaction if a microwave plasma is used. After glass deposition is completed, the remaining central hole is eliminated by heating and collapsing of the tube. The collapsed tube is then drawn into a fibre.

An IVPO process developed by Kruppers (9) uses microwave or nonisothermal plasma to obtain 100% deposition efficiency. A core glass deposition rate for multimode fibre is approximately 0.3 g/min. At a pressure of 10-30 Torr, the plasma stimulates the reactant gases to heterogenously react at the tube wall. A solid glass layer is deposited on the inside wall of tube. The plasma traverses the tube quite rapidly ($\sim$ 8 cm/sec), continuously depositing a thin glass layer as it moves in both directions. It appears that good process control is possible, especially for the index profile.

Modified Chemical Vapor Deposition (MCVD) (10)

Modifications have been made to the basic CVD process to improve deposition rates and control hydroxyl ion incorporation. An oxy-hydrogen flame is used to externally heat a rotating quartz tube. The flame thermally triggers vapor phase oxidation of the reactants (i.e. metal halide gases) flowing inside the tube causing the formation of glass particles (or soot). Hot soot flowing downstream is attracted to the cold walls of the tube where it is deposited as a thin porous film. The flame passes over the soot deposit, zone sintering it to a glassy layer. When the desired deposit thickness has been obtained, flame intensity is increased and the tube is collapsed into a solid rod blank.

The advantage of this closed environment technique is that the resultant fibre core is essentially hydroxyl-free and deposition rates are an order of magnitude higher than those with basic CVD. A disadvantage being that economics dictate deposition rates, blank sizes and starting tube needs.

A recent report by Fleming (11) indicated that rf plasma enhanced MCVD resulted in high deposition rate preforms with excellent optical properties. For any given composition the intrinsic material properties obtained with conventional MCVD can be duplicated using the plasma. The plasma process

has the additional feature that the thermophoretic deposition of glass soot is dominated by the plasma temperature and can be optimized independent of the sintering mechanism (i.e. an external heat source). Deposition rates of 3-6g/min. produced excellent single mode fibre. More recent work, using a 46 x 50 mm substrate tube and having an overall deposit diameter of 125 μm, increased the deposition rate from 6 to 20 g/min. Total process time was improved by only 25%.

Outside Vapor Phase Oxidation (OVPO) (8)

In the lateral deposition version of the OVPO process, soot is deposited from a burner onto a rotating-traversing graphite bait rod. The soot is deposited as a semisintered preform containing the desired core and (clad glass compositions. The bait rod is removed and the soot preform is sintered into a clear glass preform (or blank) by zone sintering. The fibre is drawn from this blank, at which time the center hole closes.

A strong feature of this process is the precise control over the refractive-index profile in the core, since during preform fabrication over 200 individual core glass layers are deposited. Another feature, which affects manufacturing costs, is the ability to deposit large preforms at reasonable deposition rates (i.e. 1.5-2.0 g/min.)

A problem area with this process is the center hole left after bait removal. After the preform has been sintered, tensile stresses develop at the center hole surface due to thermal expansion mismatched of core-cladding composition. The result is breakage of high numerical aperture (NA) glass blanks and limited fibre design possibilities. A second problem area is the high concentration of hydroxyl impurity in the fibre (50-200 ppm), which is introduced by flame combustion products during soot deposition. Hydroxyl ions cause undesirable fibre absorption losses at long wavelengths.

Vapor Axial Deposition (VAD) (8,12,13)

The VAD is basically a OVPO process that uses axial deposition instead of lateral deposition. The VAD process incorporates a continuous fabrication of the fibre preform in the axial direction. The core glass and, sometimes, clad glass soot are simultaneously deposited in an axial direction. A rodlike soot preform is formed without a central hole. Simultaneous consolidation into a glass blank is performed by zone sintering. Continuous preform fabrication is possible because the deposition and consolidation steps are arranged in a single line.

A number of features makes the VAD process particularly attractive. Continuous fabrication along the axial direction makes it extremely suitable for mass production (13). Long large-diameter preforms prepared by VAD significantly reduce fibre production costs. An enclosed environment for deposition and consolidation is used and there is a complete avoidance of a center hole, so that collapsing is not necessary. These features allow fabrication of excellent low-loss fibres as well as single-mode and high numerical aperture fibres (12).

A major problem, as with other processes, is hydroxyl contamination and index profile control. Hydroxyl ion removal will be discussed later in this report.

Work published by Inagaki and Edahiro (12) describes a VAD process developed by NTT laboratories (Nippon Telegraph and Telephone). This process provides a typical glass soot deposition rate of 0.5 - 1.0 g/min. with a maximum rate of 2.0 g/min. It was found that higher rates tended to adversely affect the deposition energy and refraction index. Loss and frequency properties are improved with new dehydration and profile formation techniques. A deposition efficiency of 60-80% was obtained. The continuous fabrication technique

produced a sintered glassy preform approximately 25 mm in diameter and 500-800 mm in length. This corresponds to 20-30km fibre length with 125 μm fibre diameter.

A recent report by Kyoto et al (13) indicates that improvements to the continuous fabrication VAD process has produced a sintered glass preform 1500 mm in length and 23 mm in diameter. This corresponds to a 300 km fibre length, with a 50 μm core diameter. A deposition rate of 0.5 g/min. was used.

EXPERIMENTAL SET-UP (12)

Equipment set-up for the VAD process developed by Inagaki and Edahiro (12) is shown in figure 6. The machine is similar to a single crystal pulling machine introduced by Verneuil in 1902 (15). Reactant materials such as $SiCl_4$, $GeCl_4$ and $POCl_3$ are introduced into oxy-hydrogen torches. Fine glass particles (soot) produced by a flame hydrolysis reaction are deposited on a starting silica glass rod which acts as a seed. A porous preform is then grown in the axial direction and consolidated into a transparent preform by zone sintering using a carbon ring heater. A glass (quartz) chamber encloses the reaction and deposition region. The carbon ring heater is contained in a water-cooled stainless-steel vessel. The glass chamber and the vessel are tightly connected to each other to achieve a clean environment. The starting rod is pulled upward and rotated to maintain cylindrical symmetry in the chemical deposition and to produce a porous preform with a constant diameter.

The equipment set-up for the proposed plasma torch CVD process will incorporate some features of the VAD process in figure 6 (12) and the general features of the system shown in figure 7 (5). The oxy-hydrogen torches will be substituted for a magnetically enhanced dc electrode plasma torch. A quartz tube will be used as the reaction chamber instead of the bulbous glass chamber shown in figure 6. Seed crystals on a substrate would possibly be used instead

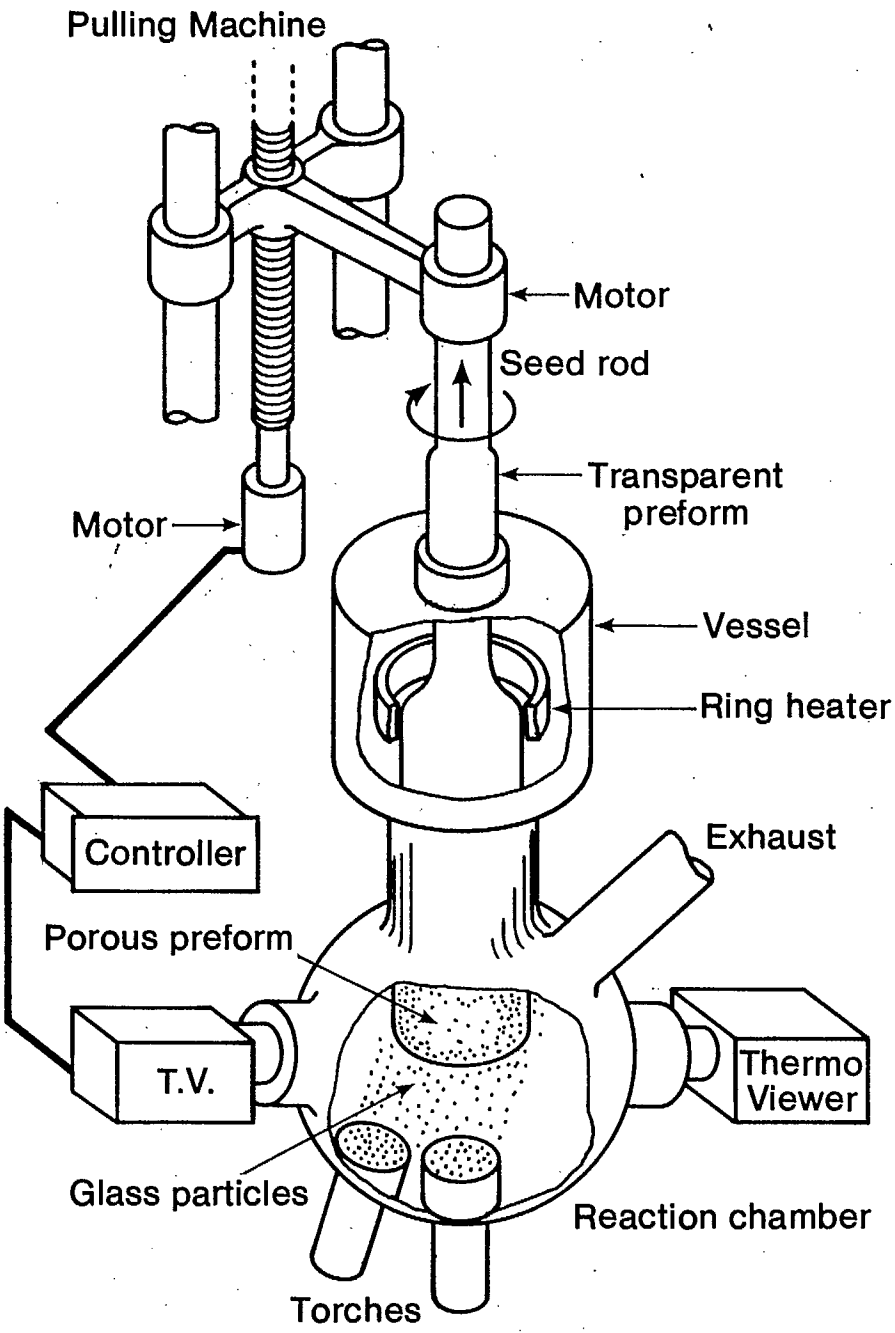

Fig. 6. Equipment for VAD process.

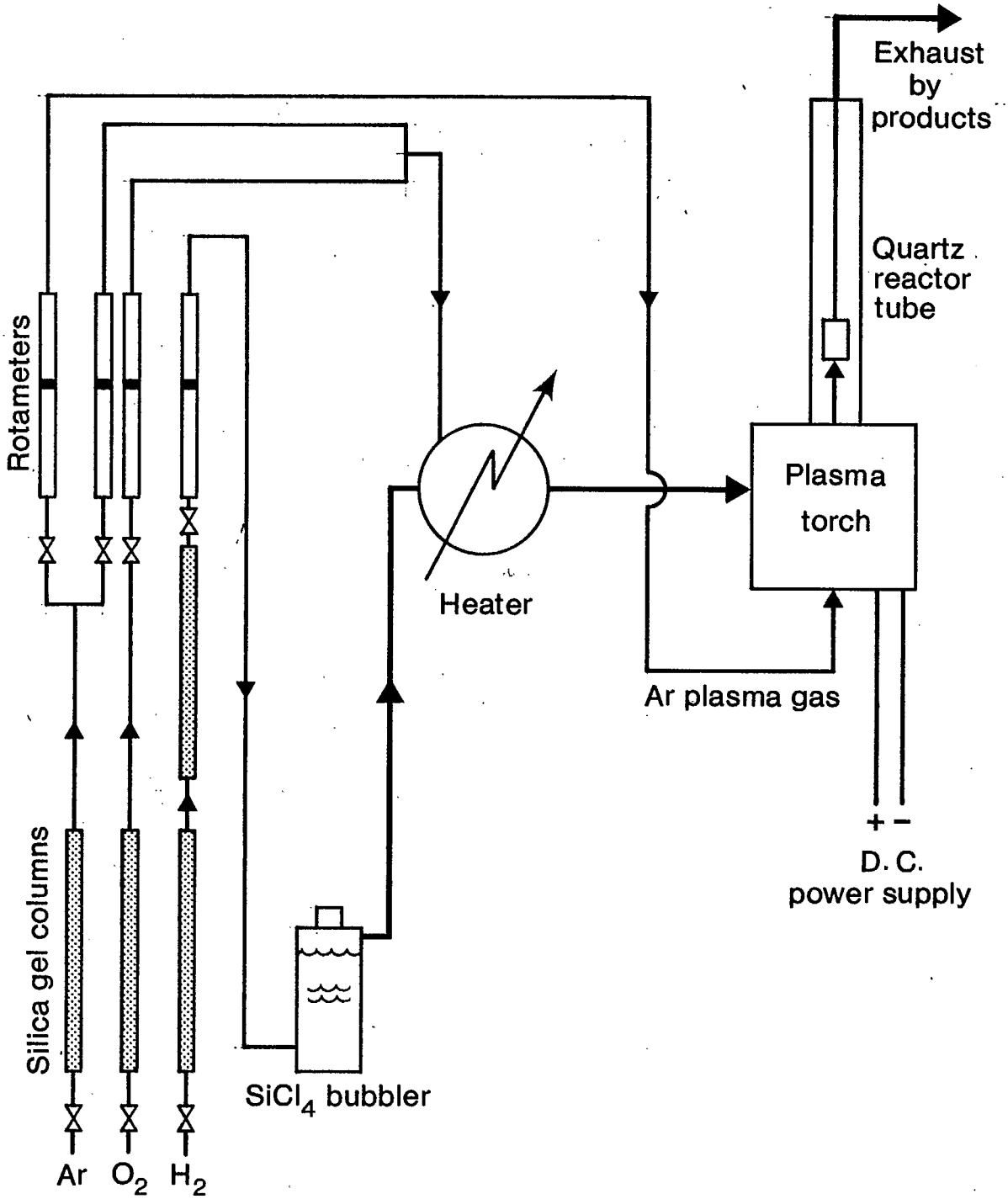

Fig. 7. - Silicon tetrachloride system flowsheet.

of a seed rod. The introduction of the reactants (i.e. $SiCl_4$, H_2 and O_2) into the plasma is as shown in figure 7. Purified hydrogen (H_2) is bubbled through $SiCl_4$ and heated to produce a vapor. Purified oxygen, a required component to produce SiO_2, is introduced into the $SiCl_4$-H_2 stream. The $SiCl_4$-H_2-O_2 vapor stream is then introduced into the plasma flame of the torch. The high temperature plasma causes a chemical reaction to occur which produces SiO_2 and HCl. SiO_2 is deposited on a cool substrate and the HCl byproduct is exhausted through an oil trap. This proposed plasma torch CVD process is in effect a VAD process with the reaction chamber under vacuum.

CHEMICAL REACTIONS (7,14)

There are a number of reactions which describe the production of SiO_2 from $SiCl_4$ (7,14):

$$SiCl_{4(\ell)} + 2H_2O_{(v)} \rightarrow SiO_{2(s)} + 2HCl_{(g)} \quad [1]$$

$$H_{2(g)} + CO_{2(g)} \xrightarrow{(400°C)} H_2O_{(g)} + CO_{(g)} \quad [2]$$

$$SiCl_{4(\ell)} + 2H_{2(g)} + 2CO_{2(g)} \rightarrow SiO_{2(s)} + 4HCl_{(g)} + 2CO_{(g)} \quad [3]$$

$$SiCl_{4(\ell)} + 2H_{2(g)} + O_{2(g)} \rightarrow SiO_{2(s)} + 4HCl_{(g)} \quad [4]$$

Equation 1 shows the hydrolysis of $SiCl_4$. The water vapor required may be formed in the gas phase by the thermal reduction of H_2 and CO_2, as shown in equation 2. If H_2O as a liquid is mixed with $SiCl_4$ a violent spontaneous reaction occurs. The result is gelatinous SiO_2 with some SiO and Si_2O_3. Equation 3 shows the hydrogen reduction of $SiCl_4$ into SiO_2. The first stage of this reaction involves vaporizing $SiCl_4$ with dry H_2 and CO_2. The second

stage involves the thermal reduction of the vapor into SiO_2, HCl and CO. Thermal reduction takes place at, near, or on a heated substrate, where SiO_2 is deposited. In the event where the plasma torch is used, thermal reduction takes place in the plasma and SiO_2 is deposited on a cool substrate. Typical plasma temperatures range between 10,000° to 20,000° K, while the heated substrate ranges between 900°-1200°C. Equation 4 uses the same reaction mechanism as equation 3 except that O_2 replaces CO_2 so that CO_2 is not a byproduct.

It is possible for equation 4 to proceed without the use of hydrogen. In which case the following reaction occurs: $SiCl_{4(\ell)} + O_{2(g)} \rightarrow SiO_{2(s)} + 2Cl_{2(g)}$. The SiO_2 is deposited out leaving an atmosphere of chlorine gas. Chlorine gas is extremely toxic and corrosive. Since it is heavier than air it tends to collect in the low lying areas and is not easily dispersed. Hydrogen chloride gas (see equation 3 and 4), on the other hand, is lighter than air and is easily dispersed. In the event of gas leaks in the torch system, it is felt that hydrogen chloride gas would be easier to deal with than chlorine gas.

There are certain gases such as water and hydrogen which can react with the silicon-oxygen (Si-O) network (8). Water and hydrogen radicals, which are present at high temperatures, break up the Si-O network, thereby modifying such properties as strength, viscosity and light absorption. Water reacts with the Si-O bond as follows:

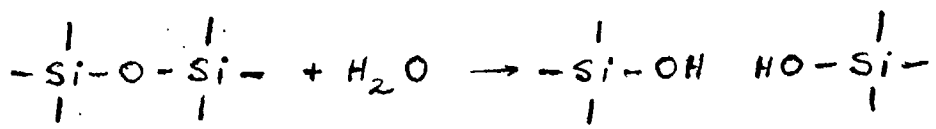

Hydrogen reacts with the Si-O bond to form hydroxyl (OH) groups.

The rate of introduction or removal of OH groups is controlled by the diffusion of hydrogen molecules, which is much faster than the diffusion of the larger water molecules. OH ion reduction is discussed later in the report.

Previous experiments (7) have provided the following deposition conditions for an amorphous SiO_2 layer (Note: Plasma torch was not used). $SiCl_4$ has a vaporization temperature of 0°C, however, a temperature of 21°C (room temperature) was used. Gas flow rates for H_2 and CO_2 are 300 cm^3/min and 100-300 cm^3/min, respectively. An excess of H_2 in the deposition atmosphere (H_2:CO_2 ratio greater than 1:1) tended to suppress the gas phase reaction which produces an oxide fog or dust at high deposition temperatures. Addition of CO to the deposition atmosphere would be more effective in supressing dust formation and powder deposits. Substrates used were molybdenum, tantalum or graphite at temperatures of 900°-1200°C. Since hydrogen reduction of $SiCl_4$ is very sensitive to the presence of impurities. Gases used must be carefully purified and the substrate must not contaminate the deposit.

FILM CHARACTERISTICS (7,14)

Chemical vapor deposition using conventional methods (i.e. where the reaction and deposition takes place on a heated substrate) results in films with greater crystallite orientation than usual. Consequently, temperature changes after deposition causes accentuated stresses. Crystallites (or grains) are often collumnar and perpendicular to the substrate. If the film is strained laterally, these grains separate and the film ruptures.

There are a number of factors that influence the nature of the film or deposit. The most important factor is the substrate temperature. Lower substrate temperatures (i.e. 800°-900°C) favor more finely crystalline deposits...virtually amorphous SiO_2. Higher substrate temperatures (i.e. 1100°-1250°C) form crystals several millimeters in length. At low or medium temperatures the structure of the

base has little or no effect upon the form of the deposit. Maximum deposition temperature is generally the melting point of the base, the deposit, or any reaction product or solid solution formed between the base and the deposit.

The crystallinity of the deposit is affected by the concentration of reactants in the reacting atmosphere and pressure of this atmosphere. Higher concentrations or pressures produce more finely crystalline deposits.

A uniform coating depends primarily upon substrate temperature uniformity and rate of supply of reactant atmosphere to the substrate surface. Non-uniform substrate temperatures result in heavier deposits on the hotter portions, except where the higher temperatures produce a premature reaction of the reacting atmosphere. Uniform substrate temperature can be easily attained with external heating, but with lower deposition efficiency. Internal heating, by induction, usually gives uniform substrate temperature if an appropriate coil design is used.

Deposit uniformity may be improved by operating at reduced pressure. This is particularly beneficial in processes where premature reduction of the reacting atmosphere is a problem. At extremely low pressures, i.e. in the order of 10^{-3} torr or less, deposition will occur only on line-of-sight surfaces.

Most of the above comments are directed at conventional CVD processes, although some may apply to plasma torch CVD. Plasma torch CVD allows the majority of chemical reactions to occur within the plasma (as opposed to the heated substrate surface). The reaction products are deposited on a cool substrate in close proximity to the plasma. This allows preferential deposition on the substrate instead of other surfaces. The following sections describe the growth factors related to vitreous SiO_2 boule growing.

GROWTH FACTORS (4,14,15)

Boule Formation

Previous experiments (4,15) have grown boules with the torch (oxy-hydrogen) flame directed downwards and the boule growing upwards. The molten material, upon leaving the flame, is deposited on a seed crystal in the form of a melt puddle. The seed crystal is held on a refractory base (sintered powdered cone). The seed, about 1-2 mm in length, is followed by a broadening phase which occurs as a consequence of a series of controlled melt runovers. As the base is lowered out of the flame, solification takes place.

The liquid-solid boundary line initially stays unchanged at the seed crystal until a definite conical form has developed. The boundary line then moves slowly upwards until it coincides with a line describing the maximum circumference of the growing boule. During this initial phase, the boule only increases directly at or above the maximum diameter. When steady state conditions have been reached, the boule grows with constant cross-section. The resulting boule may be amorphous, polycrystalline, or a single crystal.

Rotation is of marked advantage if large diameter (greater than 20 mm) boules are grown. In this way asymmetrical growth can be reduced or prevented. Fast rotation, above 135 rpm, has been found to influence the form of growth front, since the melt is driven outward by centrifugal force.

Melt Film (1)

Melt film thickness is dependent on parameters which influence the temperature in and around the melt film. Such parameters include: growth rate, length of grown boule, material which is being grown, as well as torch and growth chamber design. For large diameter boules (greater than 20 mm) melt film varies with the distance from the growth axis. There are certain effects in the melt film which originate in the process, these are: the cross-sectional shape

of the growing boule, growth striations with diffusion movements (separation phenomena), penetration of heat sinks, the shape and arrangment of gas bubbles, and convective flow. Periodic striations parallel to the growth front are due to varying growth rates. Growth rate variations may be due to apparatus faults (e.g. play in lead screw or bearings), temperature fluctuations or mechanisms of solidification.

Glass Characteristics (6, 12)

Although it is desired to grow vitreous SiO_2 directly by CVD, it may not happen. Frequently, fine glass particles (i.e. soot) are produced by the chemical reaction and deposited onto a substrate surface. A porous preform is grown in the axial direction and consolidated (12) into a transparent glossy preform by zone sintering. Consolidation of the low density porous preform comprises of two steps. The first step is the densification process in which the transition from open pore state to closed pore state occurs. The second step involves a closed pore collapsing process which results in a bubble free transparent preform. After consolidation has taken place, the transparent preform is drawn into a fibre. A description of fibre drawing techniques is given in the appendix.

Molecular Diffusion (6)

Gas can dissolve molecularly in glass because of its open structure. If the gas molecule is small it can rapidly diffuse through a simple glass such as SiO_2. Molecular diffusion is important in "fining" or removal of bubbles from melts. Gases such as hydrogen, oxygen, and water, which dissolve moelcularly in glass, also react with the glass network. These reactions affect certain glass properties, for example: optical absorption (tranmission of visible and ultraviolet light), viscosity and electrical conductivity. Gas solubility is temperature dependent from 80°-1000°C. Solubility is defined as the ratio

Ci/Cg, where Ci is the concentration of gas dissolved in the glass, and Cg is the concentration of molecules in the gas phase. Literature values for solubility ratios of some gases are given as: 0.03 for hydrogen, 0.24 for helium, 0.019 for neon, and 0.01 for argon and oxygen. Diffusion coefficients (cm^2/sec) of some gases in fused silica at 1000°C are given as: $7.3x10^{-6}$ for deuterium (heavy hydrogen), $5.5x10^{-5}$ for helium, $2.2x10^{-6}$ for neon, $1.4x10^{-9}$ for argon, $6.6x10^{-9}$ for oxygen, and $3.0x10^{-9}$ for H_2O. It is evident that hydrogen, because of its small atomic size, has the highest molecular diffusivity (in glass and metal).

OH-Ion Reduction (12, 16)

VAD fibres fabricated without dehydration usually contain hydroxyl (OH) ion concentrations of about 5-30 p.p.m. OH-ion contamination may come not only from an oxy-hydrogen flame, but also from reactant products and fibre drawing from a jacketing silica tube (which contains about 200 ppm OH-ions). Low -OH content fibers may be obtained by dehydration of the porous preform with the use of chemical reagents (for example, chlorine (Cl_2) or thionyl chloride ($SOCl_2$)).

In the last few years there has been rapid progress in dehydration techniques for VAD processes. Work by Edahiro et al (12) produced dehydrated fibres with an OH content of about 0.03 to 0.05 ppm. The porous preform is held in a furnace and rotated around its axis. $SOCl_2$ vapor, carried by O_2 gas, is introduced into the furnace. The furnace temperature for dehydration is gradually raised to between 200°C and 1450°C. At a temperature of around 100°C, OH content is 0.03 ppm, while a temperature above 1200°C reduces the OH content to below 0.1 ppm. After the dehydration treatment, $SOCl_2$ flow is stopped and the furnace temperature is raised to 1450°C for consolidation. Total time for the dehydration process is about 5 hours.

Chida et al. (16) developed a simultaneous dehydration technique with consolidation using $SOCl_2$. A muffle-type resistance furnace with an ultra-pure

graphite heating element is used for the dehydration-consolidation process. The hot zone of the heating element was designed to be narrow, effecting a sharp temperature distribution in the vertical direction for consolidation of the porous preform. The porous preform was deposited by the VAD method. It was then pulled into the furnace at a rate of 150 mm/hr and consolidated continuously to a transparent preform. During this process $SOCl_2$ vapor saturated with O_2 was introduced into the muffle furnace with helium gas. As $SOCl_2$ flow rate is increased, the OH content decreases and final fibre OH content becomes less than 0.05 ppm. The simultaneous dehydration and consolidation process is desirable for mass optical fibre fabrication.

Ultimately low -OH-content VAD fibres were obtained by Moriyama et al (16) using Cl_2 gas instead of $SOCl_2$ gas. The porous preform was inserted into a graphite heated muffle-type furnace for dehydration and consolidation. Mixed chlorine and helium gas were injected into the furnace. Dehydration treatment consisted of moving the porous preform upward in a 1200°C furnace at a speed of 200 mm/hr. Thus, the porous preform was treated for two hours. An optimum Cl_2 gas flow rate is about $80cm^3$/min. When the flow rate-exceeded 100 cm^3/min, the consolidated preform surface was attacked by excess Cl_2 gas and became rough. After dehydration, the furnace temperature was gradually raised to about 1500°C for the consolidation process. It should be noted that high temperatures are an aid in dehydration because OH-ions chemically bonded with Si are more easily removed. However, at temperatures above 1200°C the porous preform starts sintering. The residual OH content for this dehydration process was estimated at less than 1 ppb.

SUMMARY

This report has been an attempt to provide background and up-to-date information pertaining to the CVD of SiO_2 using a plasma torch. A comparison was made between dc-electrode and rf-induced plasma generation because under certain circumstances, one plasma generation method is more viable than another. Factors such as, equipment costs, power sources, and plasma velocity must be considered.

A number of chemical vapor diposition techniques have been discussed. The basic fabrication method, expected deposition rates, advantages and disadvantages are included for IVPO, MCVD, OVPO and VAD. It was found that VAD characteristics were most applicable to plasma torch CVD of SiO_2. Equipment set up for the plasma torch CVD process will incorporate some features of the VAD process shown in figures 6 and 7.

In most cases, the deposit resulting from CVD is in the form of fine glass particles (soot) or a solid boule. Growth factors pertaining to the production of porous preforms and solid boules were discussed. Hydroxyl (OH) ion contamination is a major problem with SiO_2 production. Various OH reduction techniques involve heating the porous preform in a high temperature furnace filled with $SOCl_2$ or Cl_2 for a few hours.

In some cases it is desirable to use powder material instead of liquid reactant materials. For this purpose, a discussion on the use of powder material is included in the appendix. Also included in the appendix is a brief discussion on fibre drawing.

APPENDIX

POWDER MATERIAL (15)

When growing glass or crystal boules, the occasion may arise which requires the use of powder material instead of liquid. Powder materials require special considerations in feed mechanism and boule perfection. Basic growth mechanism using a powder is as follows.

The seed crystal (on a pedestal) is heated with the plasma flame until a thin melt develops. A fine-grained powder is introduced from a supply container into the plasma flame and reaches the melt film in a molten form. Material flow from powder supply container to melt film is constant and continuous. The boule is pulled away from the flame at the same rate it is growing towards the flame. When the desired boule length has been reached, powder flow and boule rotation are stopped and the plasma flame extinguished.

Boule perfection is highly dependent on powder supply and flame characteristics. Transition from powder particle to liquid droplet requires small grain size (10-100 μm), low density, fairly constant powder flow, and chemical purity. A small grain size has a greater surface area exposed to thermal energy making it easier to melt. The melt film is very thin, so if the powder is not completely molten when it reaches the film then glass or crystal imperfection occurs.

Unfavourable growth conditions cause bubbles to form during solidification of the glass. Bubble formation is generally due to powder particles that do not fuse in the plasma so that all the gas from the powder can escape. A "pipe" of bubbles can be observed if too little energy is transferred to the powder on its way from the torch to the boule. Energy transfer is defined by a number of apparatus parameters which characterize flame size, temperature of plasma flame, location of feed tip within the flame and distance between the feed tip and growth front of the boule.

Accumulations of powder may form somewhere between the feeder mechanism and the boule top. When their weight becomes too large they free themselves as powder "avalanches". Because of their large size, such power "avalanches" cannot be fully fused and bubbles result. Causes of powder accumulations must be eliminated. The tube through which the powder is transferred from the shaking or vibration funnel to the torch should be examined to see whether powder accumulation can occur. A vibrator usually vibrates enough to prevent powder build up.

POWDER FEEDER MECHANISM (15)

There are two basic powder feeder mechanisms for introducing powder into a plasma torch at a controlled and steady rate. The first method is a single stage feeder mechanism, commonly referred to as a tapping mechanism. It's simplistic construction offers reliability of operation. The powder container is closed at one end by a sieve. Either the elastically suspended container or the sieve is tapped with a hammer at regular intervals. Small amounts of powder pass through the sieve directly into the plasma torch. Powder flow is determined by the weight of the hammer, the distance it falls, and its frequency of operation.

Powder flow decreases as the mesh aperture is reduced and approaches zero with a mesh aperture of about 70 μm. Hammer weight is independent of mesh aperture. Long term constancy depends, among other things, on the depth of powder in the container. A large mesh aperture improves constancy, i.e. approximately $\pm$ 10% for 3 hours, with a mesh aperture of 150 μm.

Short-time constancy is naturally poor for the tapping process. After each return motion of the sieve base, there is a brief suction effect following each hammer blow. This causes powder flow to momentarily cease. Therefore, the powder flow fluctuates greatly even if the shock rate is high. A typical

frequency of 100 min^{-1} has little if any effect on the glass quality. Frequency of striations is much lower than the tapping frequency.

The second powder feeder method is called the two-stage feeder mechanism. An additional stage is added between the powder container and the torch. A simple two stage device uses a feeder trough without a sieve and gives powder flow constancy of about 30%. Two-stage mechanisms with sieves have been developed which are distinguished by the manner in which vibration is imparted to the fine dosing sieve. In one feeder mechanism, the sieve vibrates in the horizontal direction; a constant powder flow is achieved with a mesh aperture of above 250 μm. A second type of feeder mechanism uses an oscillating magnet acting in a vertical direction on a sieve with asymmetrical spring retention. Vibratory movement about a horizontal axis is super-imposed on the vertical movement. Constancy of powder flow is achieved with a mesh aperture of about 150 μm. A third mechanism involves a purely vertical vibratory movement super-imposed on a purely horizontal vibratory movement. Constant powder flow can be achieved for mesh apertures of 80 μm.

Figure 8 (15) shows a schematic diagram of a two-stage powder feeder mechanism with horizontal and vertical movement of the fine dosing sieve. The fine dosing sieve [a] (80 μm mesh aperture) is held by two spring steel sheets [b] and coupled to the oscillating magnets [d] by means of two armatures [c]. One of two oscillating magnets is driven by the upper, the other by the lower halfwave of the power network voltage. Two oscillating magnets working in the vertical direction [g] also act on the fine dosing sieve [a]. The springs [f] counteract the magnets [g]. The height of the powder on the fine dosing sieve [a] is kept constant with the aid of the light barrier (light source and photocell [e]). The light barrier controls via a relay

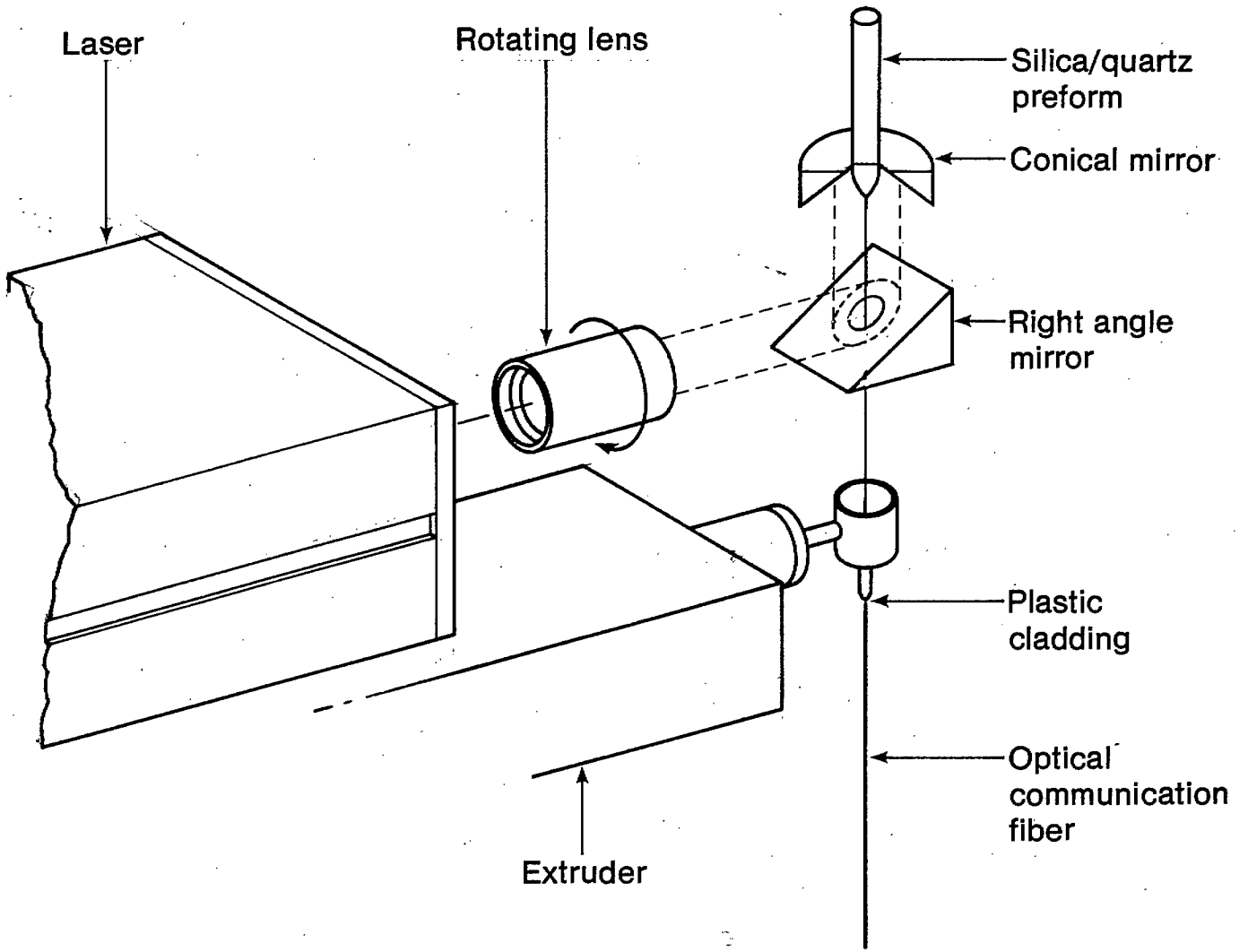

Fig. 10. Fused silica/quartz drawing with plastic cladding.

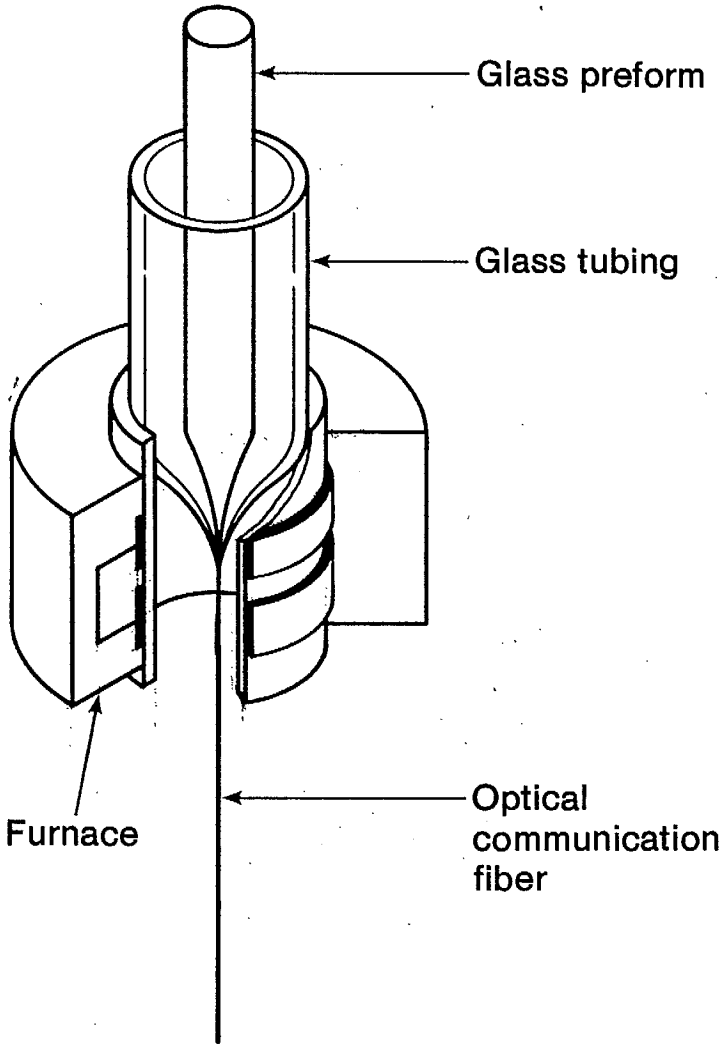

Fig. 9. Highly controlled glass fiber drawing procedure.

powder flow from the powder container [j] to the fine dosing sieve [a] by actuating the hammer [h], which acts on the coarse dosing sieve [i] (800 µm mesh aperture). Powder flow through the fine dosing sieve [a] can be regulated by altering the amplitude of the oscillations.

The effect of vibration can be enhanced by adding a layer of glass spheres (4 mm diameter) to the fine dosing sieve. Kinetic energy is transferred to the spheres by vibrating sieve; by milling and thrusting motion they contribute to passing the powder through the sieve. If a mesh aperture of 250 µm is used then a constant powder flow is achieved over a long period without using the glass spheres.

AERODYNAMIC EFFECTS (15)

When powder feeder mechanisms are used, a number of aerodynamic effects occur as a result of interactions between sieve movement, gas stream, and powder stream. A pressure compensating tube is attached to the fine dosing sieve to obtain an even powder stream. The gas, which flows past the opening of the funnel arrangement below the fine dosing sieve [a], lowers the pressure within the funnel. The air column lying above the sieve, therefore, exerts pressure on the powder, with the result that throughput is reduced. The difference in pressure between the spaces above and below the sieve is balanced by the tube, and depending on the geometry of the funnel, the throughput can be increased two or threefold.

Another disturbing effect is observed when the vibration of the fine dosing sieve has a vertical component. These oscillations are passed on by the air column and influence the throughput through the coarse dosing sieve. The throughput can no longer be controlled with the required precision. A "conveyer sphere" between coarse and fine dosing sieve reduces the cross-sectional area to a small gap and stops the interaction. An even powder

flow through the gap is obtained by rotating the sphere about a horizontal axis.

FIBRE DRAWING (17)

Once the amorphous silicon dioxide preform (or boule) has been grown to a desired length it will be drawn into an optical fibre. The glass preform must have extremely high purity as the resulting fibre will be used for fibre-optic and fibre electro-optic applications. The preform is drawn down under very carefully controlled conditions. Jacketed or clad glass preforms are produced using sophisticated methods. Figure 9 shows the glass fibre drawing procedure to obtain a glass jacketed fibre. For higher temperature compositions, such as fused silica-quartz, a laser process can be used. The laser-drawing process (see figure 10) permits temperatures in excess of 1800°C(3300°F) to be concentrated at the locus of fibre-attenuation from the preform. Although an expensive method, the drawing of pure silica-quartz optical fibres makes possible extended fibre-length transmission and ultraviolet light transmission.

A third method of producing a fibre is the vapor phase oxidation process. In this method, chemical gases which produce pure SiO_2 and associated forms are passed through the heated silica-quartz tube and become deposited on the inside surface. Following deposition, the temperature is increased and the tube is necked down to produce a finite-size preform (no center void). The preform is then reheated in another furnace and attenuated into an optical fibre. This is the most expensive optical drawing process, but costs are justified by the extreme purity of core-material gases and control of contaminants in the closed system down to one part per billion. In an important variation of this process, the composition of the gases may be sequentially varied to produce a fibre-possessing a graduated index of refraction in the cladding material.

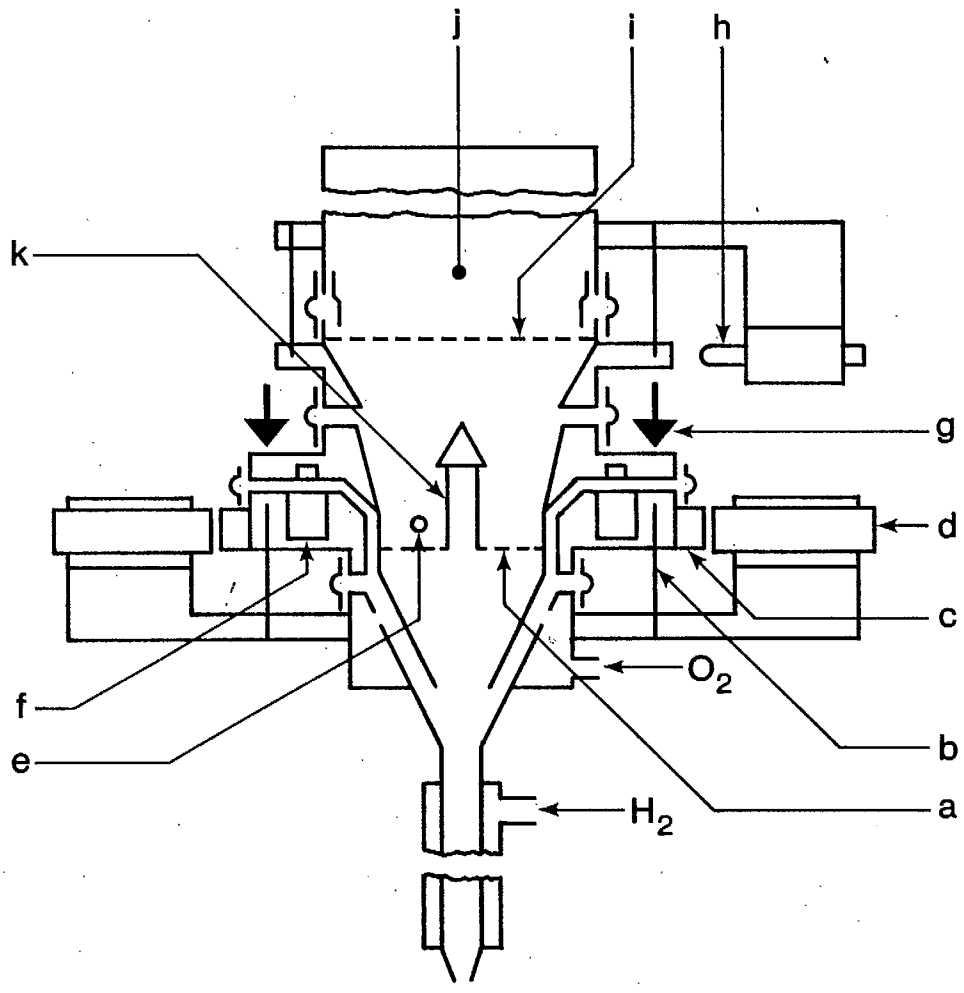

a. fine dosing sieve
b. spring steel sheet
c. armature
d. vibration magnet
e. light barrier
f. springs acting in a vertical direction
g. vibration magnets working in vertical direction
h. hammer acting in horizontal direction
i. coarse dosing sieve
j. powder container
k. pressure compensating tube

Fig. 8. Schematic diagram of a two-stage powder feeder mechanism with horizontal and vertical excitation of the fine dosing sieve.

REFERENCES

1. Reed, T.B., J. Applied Phys., 32:5 821 (1961).

2. Baddour, R.F. and R.S. Timmins, Eds. The Application of Plasma to Chemistry, M.I.T. Press, Massachusetts, 1967, pp. 14, 28-30, 36, 41-42.

3. Reed, T.B., J. Applied Physics, 32:12 2534 (1961).

4. Laudise, R.A., in The Growth of Single Crystals, Ed. by N. Holonyak, Jr., Solid State Physical Electronics Series, Prentice-Hall, Englewood Cliffs, 1970, pp. 146, 180-187, 191-195, 208-213.

5. Mahawili, I. and F.J. Weinberg, in Plasma Chemical Processing, Ed. by D.M. Benson and E. Pfender, A.I.Cb.E. Symposium Series, No. 186, Vol. 75, 1979, p. 11.

6. Doremus, R.H., Ed. Glass Science, Wiley and Sons, New York, 1973, pp. 14-16, 106, 121, 133, 239, 319.

7. Powell, C.F., J.H. Oxley and J.M. Blocher, Eds. Vapor Deposition, Wiley, New York, 1966, pp. 250-253, 260-263, 396, 404.

8. Schultz, P.C., in Optical Fiber Technology II, Ed. by C.K. Kao, IEEE Press, New York, 1981, p. 108.

9. Kuppers, D. and H. Ludtin, "Preparation Methods for Optical Fiber Applied in Philips Research, in Technical Digest, 1977 Intl. Conf. on Integrated Optics and Optical Fiber Communication, Tokyo, Japan, 1977, paper B9-1, p. 319.

10. Pearson, A.D. in Applied Solid State Science, Vol. 6, Academic Press, 1976.

11. Fleming, J.W., "Status and Prognosis for Plasma MCVD" in 1983 Optical Fiber Communication, published by Optical Society of America, 1982, p. 89.

12. Inagaki, N. and T. Edahiro, in Optical Devices and Fibers, Ed. by Y. Suematsu, Ohmasha Ltd. and North Holland Publishing Co., 1982, p. 220.

13. Kyoto, M., H. Satoh, M. Watanabe, M. Nishimura and K. Yano, "Continuous Fabrication of Graded-Index Fiber by Vapor Phase Axial Deposition," in 1983 Optical Fiber Communication, published by Optical Society of America, 1982, p. 80.

14. Berry, R.W., P.M. Hall and M.T. Harris, Eds. Thin Film Technology, Van Nostrand Co., Princeton, 1968, pp. 131-133, 266-270.

15. Goodman, C.H.L., Ed. Crystal Growth-2, Plenum Press, New York, 1978, pp. 84, 109-126, 166-170.

16. Inada, K. in Optical Devices and Fibers, Ed. by Y. Suematsu, Ohmsha Ltd. and North Holland Publishing Co., 1982, p. 241.

17. Mohr, J.G. and W.P. Rowe, Eds. Fiber Glass, Van Nostrand Reinhold Co., New York, 1978, p. 201.

APPENDIX B

Reprinted from

Applied Physics Letters

Volume 39 | 1 August 1981 | Number 3

A magnetically stabilized radial discharge for a high-powered laser

H. J. J. Seguin, C. E. Capjack, D. Antoniuk, and V. A. Seguin
Department of Electrical Engineering, The University of Alberta, Edmonton, Alberta, Canada T6G 2G7

pp. 203–205

a publication of the American Institute of Physics

A magnetically stabilized radial discharge for a high-powered laser

H. J. J. Seguin, C. E. Capjack, D. Antoniuk, and V. A. Seguin
Department of Electrical Engineering, The University of Alberta, Edmonton, Alberta, Canada T6G 2G7

(Received 8 April 1981; accepted for publication 20 May 1981)

Details of a new "magnetically stabilized" coaxial electrode system supporting a radial discharge geometry is presented. Performance was found to be largely independent of gas mixture and pressure such that high-power cw discharges were easily obtained in all the gases tested, including SF_6. The technique is exceedingly simple and appears scalable to provide a very large active volume in an unusually small physical package. A cw power loading in excess of 40 kW/l has already been attained without experiencing any glow-to-arc transitions.

PACS numbers: 52.80.Sm, 42.60.By, 42.55.Hq

It has recently been demonstrated that high-power gas laser discharges can be stabilized through the utilization of crossed electric and magnetic fields.[1] The interaction of these specially profiled fields with the discharge has been shown to cause a rapid mixing and high-velocity sheared flow near the cathode surface, and also in the plasma bulk.[2] These processes result in uniform secondary cathode emission with concomitant plasma spatial and temporal consistency, such that electrothermal bulk and electrode-induced instabilities are effectively suppressed. Consequently these "magnetically stabilized" discharges do not experience glow-to-arc transitions, as is most often the case in large-volume high-pressure cw laser plasmas under high specific power input.[3]

This letter reports on a more recent extension of this magnetic stabilization technique to a coaxial electrode and radial discharge geometry. The results are most impressive and suggest that it may be possible to build a relatively inexpensive multikilowatt cw laser device having an unusally small physical size. Such a machine would find wide industrial application.

Preliminary experiments were performed on the water-cooled coaxial electrode structure shown in Fig. 1. The required magnetic fields were provided simply by an external solenoid. This solenoid supplied both axial and radial magnetic field components B_z and B_r. The magnitude of these field components, shown in Fig. 2, was determined by using the "Potent" Code.[4]

In operation, once a radial discharge current filament has been generated, the $J_\theta B_z$ Lorentz force rapidly accelerates and distributes it into a thin rotating disk. As the current is further increased, the width of this rotating plasma body expands longitudinally into the interelectrode volume. The Hall current J_θ coupled with the radial component of the magnetic field B_r gives a Lorentz force which confines the discharge axially to the central region of the coaxial electrode device.

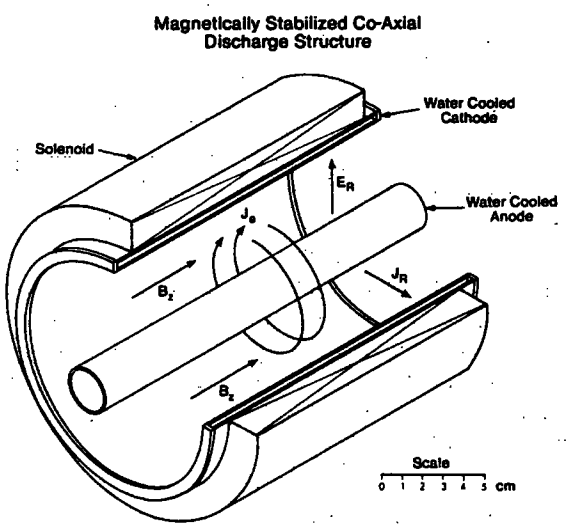

FIG. 1. Schematic diagram of experimental radial discharge electrode system.

 0003-6951/81/150203-03$00.50

Thus to uniformly fill the coaxial laser volume the radial magnetic field is "profiled" to provide only a weak end containment or "plugging" effect. This magnetic end containment feature is particularly useful, since it means that it is unnecessary to insulate or profile the distorted, high field, end sections of the coaxial electrode system, since the B_r field does not allow the discharge to run in these regions. This effect is in sharp contrast to the difficult electrode end problems previously reported in the literature.[5]

A magneto-gas-dynamic analysis, appropriate to this new discharge configuration has been undertaken so as to provide some insight and scaling information on the dominant interaction parameters. A brief version of this work follows.

As indicated previously, the magnetic field described in Fig. 2 is used to both drive a strongly sheared rotation and to axially confine the discharge to the central region of the device. Plasma dynamics can be inferred from the momentum conservation equation for the bulk gas,

$$\rho dv/dt = \mathbf{J} \times \mathbf{B} - \nabla p + \mu \nabla^2 \mathbf{v}, \tag{1}$$

where ρ is the charged plus neutral fluid mass density, $\mathbf{v}$ is the weighted average of ion, electron, and neutral velocities, $\mathbf{J}$ is the current, $\mathbf{B}$ is the imposed magnetic field, p is the sum of ion, electron, and neutral pressures, and μ is the viscosity. The current may be obtained from Ohm's Law (Mitchner and Kruger[6]) and can be written as

$$\mathbf{J} = \boldsymbol{\sigma} \cdot \mathbf{E}_T \tag{2}$$

where

$$\boldsymbol{\sigma} = \begin{bmatrix} \sigma_\perp \cos^2\phi + \sigma \sin^2\phi & -\sigma_H \cos\phi & (\sigma - \sigma_\perp) \sin\phi \cos\phi \\ \sigma_H \cos\phi & \sigma_\perp & -\sigma_H \sin\phi \\ (\sigma - \sigma_\perp) \sin\phi \cos\phi & \sigma_H \sin\phi & \sigma \cos^2\phi + \sigma_\perp \sin^2\phi \end{bmatrix},$$

$\mathbf{E}_T$ is $\mathbf{E} + \mathbf{v} \times \mathbf{B}$, and ϕ is the angle between $\mathbf{B}$ and the z axis, $\sigma_\perp$ and σ_H are the perpendicular and Hall conductivity components.

Since the Hartmann number for discharge parameters of interest in CO_2 laser systems is less than unity it can be shown that $|v_\theta| \ll E_r/B_z$. Thus with this approximation, the Lorentz forces in the azimuthal and axial directions are given by

$$F_\theta \simeq -\sigma_\perp E_r B_z, \qquad F_z \simeq -\sigma_H \cos\phi E_r B_r. \tag{3}$$

The force F_θ causes the discharge to rotate in the negative θ direction. The force F_z is negative for $z > 0$ and positive for $z < 0$ and serves to confine the plasma about the origin $z = 0$. The following approximations will be made to obtain an upper bound for the rotational velocity at the plane of symmetry ($z = 0$); (i) $J_r = I_t/(2\pi r D)$ where I_t is the total discharge current and D is the width of the discharge in z, (ii) $B_z \simeq$ constant in the interelectrode space. By using these approximations and neglecting all derivatives in z, the solution to Eq. (1) gives

$$v_\theta(r) = F_d [c_1 r + (c_2/r) + r \ln r], \tag{4}$$

where

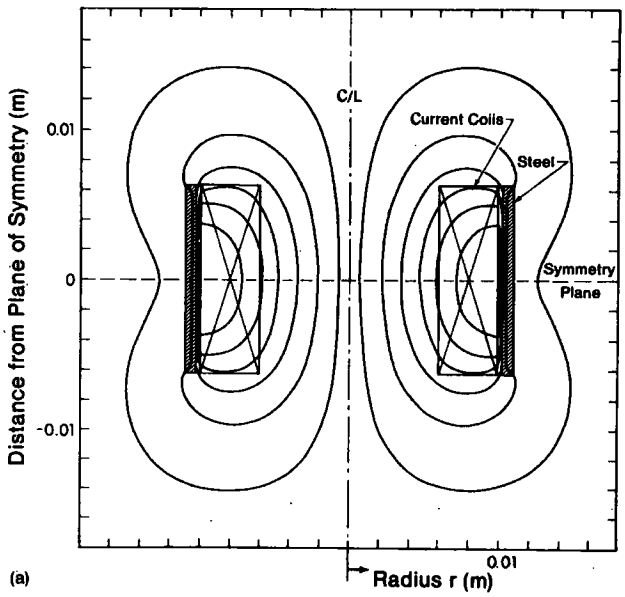

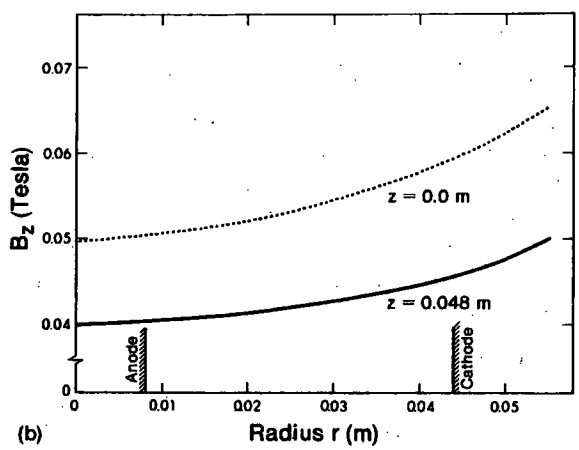

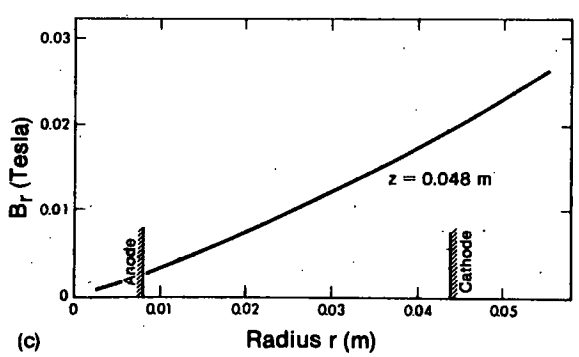

FIG. 2. (a) Computer plot of the solenoid magnetic field profiles. (b) Computer plot of the axial magnetic field at the plane of symmetry ($z = 0$) and at $z = 0.048$ m. (c) Computer plot of the radial magnetic field at $z = 0.048$ m.

$$F_d = \left(\frac{I_t B_z}{4\mu\pi D}\right), \qquad c_1 = \frac{r_1^2}{(r_2^2 - r_1^2)}\left[\ln r_1 - \left(\frac{r_2}{r_1}\right)^2 \ln r_2\right],$$

$$c_2 = \frac{r_1^2 r^2}{(r_2^2 - r_1^2)} \ln\left(\frac{r_2}{r_1}\right),$$

and r_1 and r_2 are the inner and outer radial boundaries of the discharge respectively. A plot of $v_\theta(r)$ is given in Fig. 3 for the following discharge parameters: $r_1 = 0.00794$ m, $r_2 = 0.0438$ m, $I_t = 7.0$ A, $\mu = 1.43 \times 10^{-5}$ kg/ms), $D = 0.02$ m,

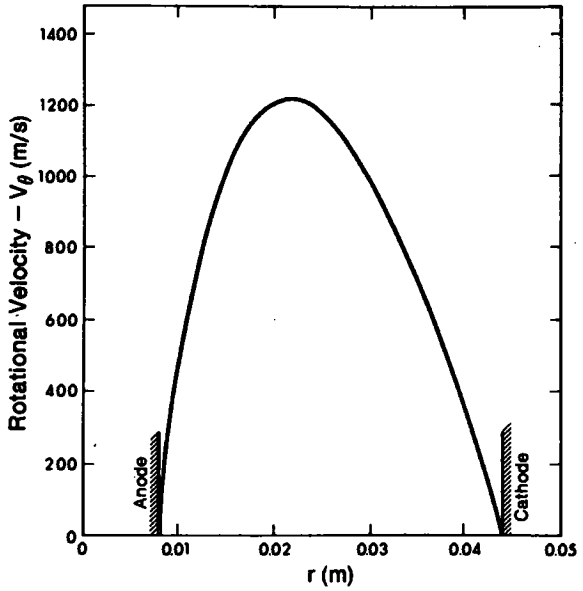

FIG. 3. Plasma rotational velocity as a function of radial position at the plane of symmetry.

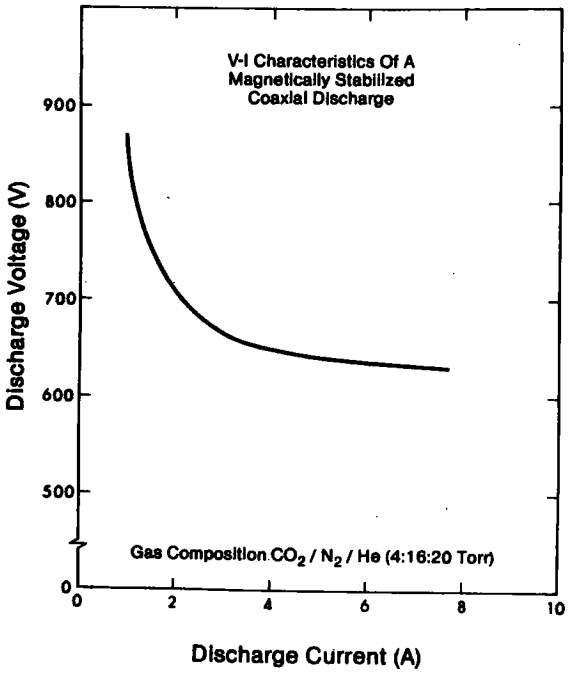

FIG. 4. *V-I* characteristics of a magnetically stabilized radial discharge. The average magnetic field strength in the interelectrode region for $z = 0$ is 0.054 T.

and $B = 0.0550$ T. This figure shows a strongly sheared velocity structure in the interelectrode space.

In an actual device the peak rotational gas velocity would be expected to be somewhat less than the 1200 m/sec predicted by Fig. 3, due to viscous drag of the fluid outside the region where J_r exists. Nevertheless this one-dimensional analysis does indeed reveal that extremely large amplitude and highly sheared mixing velocities can be expected to exist in this type of discharge structure. In addition, radial plasma containment is more easily accomplished, since the outer confining cathode surface permits higher pressure terms to augment radial $J_\theta B_z$ forces.

These effects are believed to be the principal reason for the exceptionally stable discharge performance that is observed.

Tests revealed that this radial discharge operated in a near "constant voltage" manner (Fig. 4). A specific discharge power loading of $\simeq$40 kw per litre was limited not by plasma instabilities but rather only by power supply considerations. In general plasma uniformity was observed to improve still further as the input power loading was increased.

A wide variety of gases and mixtures were tested in the structure. All gave excellent discharges, confirming that this magnetic stabilization technique is insensitive to gas composition and pressure. Stable high-power discharges were also obtained in electronegative gases such as O_2 and SF_6.

Clearly much work remains to be done in investigating the dynamics and scaling laws appropriate to the method. Nevertheless these preliminary results suggest that this new magnetically stabilized radial discharge geometry could well find application in the design of a wide range of laser devices.

[1] H. J. J. Seguin, C. E. Capjack, D. M. Antoniuk, and K. H. Nam, Appl. Phys. Lett. 37, 130 (1980).
[2] C. E. Capjack, D. M. Antoniuk, and H. J. J. Seguin, J. Appl. Phys. (to be published).
[3] A. J. Demaria, Proc. IEEE 61, 731 (1973).
[4] C. L. Thomas, *Software for Numerical Mathematics* (Academic, Loughborough, England, 1974), p. 315.
[5] K. T. K. Cheng and L. W. Casperson, Appl. Optics 18, 2130 (1979).
[6] M. Mitchner and C. H. Kruger, *Partially Ionized Gases*, (Wiley, New York 1973), Chap. 4.

Reprinted from

Journal of
APPLIED PHYSICS

Volume 55 | 1 February 1984 | Number 3

Computer simulation of gas transport in a magnetically stabilized glow discharge

D. M. Antoniuk, C. E. Capjack, and H. J. J. Seguin
Department of Electrical Engineering, University of Alberta, Edmonton, Alberta, Canada T6G 2E7

pp. 708-713

a publication of the American Institute of Physics

Computer simulation of gas transport in a magnetically stabilized glow discharge

D. M. Antoniuk, C. E. Capjack, and H. J. J. Seguin
Department of Electrical Engineering, University of Alberta, Edmonton, Alberta, Canada T6G 2E7

(Received 24 August 1983; accepted for publication 25 October 1983)

Gas flow in a magnetically stabilized glow discharge is analyzed by using a single fluid magnetogasdynamic model. The resulting system of time dependent, nonlinear, coupled partial differential equations is solved numerically on an Eulerian mesh by using an iterative alternating direction implicit finite difference method. The numerical results reveal the importance of considering the secondary flows that are driven by the strongly sheared rotational flow within the discharge volume. The numerical results are confirmed experimentally.

PACS numbers: 52.80.Hc, 52.30. + r, 42.55.Dk, 52.65. + z

I. INTRODUCTION

In recent years, gas discharges have been extensively utilized for the pumping of high power gas lasers. Experience has shown that the performance of these discharge excited lasers is strongly dependent upon the specific power loading and uniformity of the glow that is produced. The experimental scaling of such lasers to larger active volumes, higher pressures, and complex gas mixtures has been complicated by the onset of instabilities which lead to nonuniform excitation, excessive local gas heating,[1,2] and eventually glow-to-arc transitions. Recently, a promising new discharge stabilization technique has been presented[3,4] which is effective in suppressing these discharge instabilities. The technique involves the use of crossed electric and magnetic fields to create and maintain a large volume, rapidly rotating, glow discharge. To date, loadings in excess of 10 kW/l have been achieved without the benefit of external gas cooling or convection. The results obtained to date are particularly encouraging since the instability threshold has yet to be exceeded, suggesting that even higher power loadings are possible. In addition, the quality of the discharge appears relatively insensitive to gas composition and pressure.[3] The technique has also been successfully applied in other electrode geometries.[5]

The purpose of this paper is to determine the flow structure within a magnetically stabilized laser gas discharge. The solution of the two-dimensional magnetogasdynamic (MGD) equations, for the primary rotational flow, and the secondary flows within the discharge will be obtained numerically. A comparison with experimentally measured velocity values will also be made.

II. MODEL

A schematic of the discharge geometry considered in this analysis is given in Fig. 1. The magnetic field profile within the discharge was obtained by using the POTENT computer code,[6] and is given by Fig. 2. The axial (z) component of the discharge current coupled with the radial component of the magnetic field, B (r,z) gives a Lorentz force which leads to a sheared rotation of the gas discharge in the $-\theta$ direction. An initial analysis of the steady state rotational gas flow within this geometry was made by neglecting the secondary radial and axial mass flows.[4] The results indicated a strongly sheared velocity profile across the discharge region with a peak value of approximately 250 m/s. Subsequent experimental measurements indicated flow velocities almost an order of magnitude smaller, implying that a significant effect is played by the secondary flows. Therefore, in this analysis of gas transport in a magnetically stabilized glow discharge, secondary flows will be included. An MGD model will be used, of which the applicability was discussed in Ref. 4. The arguments will not be repeated here. Reference to equations developed in Ref. 4 will be made through the addition of a prefix C to the appropriate equation numbers. The equations used in this analysis include the one-fluid mass and momentum conservations equations

$$\frac{\partial \rho}{\partial t} + \nabla.(\rho \mathbf{v}) = 0\,, \tag{1}$$

$$\frac{\partial}{\partial t}(\rho \mathbf{v}) + \nabla.(\rho \mathbf{v}\mathbf{v}) + \nabla.\hat{\Pi} - \mathbf{J}\times\mathbf{B} = 0\,, \tag{2}$$

where ρ is the sum of charged and neutral fluid mass densities, $\mathbf{v}$ is the mass average of ion, electron, and neutral particle velocities, $\mathbf{J}$ the total current density, $\mathbf{B}$ the applied magnetic field, and $\hat{\Pi}$ the total pressure tensor. The pressure tensor $\hat{\Pi}$ is the sum of a viscous stress tensor[7] $\hat{\tau}$, and the hydrostatic pressure p

$$\hat{\Pi} = \hat{\tau} + p\hat{I}\,, \tag{3}$$

where $\hat{I}$ is the unit tensor and

$$\hat{\tau} = -\mu[\nabla\mathbf{v} + (\nabla\mathbf{v})^T] + (\tfrac{2}{3}\mu - \xi)(\nabla.\mathbf{v})\hat{I}. \tag{4}$$

The parameters μ and ξ are the shear and bulk viscosity coefficients, respectively, and $(\nabla\mathbf{v})^T$ the transpose of the dyadic $\nabla\mathbf{v}$. The coefficient of shear viscosity for a species "s" is given by Chapman and Cowling[8] as

$$\mu_s = \frac{1}{4Q_s}\left(\frac{m_s K T_s}{\pi}\right)^{1/2}, \tag{5}$$

where Q_s is the collision cross section for species "s." The coefficient of bulk viscosity involves the internal state of gas molecules. For dilute monatomic gases, $\xi \simeq 0$ and for polyatomic gases, ξ is still sufficiently small that it may be neglected.[9]

An expression for the current $\mathbf{J}$ in Eq. (2) may be obtained from Ohm's Law[10] and can be written as

 0021-8979/84/030708-06$02.40

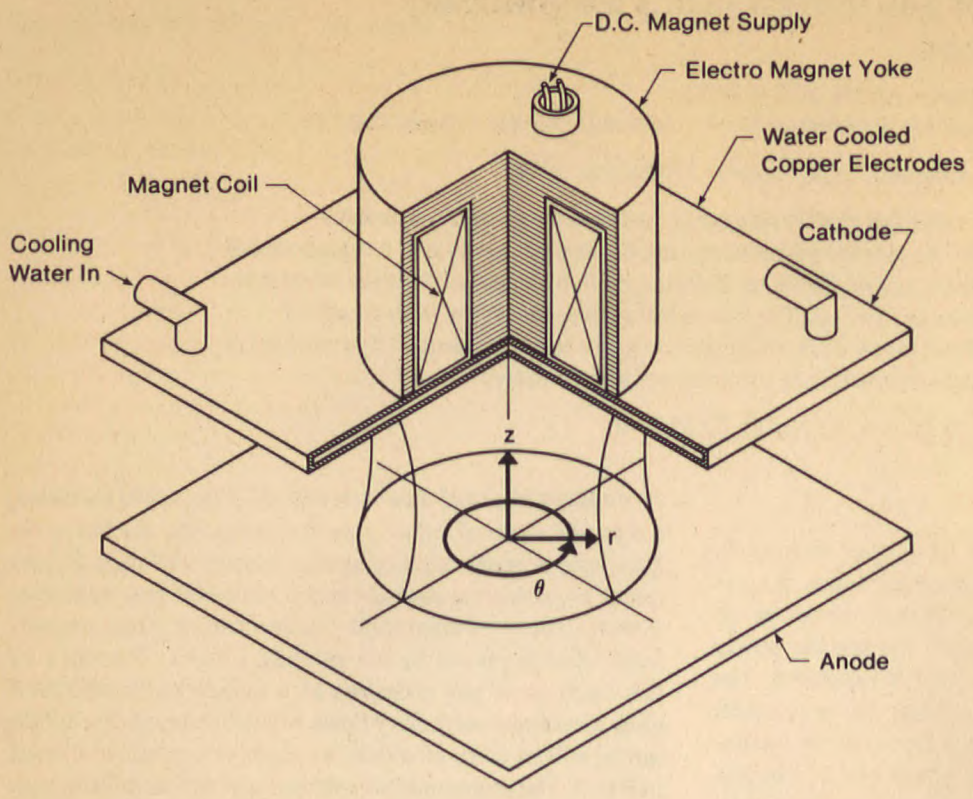

FIG. 1. Magnetically stabilized transverse discharge geometry.

$$\mathbf{J} = \hat{\sigma}.\mathbf{E}', \tag{6}$$

where $\mathbf{E}' = \mathbf{E} + \mathbf{v}\times\mathbf{B}$, and $\hat{\sigma}$ is the electrical conductivity tensor.[4] The expression for the discharge current can be considerably simplified by noting that for the cases considered, the Hartmann number $H_m < 1$. Therefore, viscous forces dominate the discharge dynamics, making $v_\theta B/E_z \ll 1$.

By applying Ohm's law and assuming a constant electron conductivity within the discharge region, it can be shown that[4]

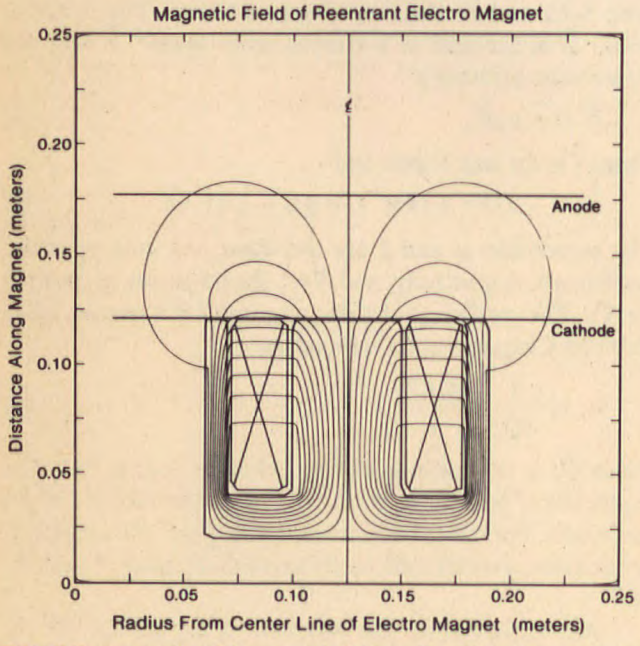

FIG. 2. Computer plot of the magnetic field profile of the reentrant electromagnet used in the experiment.

$$\frac{J_r}{J_z} = \frac{\beta_e^2 \tan\phi.}{1+(1+\beta_e^2)\tan^2\phi}, \tag{C10}$$

where J_r and J_z are the radial and axial components of the discharge current, respectively, β_e the electron Hall parameter, and $\phi = \tan^{-1}(B_z/B_r)$. This expression may be further simplified by noting that experimentally, the radial Lorentz forces confine the discharge current to an annular region where $|B_z/B_r| \ll 1$. Calculations show that a typical value of $\beta_e \simeq 1$ exists within the discharge; and with $\phi \ll 1$, Eq. (C10) indicates that $J_r \ll J_z$. Therefore, by applying the conservation of charge equation under steady-state conditions, $J_z \simeq$ const, and $J_r \simeq 0$.

The current distribution used in the numerical simulations to be described in Sec. III will assume $J_r = 0$ and J_z to be given by a Gaussian distribution centered about the midpoint r_0 of the experimentally observed annular discharge. Specifically,

$$J_z(r) = \frac{J_0}{b\sqrt{2\pi}} \exp\left[-\frac{(r-r_0)^2}{2b^2}\right], \tag{7}$$

where the variance b^2 is related to w the FWHM of the radial current distribution by $b^2 = w^2/8\ln(2)$. The constant J_0 may be determined from the expression for the total discharge current I_T, which is obtained from the integral of $J_z(r)$ over the discharge area. Evaluation of this integral yields

$$J_0 = I_T \Big/ \left\langle \sqrt{2\pi}b\left\{\exp\left(-\frac{r_0^2}{2b^2}\right) - \exp\left[-\frac{(R-r_0)^2}{2b^2}\right]\right\} + \pi r_0\left[\operatorname{erf}\left(\frac{r_0}{\sqrt{2}b}\right)\right] + \operatorname{erf}\left(\frac{R-r_0}{\sqrt{2}b}\right)\right\rangle, \tag{8}$$

where erf(x) is the error function and R the outside wall radius.

The calculation of the Lorentz force in Eq. (2) will be made by using values for the external magnetic field as calculated by the POTENT code[6] for a vacuum region. A typical value for the magnetic Reynolds number for discharges of interest is 10^{-7}. Such a small value for the magnetic Reynold's number implies that the discharge dynamics will not significantly distort the magnetic field from its vacuum profile.

To close the system of equations given by Eqs. (1) and (2), an expression for the pressure p, or equivalently, an equation of state is required. In the simulations that will be performed, the discharge will be assumed isothermal and the pressure given by the ideal gas law. A further assumption that will be made is that the discharge possess axial symmetry—that is, physical quantities are dependent upon the coordinates r and z only.

III. COMPUTATIONAL METHOD

A computer code MAGIC (MAgnetoGasdynamic Implicit Code) has been developed to numerically solve Eqs. (1) and (2), which form a system of time dependent, nonlinear, coupled partial differential equations. The equations are solved by using the method of finite differences on an Eulerian mesh. An ADI algorithm is used for the time advancement of the equations, and avoids the restrictions imposed by explicit methods on the timestep size. The development of MAGIC follows ideas presented by Finan and Killeen[11] used for the solution of time dependent, three dimensional, resistive magnetohydrodynamic equations. An overview of the development of the MAGIC computer code[12] follows.

The mass and momentum conservation equations given by Eqs. (1) and (2), respectively, can be expressed in vector form as

$$\frac{\partial}{\partial t}\mathbf{T}(\mathbf{u}) + \mathbf{F}(\mathbf{u}) + \mathbf{H}(\mathbf{u}) - \mathbf{S} = 0\,, \tag{9}$$

where $\mathbf{u} = (v_r\,, v_\theta\,, v_z\,, \rho)$ is the state vector of the system, $\mathbf{T}(\mathbf{u}) = (\rho\mathbf{v},\rho)$ the quantities advanced in time, and $\mathbf{S} = (\mathbf{J}\times\mathbf{B},\, 0)$. The function $\mathbf{F}(\mathbf{u})$ contains all the terms in Eqs. (1) and (2) that have leading derivatives with respect to r, while $\mathbf{H}(\mathbf{u})$ contains all terms with leading derivatives with respect to z. The assumption that the discharge possesses axial symmetry implies that the partial derivatives with respect to the variable θ are zero.

The solution to Eq. (9) is advanced in time by using the ADI algorithm described by Peaceman and Rachford.[13] The technique involves a two-step process for each time step, namely

$$\mathbf{T}(\mathbf{u}^*) - \mathbf{T}(\mathbf{u}^n) + \frac{\Delta t}{2}[\mathbf{F}(\mathbf{u}^*,\mathbf{u}^n) + \mathbf{H}(\mathbf{u}^n) - \mathbf{S}] = 0\,, \tag{10}$$

and

$$\mathbf{T}(\mathbf{u}^{n+1}) - \mathbf{T}(\mathbf{u}^*) + \frac{\Delta t}{2}[\mathbf{F}(\mathbf{u}^*) + \mathbf{H}(\mathbf{u}^{n+1},\mathbf{u}^*) - \mathbf{S}] = 0\,, \tag{11}$$

where $\mathbf{u}^n$ is the state vector at time t^n, $\mathbf{u}^*$ an intermediate value at $t^n + \Delta t/2$, and $\mathbf{u}^{n+1}$ is the solution at time $t^{n+1} = t^n + \Delta t$.

The procedure for obtaining the functions $\mathbf{F}(\mathbf{u})$ and $\mathbf{H}(\mathbf{u})$ from Eqs. (1) and (2) is straightforward except for the case of product and mixed derivatives which result in the need for time advanced values on either rows or columns of the mesh not yet computed. The problem was resolved by differencing the mixed derivative terms explicitly as in Finan.[14]

A straightforward solution of Eqs. (10) and (11) is unfortunately not possible because of nonlinear terms. For instance, terms such as $\mathbf{T}(\mathbf{u}^*)$ and $\mathbf{T}(\mathbf{u}^{n+1})$ will involve a product of the velocity and density sought for at the next time step. The procedure that will be used for solving Eqs. (10) and (11) for the state variables at a new time step involves a generalized Newton–Raphson iteration method described by Finan and Killeen.[11] A brief description of the technique follows.

Equation (10), which is a nonlinear vector equation, can be written in the form

$$\mathbf{W}(\mathbf{u}^*, \mathbf{u}^n) = \mathbf{W}_e(\mathbf{u}^n) + \mathbf{W}_i(\mathbf{u}^*, \mathbf{u}^n) = 0\,, \tag{12}$$

where $\mathbf{W}_e(\mathbf{u}^n)$ is the explicit part which depends only on $\mathbf{u}^n$ and an implicit part $\mathbf{W}_i(\mathbf{u}^*\,,\mathbf{u}^n)$ which depends upon $\mathbf{u}^*$ and $\mathbf{u}^n$. The problem therefore consists of finding a solution which satisfies the equation $\mathbf{W}(\mathbf{u}^*,\mathbf{u}^n) = 0$. The development of the iteration algorithm is based on the expansion of $\mathbf{W}(\mathbf{u}^*,\mathbf{u}^n)$ in a Taylor series about the lth trial solution ${}^l\mathbf{u}^*$. Since the solution desired is one where $\mathbf{W}({}^{l+1}\mathbf{u}^*, \mathbf{u}^n) = 0$, the next iteration for the solution, ${}^{l+1}\mathbf{u}^*$, can be found from

$${}^{l+1}\mathbf{W} = 0 = {}^l\mathbf{W} + \left(\frac{\partial \mathbf{W}}{\partial \mathbf{u}^*}\right)^l .({}^{l+1}\mathbf{u}^* - {}^l\mathbf{u}^*)\,, \tag{13}$$

where ${}^{l+1}\mathbf{W} = \mathbf{W}({}^{l+1}\mathbf{u}^*,\mathbf{u}^n)$, and higher order terms in the Taylor expansion are neglected. The matrix $(\partial \mathbf{W}/\partial \mathbf{u}^*)$ is a standard Jacobian whose elements are defined by

$$\hat{J} = \left(\frac{\partial \mathbf{W}}{\partial \mathbf{u}^*}\right) = \frac{\partial(W_1, W_2, W_3, W_4)}{\partial(v_r^*\,, v_\theta^*\,, v_z^*\,, \rho^*)}\,.$$

Since the Jacobian $\hat{J}$ only measures the $\mathbf{u}^*$ dependence, only the implicit portion of $\mathbf{W}(\mathbf{u}^*,\mathbf{u}^n)$ need be differentiated. By rearranging Eq. (13), a simple iteration formula is found for ${}^{l+1}\mathbf{u}^*$, namely

$${}^l\hat{J}.{}^{l+1}\mathbf{u} = \hat{J}.{}^l\mathbf{u} - {}^l\mathbf{W}\,, \tag{14}$$

where the superscript * has been suppressed. If finite difference approximations are substituted for $\mathbf{W}$ (note that a second derivative at a grid point i will also involve values at grid points i-1 and $i + 1$), a block tridiagonal form comprised of (4×4) submatrices is obtained.

$$-\hat{A}_{i,j}\,.{}^{l+1}u_{i+1,j} + \hat{B}_{i,j}\,.{}^{l+1}u_{i,j} - \hat{C}_{i,j}\,.{}^{l+1}u_{i-1,j} = D_{i,j}\,. \tag{15}$$

The subscript "i" in Eq. (15) represents a grid point in the coordinate along which the equations are being advanced implicitly, the subscript "j" represents grid points in the coordinate along which the equations are advanced explicitly. The submatrices $\hat{A}_{i,j}$, $\hat{B}_{i,j}$, and $\hat{C}_{i,j}$ are Jacobians evaluated at grid point (i, j), $\mathbf{D}_{i,j}$ contains all explicit terms. The evaluation of the terms $\hat{A}_{i,j}$, $\hat{B}_{i,j}$, $\hat{C}_{i,j}$ and $\mathbf{D}_{i,j}$ is dis-

cussed by Antoniuk.[12] Standard techniques are used to solve the resulting tridiagonal system of equations. An analogous procedure is used for obtaining a solution to Eq. (11) in the next half-time step. A detailed description of the development of the MAGIC code is given in Ref. 12.

The simulation of gas flow in the discharge shown schematically in Fig. 1 will be made by using a uniform mesh over the spatial domain $0 \leqslant r \leqslant R$ and $0 \leqslant z \leqslant d$. The effects of viscosity and the assumption of solid electrodes imply homogeneous Dirichlet boundary conditions on all velocity components at the electrode surfaces. A homogeneous Dirichlet condition is also used on all velocity components at the axis of symmetry ($r = 0$). The computational grid does not extend to the chamber walls in the experiment, but rather to a radius R which is still well removed from the active discharge region. A homogeneous Neumann condition will be used for the azimuthal velocity v_θ on the boundary $r = R$, while homogeneous Dirichlet conditions are used for v_r and v_z on this boundary. The homogeneous Neumann condition is used for ρ on all boundaries.

The use of the iterative ADI computer code described in this section is cost effective in analyzing time dependent viscous flow problems. In performing the simulations to be described in Sec. IV, time steps of about twice that of the Courant–Friedrichs–Lewy (CFL) limit[15] were used without incurring significant error. This result makes the ADI scheme very attractive since most explicit codes of this complexity can only run at a fraction of the Courant limit (typically 20%) to ensure stability. However, ADI direction splitting techniques can lead to difficulties when large time steps are used. Craxton and McCrory[16] have found that the direction splitting technique produced smooth solution profiles in the last implicit direction scanned, but noisy profiles in the other direction scanned explicitly. This noise was also observed in MAGIC, but could easily be eliminated by reducing the time step size.

IV. NUMERICAL RESULTS

The flow structure within a magnetically stabilized glow discharge structure given schematically by Fig. 1 will now be obtained. For this case the externally applied magnetic field profile is as given by Fig. 2 and the discharge current radial distribution is given by Eq. (7). The numerical solution to Eqs. (1) and (2) which govern viscous isothermal flow, will be obtained numerically by using the large time-step ADI techniques described in Sec. III. The experimental parameters that are chosen are essentially those used in the analysis of Ref. 4 where secondary flow effects were neglected. A gas mixture of $CO_2/N_2/He$ in the proportions 2/2/16 Torr is assumed at a temperature of 425 °K. The peak value of the magnetic field near the cathode surface is approximately 0.07 T and approximately 0.025 T in the central region of the discharge. The remaining parameters are $R = 0.1$ m, $d = 0.056$ m, $\mu = 6.6 \times 10^{-6}$ kg/m s, $I_T = 5$ A, $r_0 = 0.03$ m, and $w = 0.025$ m. The results of the simulation for the flow velocities are given at a time 4 ms after discharge initiation in Figs. 3–5. Essentially steady state conditions exist at this time.

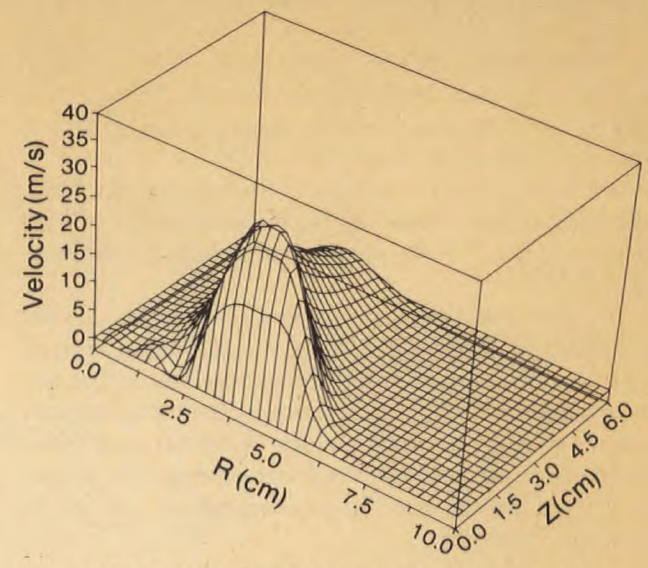

FIG. 3. Rotational velocity distribution as a function of r and z.

The rotational velocity v_θ is given as a function of r and z in Figs. 3 and 4. The results indicate a maximum velocity of 35 m/s, which is substantially below the value of 250 m/s predicted by the earlier numerical simulation[4] which neglected secondary flows. The peak rotational velocity occurs near the cathode surface (see Fig. 4) where the Lorentz driving force is strongest. Also evident is the strong shear in v_θ throughout the discharge volume. Equation (2) shows the velocity to be proportional to the Lorentz force. Larger rotational velocities can therefore be realized by using either a larger discharge current or a stronger magnetic field. This has been confirmed by numerical simulations.

The resulting secondary flows are given in Fig. 5. The flow direction and magnitude is indicated by the direction and length of the arrows, the longest of which represents velocities of approximately 18 m/s. It is important to note that the secondary flow forms a convective cell which is driven by the strongly sheared velocity distribution in v_θ (see Figs. 3 and 4). This secondary flow is responsible for the reduction in magnitude of the rotational velocity. The mechanism by which this occurs is as follows. The fluid is accelerated in the v_θ direction predominantly near the cathode surface where the Lorentz forces are strongest. The fluid is then convected radially outward and subsequently losses a significant fraction of its azimuthal momentum through viscous drag on the electrodes and on the vessel walls. Near the anode region, fluid that has lost most of its azimuthal momentum (Figs. 3 and 4) is convected back into the discharge region where it is again accelerated and the process repeated. The secondary flow effectively "loads down" the rotating discharge by convecting fluid with a reduced angular momentum into the discharge region.

In this MGD system, the normally neglected secondary flows have been found to be of the same order of magnitude as the principle rotational flow v_θ. The existence of such large axial and radial flows serve to stabilize the discharge against bulk instabilities. One mechanism by which this is

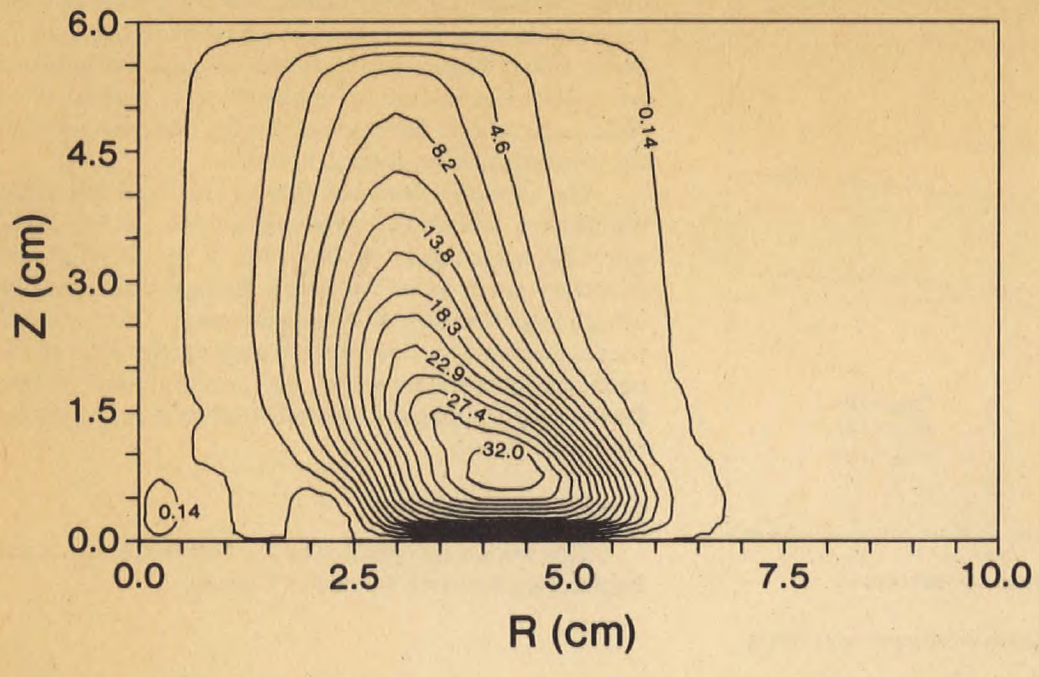

FIG. 4. Contour plot of the sheared rotational velocity distribution.

achieved can be attributed to the strongly sheared rotational flow (Figs. 3 and 4) and the convective secondary flows (Fig. 5) which rapidly spread any localized nonuniformities in density, temperature or current over the entire discharge volume in a time much less than the normal instability formation time.

With suitable modifications to the experiment, it may be possible to exploit the large radial flows in order to cool the hot gas produced within the discharge. This would allow the hot neutral gas to be transported radially outward towards a heat exchanger where it could be cooled and then returned to the discharge region. In this radial flow system, the hot gas would only have to travel across one-half of the electrode length in order to escape the excitation processes. Consequently, such a system would have only one-half of the normal gas residence time found in conventional transverse devices.

It must be noted that the calculated flow velocities represent the mass averaged flow of the gas discharge system as determined by a one-fluid MGD model. Since the degree of ionization is only 2.6×10^{-7}, the plotted values are essentially those of the neutral gas and do not represent the flow pattern of the charged species.

V. EXPERIMENTAL RESULTS

The observation of a radial afterglow ejected out of the discharge in the experiments suggested the presence of strong radial gas flow predicted by the numerical simulations. The presence of this flow was confirmed by measurements made by using a Pitot tube connected to a capacitance manometer, the results of which are given in Fig. 6. The magnitude of the measured flow velocities are in good agreement with the computer simulation results in Fig. 5. The measurements also confirm that larger flow velocities are

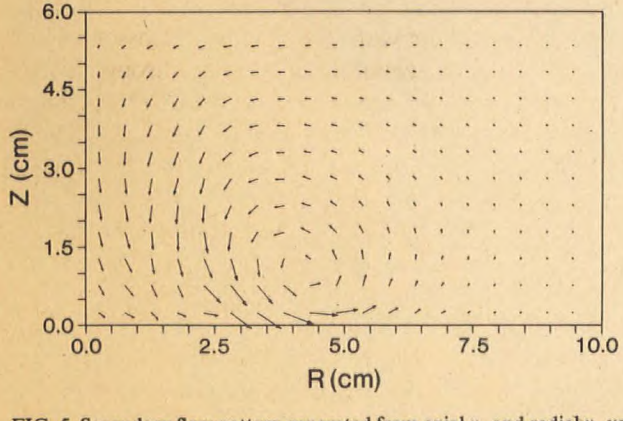

FIG. 5. Secondary flow pattern generated from axial v_z and radial v_r velocity components.

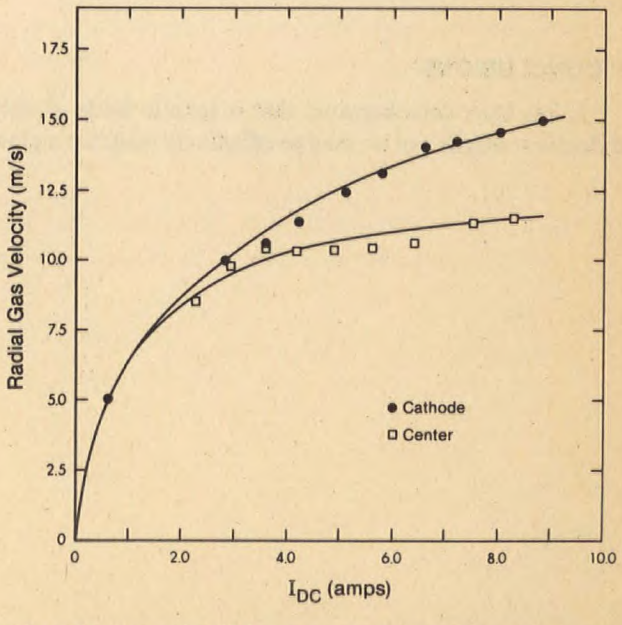

FIG. 6. Effect of applied discharge current on the radial gas velocity profile.

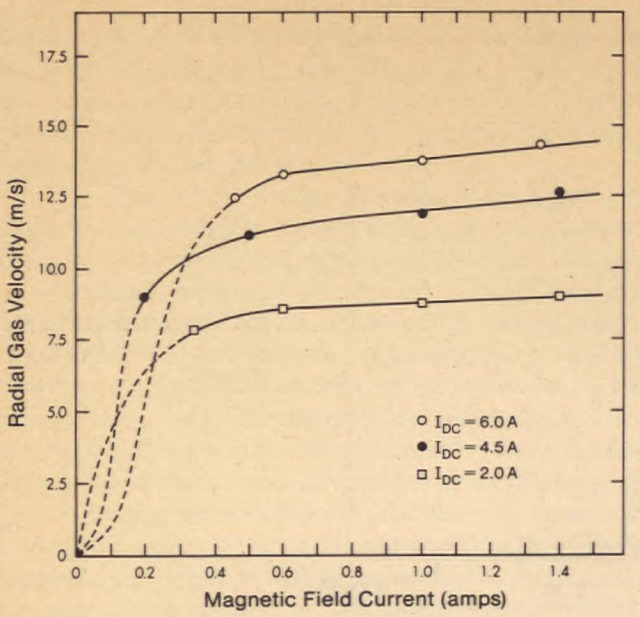

FIG. 7. Dependence of radial gas velocity on magnetic field strength.

realized near the cathode region as compared to those near the anode. The results in Fig. 6 also verify that larger flow velocities can be realized by increasing the magnitude of the Lorentz force [see Eq. (2)]. In this case the magnetic field is held constant and the magnitude of the discharge current varied. The effect of an increased Lorentz force on the radial gas flow velocity is again seen in Fig. 7 where the discharge current is now fixed and the magnetic field strength is varied. The current in the magnetic field coils is used for the abscissa because the magnetic field strength has a strong spatial dependence (see Fig. 2). The average magnetic field strength $|B|$ in the discharge is linearly related to the current in the field coils (neglecting ion core saturation effects). As a rough guide, each ampere of current in the field coils corresponds to an average magnetic flux density of approximately 400 G.

VI. CONCLUSIONS

It has been demonstrated that magnetic fields of only moderate strength can be used to effectively stabilize a glow discharge. Stabilization is achieved as a result of the strongly sheared rotational flow v_θ and the convective cell formed by the secondary flows v_r and v_z . The flows cause any localized nonuniformities in density, temperature, or current to be rapidly spread over the entire discharge, in a time less than the normal instability formulation time.

The secondary flows also play an important role in the stabilization process by convecting the hot gas out of the active discharge region. A simulation of the rotational and secondary gas flows within such a discharge was made by using a large time step ADI computer code. The numerical results that were obtained were in good agreement with experimentally measured values, and provide further insight for the design of magnetically stabilized glow discharges for laser applications.

ACKNOWLEDGMENTS

This work was supported by the National Sciences and Engineering Research Council of Canada.

[1]R. A. Haas, Phys. Rev. A **8**, 1017 (1973).
[2]W. L. Nighan and W. J. Wiegand, Appl. Phys. Lett. **25**, 633 (1974).
[3]H. J. J. Seguin, C. E. Capjack, D. M. Antoniuk, and K. H. Nam, Appl. Phys. Lett. **37**, 130 (1980).
[4]C. E. Capjack, D. M. Antoniuk, and H. J. J. Seguin, J. Appl. Phys. **52**, 4517 (1981).
[5]C. E. Capjack, H. J. J. Seguin, D. M. Antoniuk, and V. A. Seguin, Appl. Phys. B **26**, 161 (1981).
[6]C. L. Thomas, *Software for Numerical Mathematics* (Academic, Loughborough, England, 1974), p. 315.
[7]L. D. Landau and E. M. Lifshitz, *Fluid Mechanics* (Pergamon, London, 1959).
[8]S. Chapman, and T. G. Cowling, *Mathematical Theory of Non-Uniform Gases*, 3rd ed. (Cambridge University , London, 1970).
[9]J. O. Hirschfelder, C. F. Curtis, and R. B. Bird, *Molecular Theory of Gases and Liquids* (Wiley, New York, 1954).
[10]G. W. Sutton and A. Sherman, *Engineering Magnetohydrodynamics* (McGraw-Hill, New York, 1965).
[11]C. H. Finan III and J. Killeen, Comp. Phys. Comm. **24**, 441 (1981).
[12]D. M. Antoniuk, Ph.D. thesis, University of Alberta, 1983.
[13]D. W. Peaceman and H. H. Rachford, Jr., J. Soc. Indust. Appl. Math **3**, 28 (1955).
[14]C. H. Finan III, Ph.D. thesis, UCRL-53086, December 1980.
[15]R. D. Richtmyer and K. W. Morton, *Difference Methods for Initial Value Problems* (Interscience, New York, 1967).
[16]R. S. Craxton and R. L. McCrory, Report No. 99, Laboratory for Laser Energetics, University of Rochester, 1980.

LANCASTER PRESS, INC., LANCASTER, PA.